

UNIVERSITÄTSKLINIKUM HAMBURG-EPPENDORF

Zentrum für Experimentelle Medizin
Institut für Zelluläre und Integrative Physiologie

Prof. Dr. med. Heimo Ehmke

Tripartite Separation of Glomerular Cell Types and Proteomes from Reporter-Free Mice

Dissertation

zur Erlangung des Grades eines Doktors der Medizin
an der Medizinischen Fakultät der Universität Hamburg.

vorgelegt von:

Favian Alexander Hatje
aus Hongkong

Hamburg 2023

**Angenommen von der
Medizinischen Fakultät der Universität Hamburg am:
09.07.2024**

**Veröffentlicht mit Genehmigung der
Medizinischen Fakultät der Universität Hamburg.**

**Prüfungsausschuss, der/die Vorsitzende:
Prof. Dr. Hartmut Schlüter**





**Prüfungsausschuss, zweite/r Gutachter/in:
Prof. Dr. Catherine Meyer-Schwesinger**

Inhaltsverzeichnis

1. Publikation.....	4
2. Dissertation	43
2.1. <i>Einleitung</i>	43
2.1.1. Anatomie der Niere und des Nierenkörperchens	43
2.1.2. Die Zellen des Glomerulus	45
2.1.2.1. Podozyten	45
2.1.2.2. Mesangialzellen.....	45
2.1.2.3. Endothelzellen	45
2.1.3. Podozyten, Mesangial- und Endothelzellen im Kontext glomerulärer Pathologien ...	45
2.1.4. Das Ziel meiner Arbeit	46
2.2. <i>Ergebnisse</i>	46
2.2.1. Arbeitshypothese.....	46
2.2.2. Tiere.....	47
2.2.3. Isolation von Glomeruli.....	48
2.2.4. Entwicklung eines Protokolls zur Lösung glomerulärer Zellen aus ihrem Verband ..	48
2.2.4.1. Podoplanin	48
2.2.4.2. CD73.....	49
2.2.4.3. CD31.....	49
2.2.5. Zellen sortieren.....	50
2.2.6. Reinheit isolierter Zellpopulationen	50
2.2.6.1. Konfokale Mikroskopie.....	50
2.2.6.2. Quantitative polymerase chain reaction	51
2.2.6.3. Western Blot.....	52
2.2.6.4. Proteomics	52
2.2.7. Weiterführende Untersuchungen	53
2.2.7.1. Angereicherte Proteine in den Zellpopulationen.....	53
2.2.7.2. Ergebnisse proteomischer Untersuchungen sortierter Zellpopulationen	53
2.2.7.3. Spezifische Reaktionen glomerulärer Zellen im Mausmodell der anti-THSD7A membranösen Glomerulonephritis	53
2.3. <i>Diskussion</i>	53
2.3.1. Der Verlust von Antigenen	53
2.3.2. Die membranöse Glomerulonephritis.....	54
2.3.3. Relevanz von timMEP im Kontext medizinischer Grundlagenforschung	55
3. Zusammenfassung.....	55
3.1. <i>Deutsch</i>	55
3.2. <i>Englisch</i>	55
4. Abkürzungsverzeichnis.....	56
5. Abbildungsverzeichnis	56
6. Literaturverzeichnis	56
7. Erklärung des Eigenanteils an der Publikation	58
8. Danksagung	59
9. Lebenslauf.....	60
10. Eidesstaatliche Versicherung	61

1. Publikation

Tripartite Separation of Glomerular Cell Types and Proteomes from Reporter-Free Mice

Favian A. Hatje,¹ Uta Wedekind,¹ Wiebke Sachs,¹ Desiree Loreth ¹, Julia Reichelt,¹ Fatih Demir ², Christopher Kosub ¹, Lukas Heintz ¹, Nicola M. Tomas,³ Tobias B. Huber,³ Sinah Skuza,¹ Marlies Sachs,¹ Stephanie Zielinski,¹ Markus M. Rinschen,^{2,3,4} and Catherine Meyer-Schwesinger¹

Due to the number of contributing authors, the affiliations are listed at the end of this article.

ABSTRACT

Background The glomerulus comprises podocytes, mesangial cells, and endothelial cells, which jointly determine glomerular filtration. Understanding this intricate functional unit beyond the transcriptome requires bulk isolation of these cell types for biochemical investigations. We developed a globally applicable tripartite isolation method for murine mesangial and endothelial cells and podocytes (timMEP).

Methods We separated glomerular cell types from wild-type or mT/mG mice via a novel FACS approach, and validated their purity. Cell type proteomes were compared between strains, ages, and sex. We applied timMEP to the podocyte-targeting, immunologic, THSD7A-associated, model of membranous nephropathy.

Results timMEP enabled protein-biochemical analyses of podocytes, mesangial cells, and endothelial cells derived from reporter-free mice, and allowed for the characterization of podocyte, endothelial, and mesangial proteomes of individual mice. We identified marker proteins for mesangial and endothelial proteins, and outlined protein-based, potential communication networks and phosphorylation patterns. The analysis detected cell type-specific proteome differences between mouse strains and alterations depending on sex, age, and transgene. After exposure to anti-THSD7A antibodies, timMEP resolved a fine-tuned initial stress response, chiefly in podocytes, that could not be detected by bulk glomerular analyses. The combination of proteomics with super-resolution imaging revealed a specific loss of slit diaphragm, but not of other foot process proteins, unraveling a protein-based mechanism of podocyte injury in this animal model.

Conclusion timMEP enables glomerular cell type-resolved investigations at the transcriptional and protein-biochemical level in health and disease, while avoiding reporter-based artifacts, paving the way toward the comprehensive and systematic characterization of glomerular cell biology.

JASN 32: 2175–2193, 2021. doi: <https://doi.org/10.1681/ASN.2020091346>

The glomerular filtration barrier (GFB) represents a sophisticated syncytium of individual cell types, *i.e.*, podocytes, mesangial cells, and glomerular endothelial cells, which sustain the structure and regulate the function of the filtration barrier.¹ Podocytes embrace the glomerular capillaries and form an intricate mesh with their interdigitating processes that are interconnected by a modified form of an adherens junction, the slit diaphragm, which ultimately bridges the filtration slits. The intraglomerular mesangial cells are situated in close contact with the endothelial cells and represent a specialized form of pericytes that provide

structural support. The fenestrated endothelial cells line the glomerular capillaries and reside opposite the podocytes, separated by the glomerular

Received September 20, 2020. Accepted April 9, 2021.

Correspondence: Prof. Catherine Meyer-Schwesinger, Institute of Cellular and Integrative Physiology, University Medical Center Hamburg-Eppendorf, Martinistrasse 52, 20246, Hamburg, Germany. Email: c.meyer-schwesinger@uke.de

Copyright © 2021 by the American Society of Nephrology

basement membrane (GBM). Malfunction of any of these cell types leads to a loss of glomerular function and proteinuria, leading to the concept that these glomerular cell types interact,² a finding also supported *in silico* by single-cell transcriptomic studies. However, limitations of single-cell approaches include the lack of depth of transcriptomes and the difficulty in subjecting single cells to biochemical applications to analyze their function. Therefore, analysis of glomerular injury would also benefit from the bulk isolation of all three cell types from the glomeruli of individual mice for subsequent protein-biochemical investigations.

The establishment of a globally applicable, large-scale method to isolate glomeruli from mice, using magnetic beads,³ revolutionized our understanding of glomerular injury pathways. Later, a FACS-based method to isolate podocytes from mice was developed, which has further enhanced the cellular resolution of glomerular injury patterns, but with an isolated focus on podocytes.^{4–6} This technique relies on the use of mT/mG mice that exhibit a transgenic, intracellular expression of enhanced green fluorescent protein (eGFP) in podocytes, and of tdTomato in nonpodocytes, under control of a Cre promoter⁷ or other genetically encoded reporters.⁸ However, this method has significant limitations. First, before podocyte isolation, the mouse models of interest are required to be crossed to mT/mG mice, resulting in costly, time-, and mouse-consuming breeding, with the risk of genetic background changes that are often accompanied by a change in susceptibility to established injury models. Further, only podocytes are isolated from the mouse, the other glomerular cells are indistinguishable from each other through the expression of tdTomato. These limitations are particularly important in diseases with altered glomerular composition, such as podocyte loss or mesangial expansion.

The aim of this study was to develop a (1) globally applicable, and (2) economic (in terms of cost, time, and mice) isolation protocol of all three glomerular cell types, from an individual mouse, in sufficient amounts and at a sufficient purity to enable physiologic, pathophysiologic, protein-biochemical, and omics investigations of *in vivo* mouse models. This glomerular cell isolation technique adds a new level of biochemical resolution of glomerular cell types that is not possible using single-cell technologies, spatial transcriptomics, or spatial proteomics.

METHODS

Animals

Male and female C57BL/6 mice and BALB/c mice were purchased from Charles River (Sulzfeld, Germany) at the age of 10–14 weeks. mT/mG mice (ICR;Sv129/J;C57BL/6)⁵ were provided by T.B.H. (III Medical Clinic, University Medical Center Hamburg-Eppendorf, Hamburg, Germany). Mice

Significance Statement

Renal blood filtration occurs in a functional unit called the glomerulus. The filtration barrier comprises resident cell types, *i.e.*, podocytes, mesangial cells, and glomerular endothelial cells. We introduce a glomerular cell isolation protocol that separates these three cell types at a sufficient quantity and purity to allow for detailed protein-biochemical investigations. We demonstrate that the expression of fluorescent transgenes in glomerular cells can result in proteome artifacts, and that different mouse strains have different glomerular cell type proteomes. Further, we demonstrate the power of this globally applicable technique to identify new proteins enriched in glomerular cells and to dissect cell-specific disease responses and crosstalk between different intra-glomerular cell types.

had free access to water and standard chow, were synchronized to a 12-hour light/dark cycle, and euthanized by cervical dissection for kidney removal. Anti-THSD7A membranous nephropathy (MN) was induced by intravenous injection of 180 μ l (1.4 mg per 30 g mouse) rabbit anti-THSD7A antibodies, or unspecific rabbit IgG as control, in male BALB/c mice aged 12–22 weeks.⁹ Urine was collected after spontaneous urination on day 1 and 7 before euthanasia. Cells isolated *via* the tripartite isolation method for murine mesangial and endothelial cells and podocytes (tim-MEP) were analyzed by quantitative PCR (qPCR; days 1 and 7) and by proteomics (day 7).

Measurement of Proteinuria

Urine samples were collected over 3–5 hours in a metabolic cage with free access to water. Urinary albumin content was quantified using a commercially available ELISA system (Bethyl) according to the manufacturer's instructions, using an ELISA plate reader (BioTek), as described.¹⁰ Albumin levels were standardized against urine creatinine values, determined according to the Jaffe method, for the same individuals.

Glomerular Cell Isolation

Kidneys were harvested, perfused with magnetic DynaBeads, and glomeruli were isolated as previously described.³ We then isolated podocytes, mesangial cells, and endothelial cells (a detailed protocol is provided in Supplemental Appendix 1). In brief, collected and pelleted, decapsulated glomeruli were dissolved in digestion buffer. The digestion buffer contained 1000 μ g/ml Liberase TL (Roche), 100 U/ml DNase1 (Roche), 10% FCS, 1% insulin/transferrin/selenium, 1% penicillin/streptomycin, and 25 mM HEPES dissolved in 1 \times RPMI 1640 (Gibco). Cells were incubated for 2 hours at 37°C and 1400 rpm, and repeatedly, diversely, mechanically stressed by vortexing, shearing (with a 27-gauge needle), and pipetting (inspired by Boerries *et al.*⁵) using Pasteur and Eppendorf pipettes to promote maximum cellular separation. A DynaMag magnet was used to separate glomerular remnants and DynaBeads from single cells. After 5 minutes in the DynaMag, the single cell-containing supernatant was

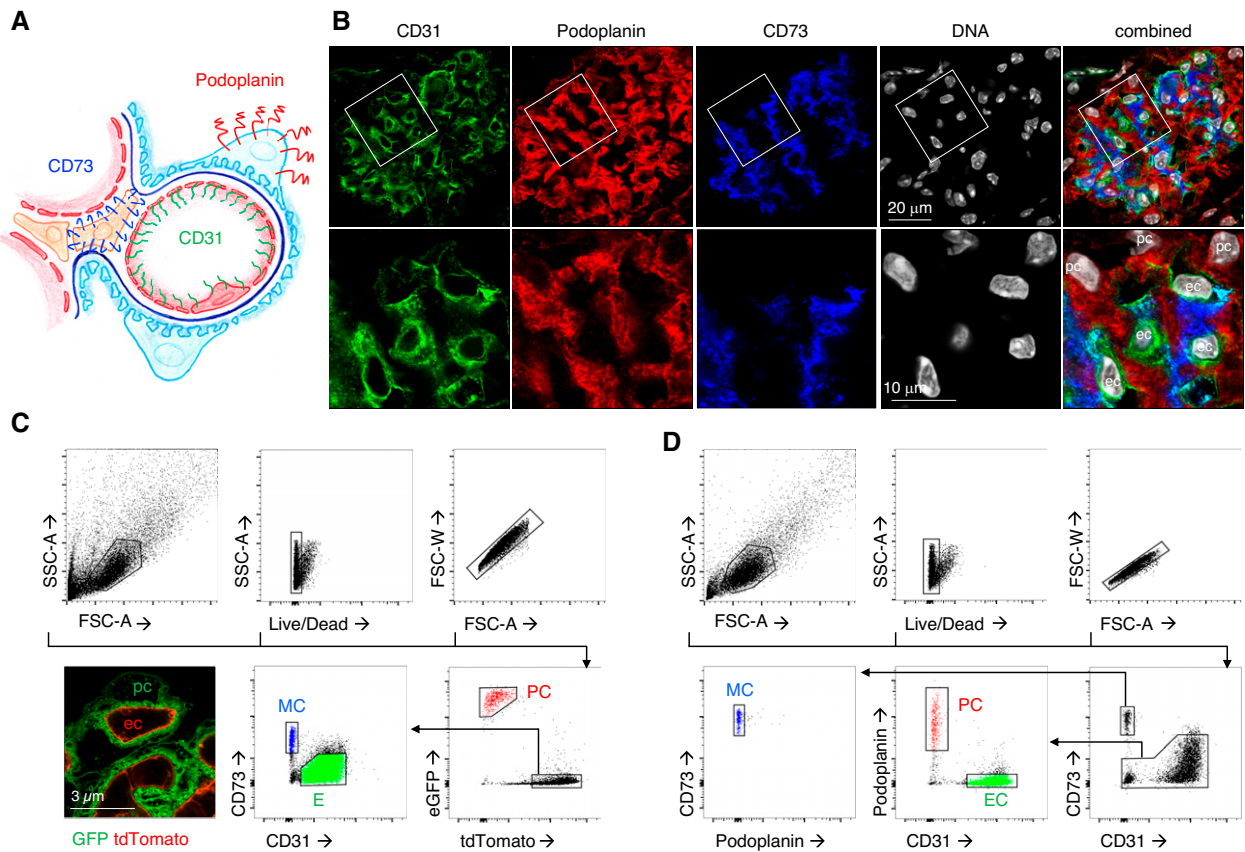


Figure 1. FACS strategy from wild-type and mT/mG mice for tripartite isolation of glomerular cell types allows bulk isolation of podocyte, mesangial and endothelial cells. (A) Scheme of a glomerular loop depicting the localization of the cell-specific markers used for the FACS strategy. (B) Confocal micrographs depicting labeled podocytes (pc; podoplanin, red), endothelial cells (ec; CD31, green), and mesangial cells (CD73, blue) in a 4% PFA fixed-frozen section of a murine kidney. DNA was visualized using Hoechst. (C) Gating strategy of glomerular single cells derived from an mT/mG mouse, demonstrating a distinct podocyte (eGFP⁺/tdTomato⁻, red), endothelial cell (tdTomato⁺/eGFP⁻/CD31⁺/CD73⁻, green), and mesangial cell (tdTomato⁺/eGFP⁻/CD73⁺/CD31⁻, blue) population. The unlabeled cells represent contaminating cells such as tubular cells. The left lower panel exhibits a representative high-resolution confocal image of the intrinsic GFP and tdTomato expression in an mT/mG glomerulus from an optically cleared kidney section. The histologic panel exhibits intrinsic GFP and tdTomato fluorescence of a glomerular capillary loop of an optically cleared 300- μ m kidney slice. (D) Gating strategy of glomerular single cells isolated from a wild-type mouse exhibiting a distinct podocyte (PC; podoplanin⁺/CD73⁻/CD31⁻, red), endothelial cell (EC; CD31⁺/CD73⁻/podoplanin⁻, green), and mesangial cell (MC; CD73⁺/CD31⁻/podoplanin⁻, blue) population. The unlabeled cells represent contaminating cells such as tubular cells. FSC-A, forward scatter area; FSC-W, forward scatter width; SSC-A, side scatter area.

collected. Cells were pelleted (10 min, 4°C, 1000 \times g) and washed once with magnetic cell sorting buffer (PBS with 0.5% BSA and 2 mM EDTA). After centrifugation, the supernatant was carefully removed to avoid any disturbance of the very fragile cell pellet. Subsequently, cells were stained with the cell-specific antibodies Podoplanin (podocytes), CD73 (mesangial cells), CD31 (endothelial cells), CD45 (leukocytes), and a LIVE/DEAD stain (Invitrogen), as listed in Supplemental Table 1. After incubation (30 minutes at 4°C in complete darkness), cells were washed once more, resuspended in magnetic cell sorting buffer, and sieved through 40- μ m sieves into the FACS tubes. Cells for the native proteomic experiments were sorted using a FACSAria Fusion (BD Biosciences), applying the strategy shown in

Supplemental Figure 1A. However, we then revised this strategy to compensate for slight and minor cross-contamination of podocytes in the mesangial cells, which became evident in this proteomic dataset (Supplemental Figures 1B and 2). We only recommend using the strategy shown in Figure 1D for sorting, which was used for all other depicted experiments (*i.e.*, qPCR and proteomics of THSD7A-MN glomerular cells, cell culture, and Western blot).

Sample Preparation and Mass Spectrometry Analysis

Cell pellets were snap frozen and stored at -80°C . For comparison of different strains, approximately 50,000 cells were

analyzed. Cells were resuspended in 4% SDS and 10 mM Tris and heated at 95°C for 10 minutes. Then, solubilized proteins were reduced and alkylated using 5 mM dithiothreitol and 10 mM iodoacetate, respectively. Proteins were digested and prepared using the SP3 protocol, with modifications, as previously described.^{11,12} For deeper protein analysis, we obtained pellets of 1 million cells from mT/mG mice. These pellets were resuspended in 8 M urea and 5 mM Tris in liquid chromatography–mass spectrometry–grade water, sonicated for 1 minute using an ultrasonication pulse (0.1 second cycle, 10% strength), and spun down at 16000 × g at 4°C. Protein concentration (for 1 million cells) was determined using a commercial BCA assay (Thermo). Proteins were then reduced and alkylated as described above. Proteins were digested using a protease in-solution digestion protocol, with a modified SP3 protocol^{11,13} (50,000 cells), or in-solution digestion.¹⁴ We used trypsin for all digestion steps. Tryptic peptides were analyzed using a nanoscale liquid chromatography–tandem mass spectrometry hardware setup, consisting of a nanoflow LC (flow, 200 nl/min) coupled to an Orbitrap QExactive Plus tandem mass spectrometer. The peptides were separated using a gradient for reverse-phase separation, consisting of buffer A and buffer B, with ascending concentrations of buffer B (80% acetonitrile, 0.1% formic acid) over buffer A (0.1% formic acid). The peptides from 50,000 cells were separated using a 1 hour gradient. The peptides from 1 million cells were separated using a 2.5 hour gradient.

Bioinformatic Analysis

Protein raw files were searched using MaxQuant and the LFQ algorithm^{15,16} with searches against a UniProt mouse proteome reference database released in January 2018. Search criteria were alkylation on cysteines as a fixed modification, and amino-terminal acetylation and methionine oxidation as variable modifications. Default criteria were used, meaning that PSM, peptide, and protein false discovery rates (FDRs) were set at 0.01. The LFQ algorithm was enabled, and “match between run” was enabled. The data were analyzed using Perseus version 1.5.5.3, with filtering for the embedded annotations as contaminant, reverse, or proteins identified by site only. Only proteins in at least 60% of samples were retained, and missing values were imputed using default imputation parameters (downshift SD, 2; width, 0.3). Gene Ontology term and UniProt keyword annotation and enrichment were performed using the embedded terms.¹⁷ Radar plots were generated using the ggradar package (Rstudio; <https://github.com/ricardo-bion/ggradar>), with default settings. The generated .txt files have been shared (see *Data Sharing Statement*). Differentially expressed proteins were defined by ANOVA with an FDR-corrected *P* value of <0.01 to adjust for multiple testing. For these proteins, we defined criteria for the identification of new glomerular cell–enriched proteins as follows: (1) a log₂ fold change of

two between podocytes and nonpodocytes; (2) a negative search result in PubMed (<https://www.ncbi.nlm.nih.gov/pubmed>) with the keywords “protein of interest” and “podocyte” or “glomerular” or “renal” or “kidney,” “protein of interest” and “mesangium” or “mesangial” or “glomerular” or “renal” or “kidney,” and “protein of interest” and “endothelial” or “endothelium” or “glomerular” or “renal” or “kidney”; and (3) a validated cell-of-interest expression pattern in the human protein atlas (<https://www.proteinatlas.org/search>). From significantly enriched podocytes, protein-protein interaction networks were generated using STRINGdb¹⁸ and filtered for high confidence (>0.9) on the basis of experimental or database evidence only. Then, protein networks were imported into Cytoscape version 3.3,¹⁹ and all edges that were not between two different cell types and the associated nodes were removed.

Phosphorylation Patterns

To determine phosphorylation patterns, we used MaxQuant to search our raw spectral data against a mouse database, with phosphorylation as a variable modification, as previously described.²⁰ Sequence windows of phosphorylation sites with a localization probability >0.8 were used for further analysis. Phosphorylation patterns were determined using Seq2Logo,²¹ using the Kullback–Leibler sequence logo type, Hobohm-1 clustering with a threshold of 0.63, and weight on prior set to 200.

qPCR Analysis

Total mRNA was extracted from FACS-sorted cells and isolated glomeruli using the NucleoSpin RNAII kit and NucleoSpin RNA Plus XS (both Macherey–Nagel), according to the manufacturer’s instructions, and was reverse transcribed with a random hexamer primer (Invitrogen) and RevertAid (Thermo Fisher). mRNA expression was quantified with QuantStudio 3 using SYBR green, as recently described.²² The exon-spanning primer pairs for murine cDNA are listed in Supplemental Table 2. 18S was used as an internal control to correct for small variations in RNA quality and cDNA synthesis. Amplicons of random samples for each primer pair were determined by automatic PCR sequencing to demonstrate the specificity of the PCR reaction (data not shown). Δ CT values were calculated using 18S as a housekeeping gene. $\Delta\Delta$ CT values were calculated as the difference between the glomerular and sorted cell Δ CT; relative expression (RE) is $2^{\Delta\Delta$ CT}. The RE of sorted cells are expressed as a percentage of the glomerular RE, which is calculated as follows: $100\% \times (\text{cell RE} / \text{glomerular RE} - 1)$.

Immunoblotting

Immunoblots were performed from isolated glomerular cells or glomeruli from one mouse per lane. Samples were lysed in T-PER (Thermo Scientific) containing 1 mM sodium fluoride, 1 mM sodium vanadate, 1 mM calyculin A, and

cOmplete Protease Inhibitor (Roche), and denatured in 5× SDS. Samples were separated on a 4%–12% Mini Protean TGX gel (Bio-Rad, Hercules, CA) in a Tris-glycine migration buffer (0.25 M Tris, 1.92 M glycine, 1% SDS, pH 8.3). Protein transfer was performed in transfer buffer (0.192 M glycine, 25 mM Tris base, 20% ethanol in double-distilled water) in a TransBlot Turbo System (Bio-Rad). After the transfer, all proteins were visualized by Ponceau S staining. Polyvinylidene difluoride membranes (Millipore) were blocked (5% nonfat milk) before incubation with primary antibodies diluted in SuperBlock blocking reagent (Thermo Scientific). We used the following primary antibodies: guinea pig anti-Nephrin (1:2000; Progen), rabbit anti-PDGFR- β (1:1000; Cell Signaling), rat anti-VE-Cadherin (1:1000; BD Biosciences), rabbit anti-THSD7A (1:1000; Atlas), rabbit anti-Synaptopodin (1:1000; Synaptic Systems), guinea pig anti-Neph1 (1:1000, gp2; made by T.B.H.), rabbit anti-Podocin (1:500; Sigma), rabbit anti- α -Actinin 4 (1:1000; Immunoglobe). Binding was detected by incubation with horseradish peroxidase-coupled secondary antibodies (1:10000, 5% nonfat milk). Protein expression was visualized using ECL SuperSignal (Thermo Scientific), according to the manufacturer's instructions, on an Amersham Imager 600 (GE Healthcare, Little Chalfont, United Kingdom). We analyzed Western blots using software from ImageJ.²³

Immunofluorescence

A kidney section (300 μ m thick) from an mT/mG mouse was fixed with 4% paraformaldehyde (PFA; EMSciences) for 6 hours, washed with PBS, and optically cleared for 24 hours using SCALEVIEW-A2 (FUJIFILM Wako Chemicals). FACS-sorted glomerular cells were seeded on collagen type IV-coated (Sigma), 35-mm culture dishes (Sarstedt) for 24 hours, and fixed with 4% PFA for 8 minutes at room temperature (RT). For immunofluorescence, nonspecific binding was blocked with 5% normal horse serum (Vector) in PBS with 0.05% Triton X-100 (Sigma) for 30 minutes at RT. Subsequently, cells were stained with Alexa Fluor 488-phalloidin (1:400; Molecular Probes), rhodamine-Wheat germ agglutinin (WGA; 1:400; Vector), and Hoechst (1:1000; Molecular Probes) for 30 minutes at RT and then coverslips were applied using Fluoromount (SouthernBiotech). Paraffin sections (3 μ m) were deparaffinized and rehydrated in water. Antigen retrieval was performed by cooking at a constant temperature of 98°C in DAKO (pH 9) or citrate (pH 6.1) buffer for 30 minutes. Frozen sections were dried and fixed with 4% PFA for 8 minutes at RT. Nonspecific binding in frozen and paraffin sections was blocked with 5% normal horse serum in 0.05% Triton X-100 for 30 minutes at RT. The following primary antibodies were incubated overnight in blocking buffer at 4°C: goat anti-THSD7A (1:200; Santa Cruz), Cy3 anti-mouse IgG, rat anti-ubiquitin carboxy-terminal hydrolase L1 (anti-UCH-L1; U104; 1:50),²⁴ guinea pig anti-Nephrin (1:200; Acris),

PE-Podoplanin (1:50; BioLegend), Alexa Fluor 647-CD73 (1:50; BioLegend), CD31 (PECAM1, 1:100; BD Pharmingen), guinea pig anti-Neph1 (gp2, 1:100), rabbit anti-Neph1 (1:100; made by T.B.H.), and guinea pig anti-Synaptopodin (1:200; Synaptic Systems). After washing in PBS, fluorochrome-labeled donkey secondary antibodies (all from Jackson ImmunoResearch Laboratories) and Hoechst (Molecular Probes) were applied, where appropriate, for 30 minutes at RT. After washing in PBS, sections were mounted in Fluoromount. Staining was visualized using an LSM800 with Airyscan and the ZenBlue software, or with an ELYRA PS.1 SIM microscope and the ZenBlack software (all Zeiss). To quantify foot process morphology, analysis of filtration slit density was performed, as previously described.^{25,26} To quantify protein intensity at the slit diaphragm (Nephrin and Neph1), or at the foot processes (Synaptopodin), the amount of white/black pixels was measured in a standardized region of interest at the GFB using FIJI.

Uniform Manifold Approximation and Projection Visualizations

To further visualize the separation of podocytes, mesangial cells, and endothelial cells, we performed Uniform Manifold Approximation and Projection (UMAP), a dimensionality reduction method (<https://joss.theoj.org/papers/10.21105/joss.00861>). This algorithm can be used to map high-dimensional data into two dimensions. Visualizations were created from cytometry channel data and gates were used as labels for coloring. Only living, single cells were included in analyses.

Statistical Analysis

Results were expressed as means \pm SEM or SD, and significance was set at $P < 0.05$. The means were compared using the two-tailed, nonparametric Mann-Whitney U test to enable robust conclusions on the effect's significance in case of departures from normality, which is associated with small sample sizes. We used biologic replicates, measured using different samples derived from distinct mice. More than two groups and points in time were analyzed using the two-way ANOVA with the Sidak multiple comparison.

RESULTS

Establishment of the Glomerular Cell Isolation Method

First, we established and validated fluorescently labeled antibodies directed against extracellular antigens that would prove suitable for labeling of individual glomerular cell types, after an extensive protocol of enzymatic digestion and mechanical disruption (Figure 1A). Immunofluorescence analysis of frozen murine kidney sections (Figure 1B) demonstrated a specific labeling of podocytes with antibodies directed against Podoplanin²⁷; of endothelial cells with

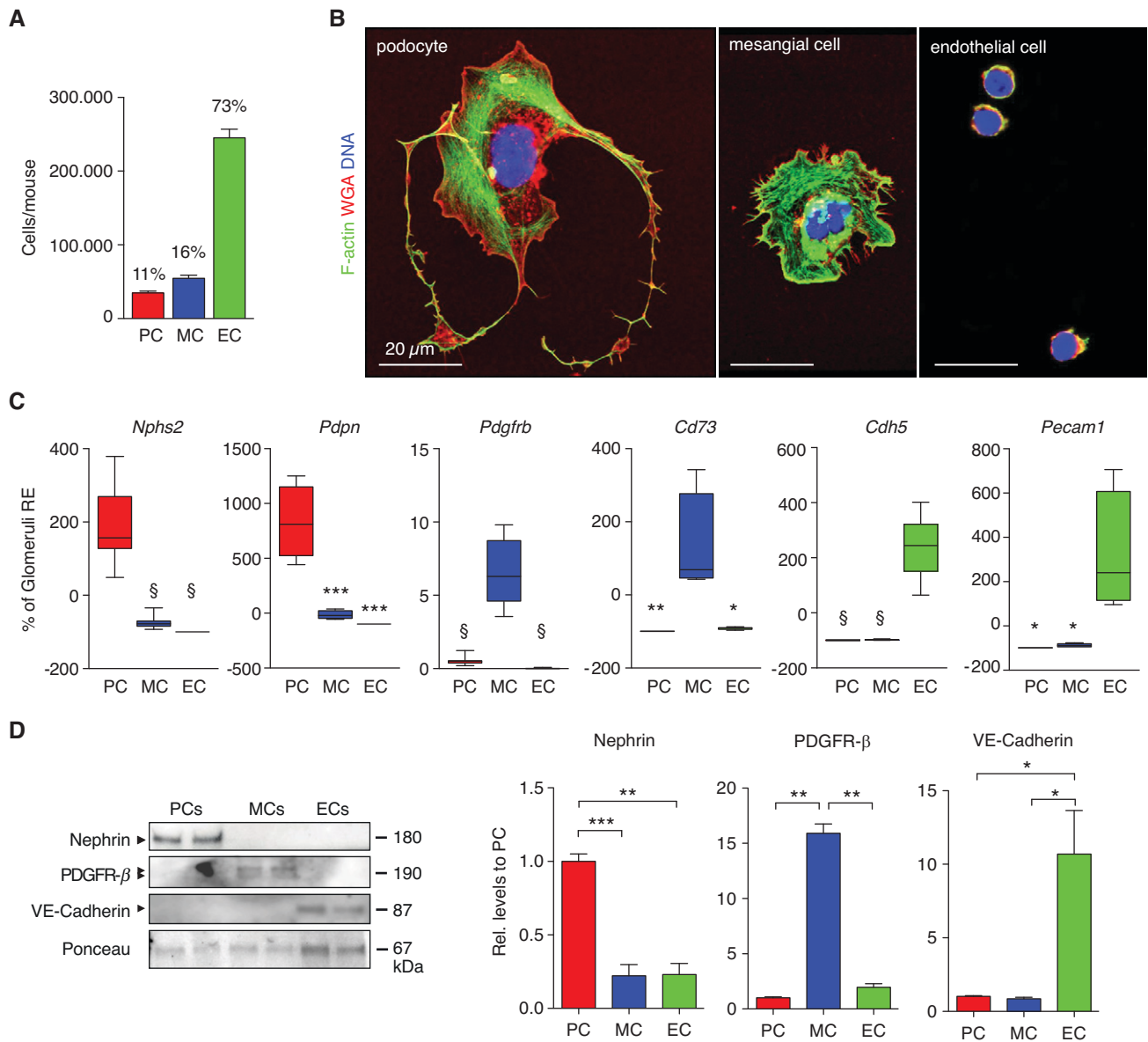


Figure 2. FACS-sorted cells are pure and in sufficient amounts to perform protein-biochemical investigations. (A) Graph depicting the mean cell harvest per mouse in absolute numbers (mean±SEM, $n=149$ mice, pooled data from 20 independent experiments). Percentages indicate the relative number of each cell population from the total amount of isolated cells. (B) Representative confocal images of FACS-sorted podocytes (PC), mesangial cells (MC), and glomerular endothelial cells (EC) plated on collagen IV. F-actin (green) demarcates the actin cytoskeleton, WGA (red) the glycocalyx; DNA was stained with Hoechst (blue). (C) Real-time qPCR analysis exhibiting the expression of cell-specific transcripts. mRNA was isolated from FACS-sorted podocytes, mesangial cells, and endothelial cells, and from isolated glomeruli derived from the same individual. Δ CT values were calculated using 18S as a house-keeping gene. $\Delta\Delta$ CT values were calculated as the difference between the glomerular and FACS-sorted cell type Δ CT. Displayed is the RE of FACS-sorted cell types in percent of the glomeruli. Note the significant enrichment of cell-specific transcripts in the FACS-sorted cell types compared with the glomerulus. Mean±SEM, $n=8$ (*Nphs2*, *Pdgfrb*, *Cdh5*), $n=4$ (*Pdpn*, *Cd73*, *Pecam1*), pooled data from three independent experiments, one-way ANOVA and Bonferroni's multiple comparisons test. (D) Cell number-adapted lysates of FACS-sorted cells from individual mice were separated by SDS-PAGE and analyzed by immunoblot for the expression of cell-specific markers. Graphs exhibit densitometric quantification, values were normalized to Ponceau S staining of the same membrane, and are expressed as mean±SEM RE levels to podocytes. $n>4$ pooled data from two to five independent blots, with $n=2$ mice per blot. * $P<0.05$, ** $P<0.01$, *** $P<0.005$, § $P<0.0001$. Rel., relative.

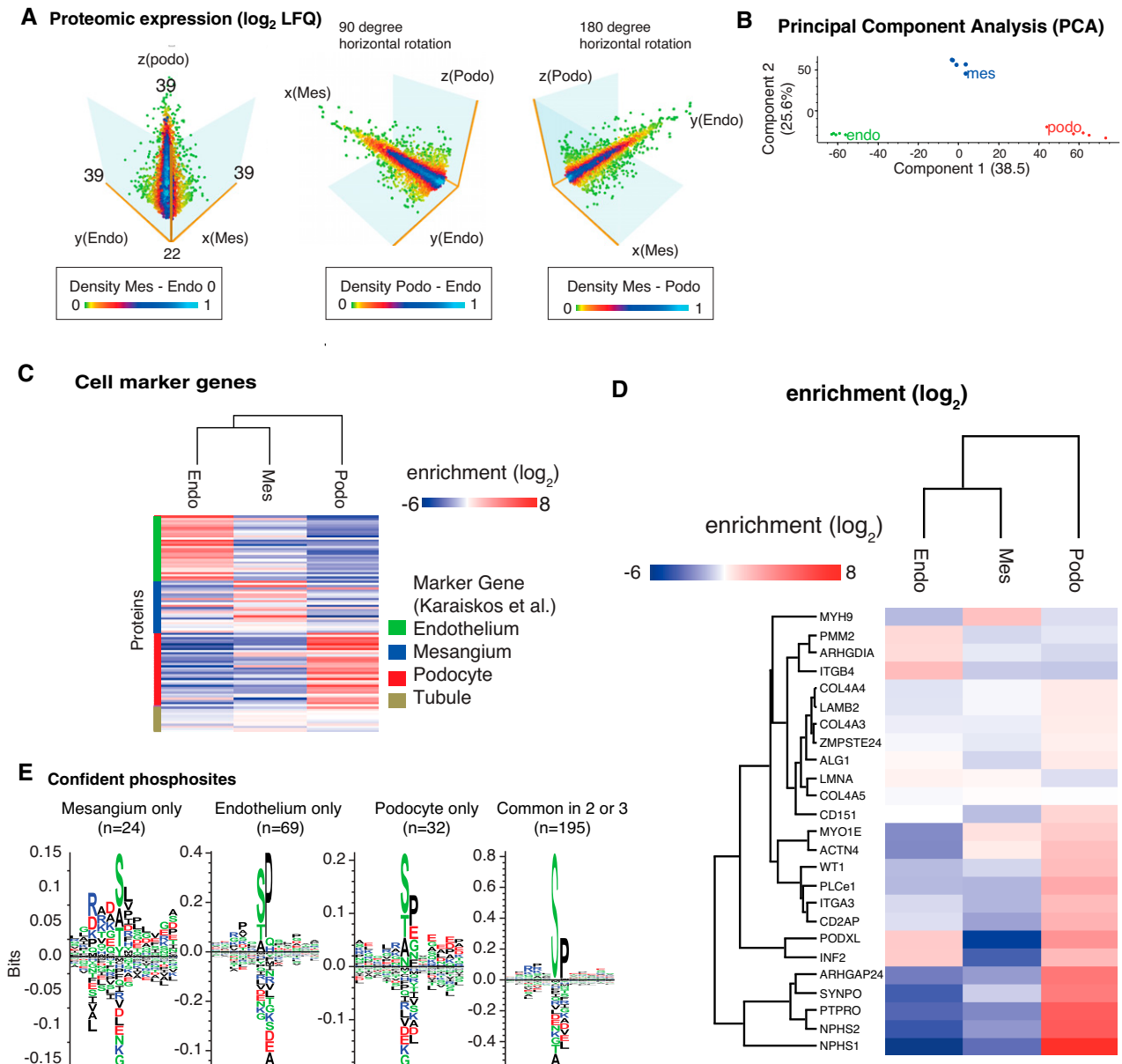


Figure 3. Tripartite cell type isolation and proteomic analysis from mT/mG mice shows cell specific profiles. (A) Three-dimensional view of the tripartite cell proteomes containing 6600 proteins and quantification of 4400 proteins. (B) PCA showing clear separations of endothelial cell (endo), mesangial cell (mes), and podocyte (podo) proteomes. (C) Cell marker gene products derived from Karaiskos et al.,³⁰ and their proteomic expression from mesangial cells, podocytes, and endothelial cells. (D) Expression of annotated proteinuria genes. (E) Position-weighted matrices of phosphorylation motifs in podocytes, mesangial cells, and endothelial cells. Letter height represents frequency around the central (serine) phosphorylation site. (F) Visualization of glomerular cell crosstalk systems. Protein-protein interaction networks were generated in STRING using high-confidence interactions (database and experimental evidence, confidence >0.9).

antibodies directed against CD31²⁸; and of mesangial cells with antibodies directed against ecto-5'-nucleotidase/CD73, an enzyme responsible for adenosine formation from AMP expressed in mesangial cells.³⁰ Two protocols were used for the initial comparison of glomerular cell types isolated on the basis of cell type reporter expression (Figure 1C) with those isolated from reporter-free mice (Figure 1D). As a

reference for reporter-free glomerular live cell isolation, mT/mG mice were used, in which podocytes are already marked by the intrinsic expression of eGFP and all of the other murine cells by the intrinsic expression of tdTomato. To differentiate glomerular endothelial and mesangial cells, the remaining tdTomato-positive glomerular cells were separated into tdTomato⁺/CD31⁺/eGFP⁻/CD73⁻ endothelial

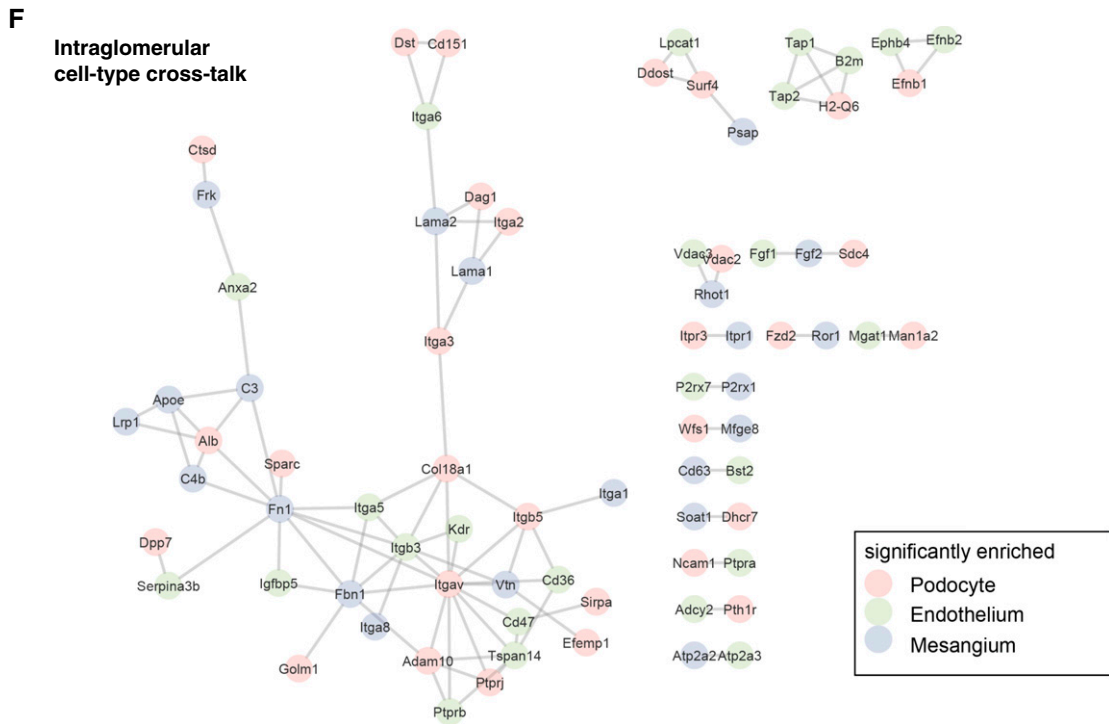


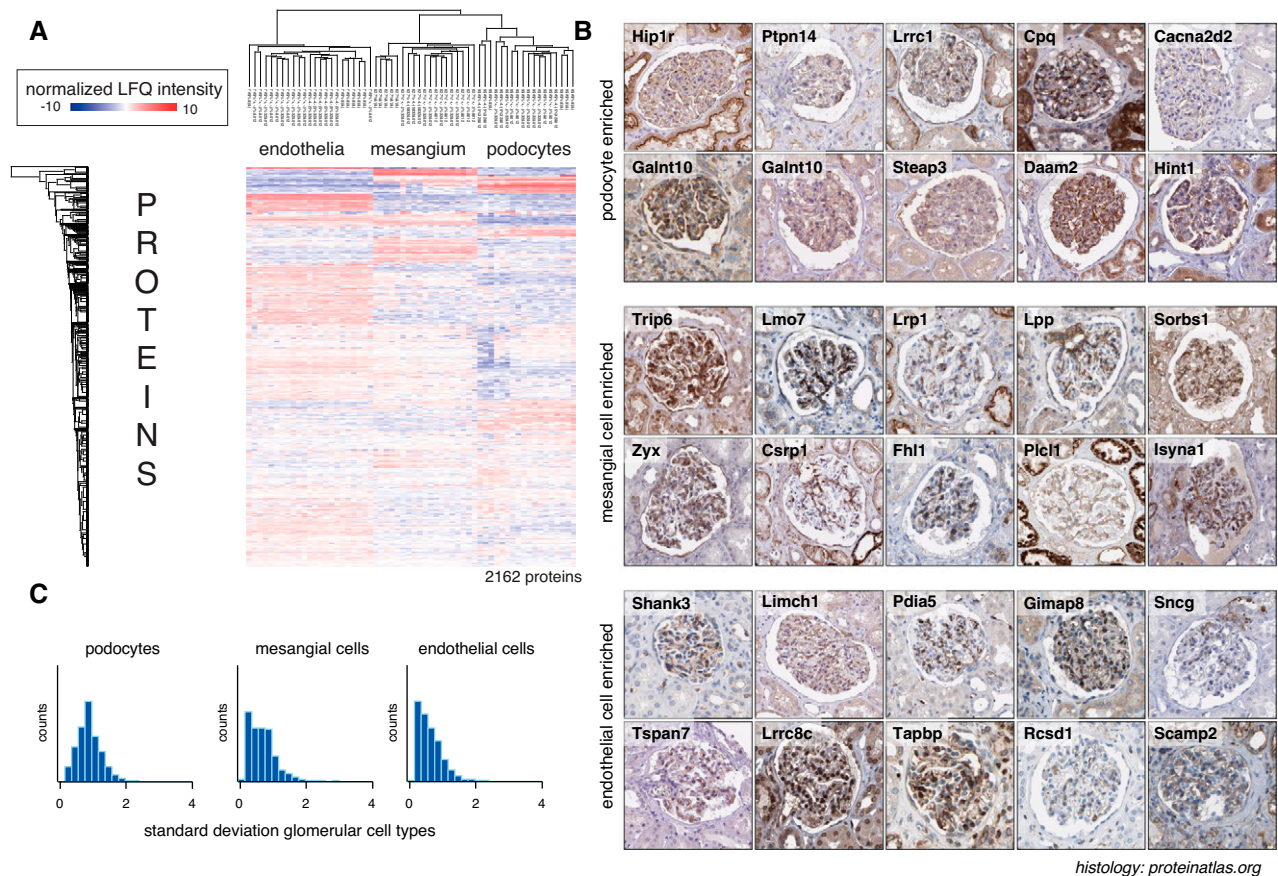
Figure 3. (Continued)

cells and into tdTomato⁺/CD73⁺/eGFP⁻/CD31⁻ mesangial cells (Figure 1C). This gating strategy was then modified for the use in wild-type mice, using a combination of fluorophore-conjugated anti-Podoplanin, anti-CD31, and anti-CD73 antibodies, resulting in three distinct glomerular cell populations: Podoplanin⁺/CD31⁻/CD73⁻ podocytes, CD73⁺/Podoplanin⁻/CD31⁻ mesangial cells, CD31⁺/CD73⁻/Podoplanin⁻ endothelial cells, and a population of nonlabeled cells. These nonlabeled cells most likely represented contaminating tubular cells, because they expressed higher levels of the tubular transcripts *Slc12a1* (encoding for Nkcc2) and *Aqp4* (encoding for Aquaporin 4) relative to isolated glomeruli (Figure 1D, Supplemental Figure 3). UMAP analysis demonstrated a clear separation of the three glomerular cell types in wild-type mice (Supplemental Figure 2A).

Isolated Glomerular Cells Are Pure

To evaluate purity and to assess further usability of the isolated cell populations, we performed several experiments. First, we established the typical cellular yield obtained by this isolation technique (Figure 2A). In total, 11% (mean ± SEM, 35,600 ± 1,722) of glomerular cells isolated were podocytes, 16% (55,300 ± 3,600) were mesangial cells, and 73% (245,000 ± 11,000) were endothelial cells. These percentages and absolute cell numbers were stable across species and sex (Supplemental Figure 4, A and B). In old mice (61–69 weeks old), the efficiency of podocyte, mesangial cell, and

endothelial cell isolation decreased significantly, when compared with younger (11–14 weeks old) mice (Supplemental Figure 4C). The percentages of isolated cell types were not different between wild-type and mT/mG mice, although mT/mG mice resulted in higher absolute number of podocytes, mesangial cells, and endothelial cells than wild-type mice (Supplemental Figure 5). We then plated the FACS-sorted cells onto collagen type IV-coated culture plates to assess the morphologic characteristics of the different cell populations by visualizing the actin cytoskeleton with F-actin and the glycocalyx by staining with WGA (Figure 2B). FACS-sorted podocytes were the largest cells and exhibited an elaborate phenotype with long arborizations and a cortical actin ring, as expected.¹ FACS-sorted mesangial cells were generally smaller than podocytes, with a coarse actin cytoskeleton and smaller membrane arborizations. FACS-sorted endothelial cells were the smallest of all cell types, round in morphology, with a prominent WGA-positive glycocalyx. We then analyzed the RE of cell-specific transcripts in the FACS-sorted cell population relative to the transcript levels present in whole glomeruli from the same mouse (Figure 2C). The expression of the podocyte-specific transcripts *Nphs2* (encoding for Podocin) and *Pdpn* (encoding for Podoplanin) was enriched in podocytes, compared with glomeruli, and significantly lower in mesangial and endothelial cells. The expression of the mesangial cell-specific transcripts *Pdgfrb* (encoding for PDGFR-β) and *Cd73* (encoding for CD73) was enriched in mesangial cells compared with glomeruli, and significantly lower in podocytes and



histology: proteinatlas.org

Figure 4. TimMEP identifies new podocyte-, mesangial cell-, and glomerular endothelial cell-enriched proteins in reporter-free single mice. (A) Heat map showing Euclidean distance clustering of single-mouse, single-shot proteomics results from male C57BL/6, female C57BL/6, female BALB/c, and female mT/mG mice. Each column represents a cell type proteome from a single mouse. (B) To identify new proteins enriched in podocytes, mesangial cells, and glomerular endothelial cells, glomerular cell type proteome lists of individual mice were compared. For the comparisons, we defined (1) a *t*-test difference cutoff of greater than two between podocytes and nonpodocytes; (2) a negative search result in PubMed (<https://www.ncbi.nlm.nih.gov/pubmed>); and (3) a validated podocyte expression pattern in the Human Protein Atlas (<https://www.proteinatlas.org/search>), from which the histologic micrographs are taken. (C) SD distributions of proteins in each cell type reveal low variance of expression in endothelial cells.

endothelial cells. The expression of the endothelial cell-specific transcripts *Cdh5* (encoding for VE-Cadherin) and *Pecam1* (encoding for CD31) was enriched in endothelial cells, compared with glomeruli, and significantly lower in podocytes and mesangial cells. To control for parietal epithelial cell and tubular cell contamination of our glomerular cell type preparations, we first ensured that our glomerular isolation resulted in a preferential enrichment of decapsulated glomeruli, without appending tubuli, by phase-contrast microscopy. Second, potential contamination was excluded by qPCR for the parietal cell-specific transcripts *Lad1* (encodes for Ladinin) and *Scin* (encodes for Scinderin),²⁷ and for transcripts specific to tubular cells, *Aqp4* (encodes for Aquaporin 4) and *Slc12a3* (encodes for the sodium chloride channel NCC) (Supplemental Figure 6A). Additionally, we controlled for the absence of the parietal cell-specific protein Claudin1 in the podocyte cell population by Western blot

(Supplemental Figure 6B). We next proceeded to evaluate the expression of cell-specific markers by immunoblot (Figure 2D). Cell number-adapted lysates of FACS-sorted cells from individual mice were separated by SDS-PAGE and blotted for cell-specific markers. Corroborating the qPCR results, only podocytes expressed the slit membrane protein Nephryn, only mesangial cells expressed PDGFR- β , and only endothelial cells expressed VE-Cadherin. Taken together, these analyses demonstrate the successful isolation of podocytes, glomerular endothelial cells, and mesangial cells from individual mice in sufficient amounts to perform protein-biochemical investigations.

Proteomic Analyses Unravel Glomerular Cell-Specific Molecular Reference Profiles and Signaling Networks

Using gating strategy 1 (applied to transgenic mice; Figure 1C), we first generated a proteomics profile from mT/mG

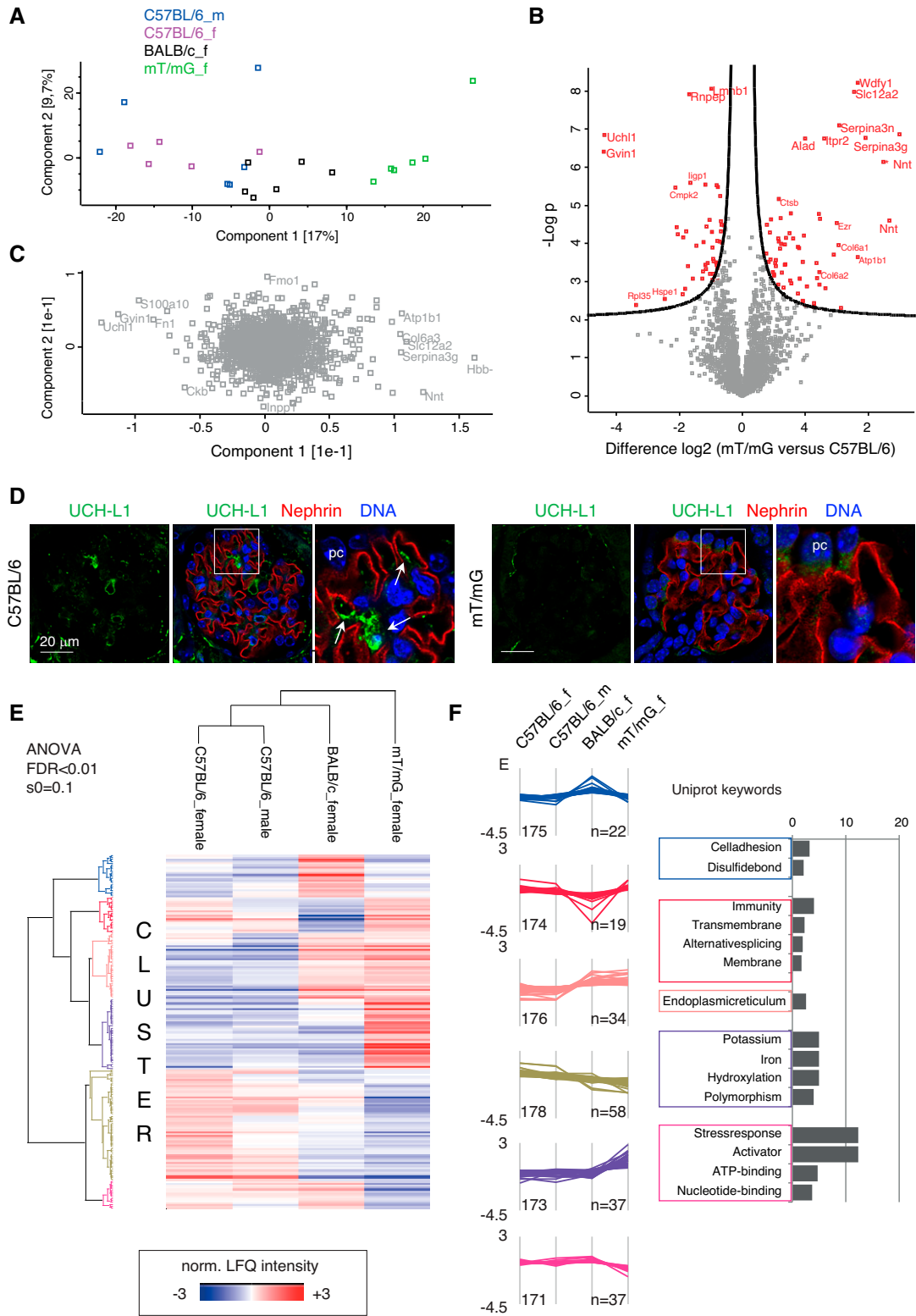


Figure 5. TiMEP unravels strain-dependent differences in endothelial proteomes. (A) Analysis of glomerular endothelial proteome from wild-type and mT/mG mice. (B) PCA of proteins. (C) Volcano plot showing differences between proteins highly expressed in mT/mG (right side of the plot) and C57BL/6 (left side of the plot) endothelial cells. (D) Representative confocal images of UCH-L1 (green) expression in a C57BL/6 and in a mT/mG glomerulus. Nephtrin (red) was used to demarcate the GFB (DNA, blue). Arrows point toward endothelial UCH-L1 expression. (E) Hierarchic clustering of mean normalized protein expression (log₂ LFQ) from four different mouse strains. (F) Clustering combined with Gene Ontology term enrichment reveals stress response proteins in endothelia from mT/mG mice. f, female mice; m, male mice; norm., normalized; pc, podocyte.

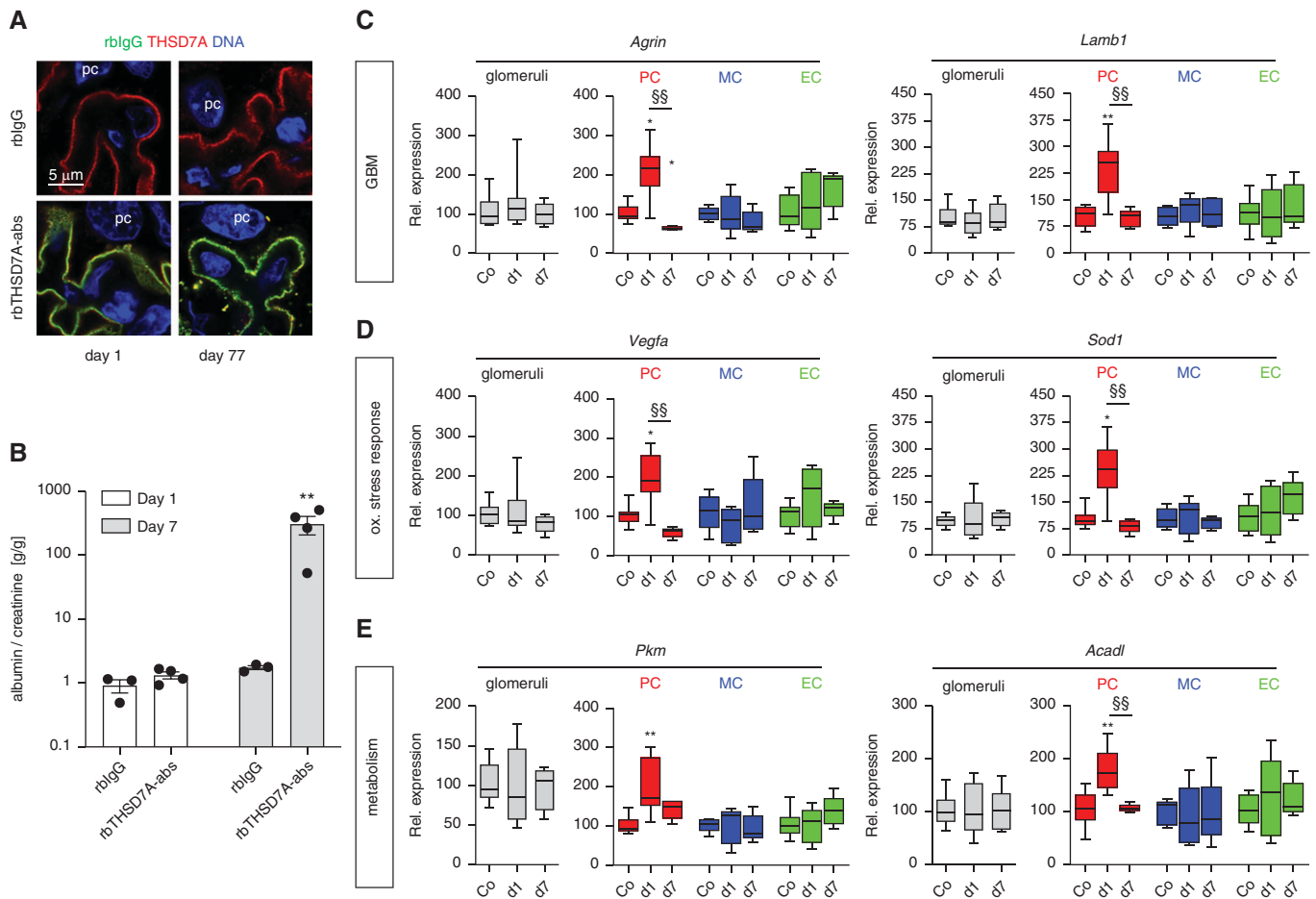


Figure 6. Glomerular cell-specific analyses in the experimental model of THSD7A MN unravels acute transcript regulation. Experimental THSD7A MN was induced in male BALB/c mice by injection of podocyte-targeting rbTHSD7A-abs or nonspecific control rblgG. Analyses were performed on day 1 (d1) and 7 (d7) after antibody injection. (A) Confocal analyses demonstrating rblgG (green) deposition in a linear (day 1) and a more granular (day 7) pattern in rbTHSD7A-abs-injected mice. Yellow color exhibits colocalization of the injected rabbit antibodies with the antigen THSD7A (red), as a sign for successful induction of MN (DNA, blue). (B) Urinary albumin-creatinine ratio on days 1 and 7. $**P < 0.01$ to day 7 rblgG, Mann-Whitney *U* test. (C–E) qPCR analyses were performed in isolated glomeruli (as the conventional method, graphs with gray bars) and in FACS-sorted (right graphs) podocytes (PC, red bars), glomerular endothelial cells (EC, green bars), and mesangial cells (MC, blue bars) of the same mouse. Graphs exhibit RE in comparison with rblgG-treated mice (control [Co], striped bar) of the respective time point (day 1 rblgG to day 1 rbTHSD7A-abs, and day 7 rblgG to day 7 rbTHSD7A-abs) after normalization to 18S as a housekeeping gene. The control bars exhibit the pooled day 1 and day 7 rblgG values for simplification. $*P < 0.05$, $**P < 0.01$ to control, $^{\$}P < 0.01$ to day 7 rblgG, Mann-Whitney *U* test. Ox, oxidative; Rel., relative.

mice using cell pellets consisting of 1 million cells. The dataset quantified 4753 proteins from these cells out of >6600 proteins, allowing for a three-dimensional view of protein quantification (Figure 3A). Principal component analysis (PCA) and hierarchic clustering revealed a strong separation of the cell types (Figure 3, B and C). Using *t*-test analyses, we defined lists of podocyte-, endothelial cell-, and mesangial cell-specific proteins that were significantly enriched over the other cell types. These can be found in Supplemental Table 3 for mT/mG mice, and in Supplemental Table 4 for wild-type mice across sex, species, and age. On the basis of statistical enrichment followed by

statistical testing with correction for multiple testing, we defined 1150 endothelial cell-, 366 mesangial cell-, and 718 podocyte-specific proteins (FDR < 0.01, at least two-fold \log_2 enrichment, $P < 0.05$). To confirm the purity of the preparation, we mapped these cell type-specific proteins against previously defined cell marker genes obtained by single-cell RNA sequencing.³⁰ The data were largely consistent with the protein expression defined on these clusters; however, some genes were differently expressed (Figure 3C). We mapped known proteinuria genes³¹ against the enrichment and found the majority of proteinuria genes in podocytes (Figure 3D). We also mapped 365 high-confidence

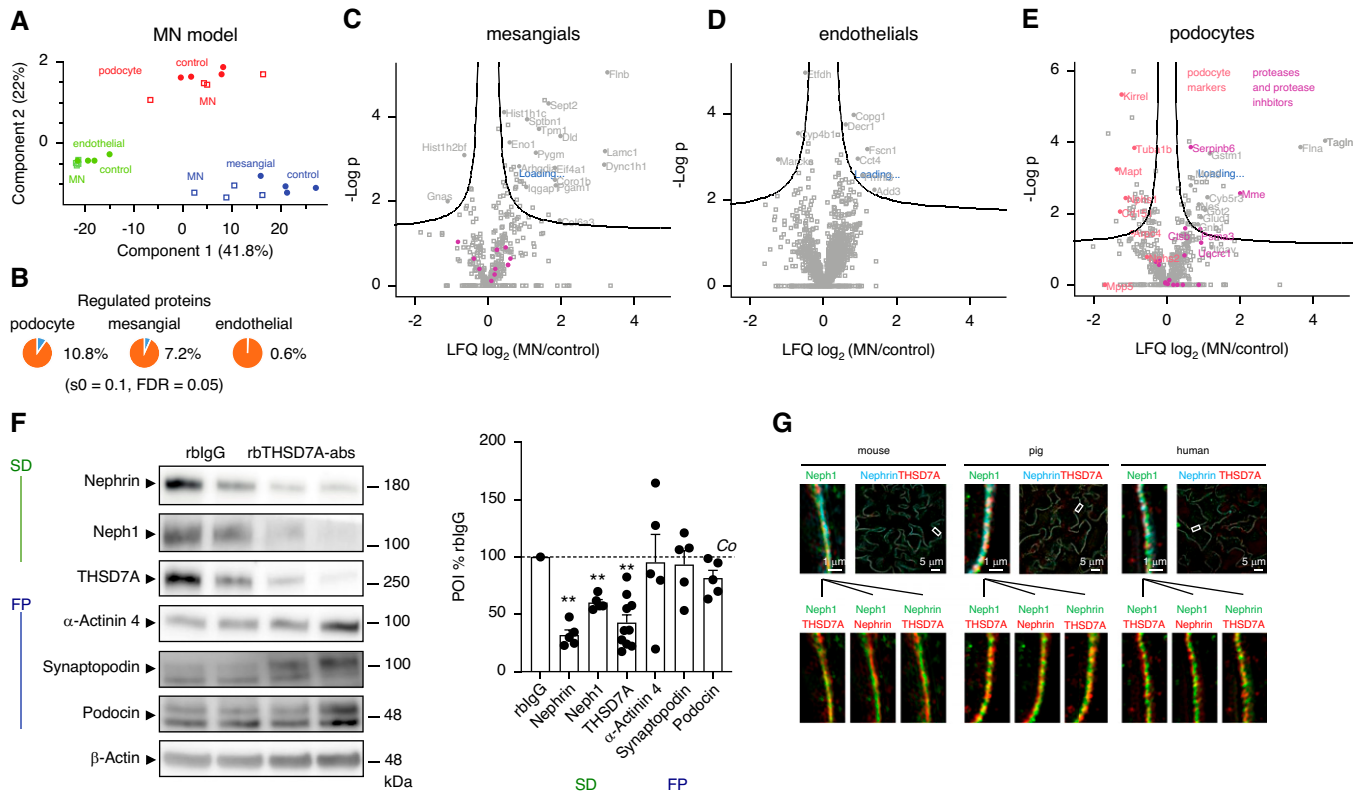


Figure 7. TimMEP dissects reduced slit diaphragm protein levels in THSD7A-associated MN. Experimental THSD7A-associated MN was induced in male BALB/c mice by injection of podocyte-targeting rbTHSD7A-abs or unspecific control rblgG. (A) Glomerular cell types were isolated by timMEP on day 7 after antibody injection and bulk proteomics were performed. PCA showing clear separation of endothelial cell, mesangial cell, and podocyte proteomes from control- (filled circles) and THSD7A-MN–derived (open squares) cell types. (B) Percentages of significantly regulated proteins are indicated in timMEP-isolated glomerular cell types. (C–E) Volcano plots showing differences between proteins highly expressed in control (right side of the plot) and MN (left side of the plot) glomerular cell types. Proteins beyond the lines are of significance (FDR<0.05, s0=0.1 [fudge factor]). (F) Western blot from isolated glomeruli of experimental mice on day 12 for the slit diaphragm (SD) proteins Neph1 and Nephrin, for THSD7A, and for the foot process (FP) proteins α-Actinin 4, Synaptopodin, and Podocin. β-Actin of the same membrane was used as a loading control. Graph exhibits relative protein-of-interest (POI) abundance in comparison with rblgG-treated mice (control [Co], striped line and white bar) of the respective POI (after normalization to β-actin of the same membrane). n≥5, pooled data from two independent experiments. **P<0.01 to control, Mann–Whitney U test. (G) Super-resolution structured illumination microscopy micrographs of triple immunostaining for Neph1 (green), THSD7A (red), and Nephrin (cyan) in a healthy mouse, pig, and human glomerulus. Note the close localization of THSD7A to Neph1 and Nephrin in all species (arrows).

phosphorylation sites in the proteomics data; among these, protein phosphorylation of Kirrel (Neph1) and Synaptopodin were only detected in podocytes. Motif analysis of the phosphorylation sites uniquely localized to cell types revealed higher distinct sequence logos in each cell type. For instance, phosphorylation sites unique to podocytes had more acidic (D/E) amino acid residues on the carboxy-terminal of the phosphorylation site (Figure 3E). This phosphorylation motif is increasingly found in proteins at the filtration barrier, for instance, a phosphorylation site of Neph1 at S584 (sequence window REPLTMHS*DREDDT) that was previously described.^{32,33} We also used *in silico* protein-protein interaction analyses and data resources to map potential intercellular protein crosstalk and communication. The analysis revealed contribution of different cell types to

the extracellular matrix, and a distinct signaling system. One example here was the ephrin-ephrin receptor system, with *Epha2* and *Efnb1* expressed in podocytes, and *Epha2*, *Ephb4*, and *Efnb2* expressed in endothelial cells (Figure 3F). Furthermore, we constructed cell type-enriched signal transduction networks using a protein-protein interaction network and the NetBox algorithm (Supplemental Figure 7).³⁴ Both analyses support the view of podocytes being active in proteostasis.

Proteomic Analyses Unravel New Glomerular Cell-Specific Proteins

We applied the newly generated method to cell populations from a single mouse, comparing male and female mice in a

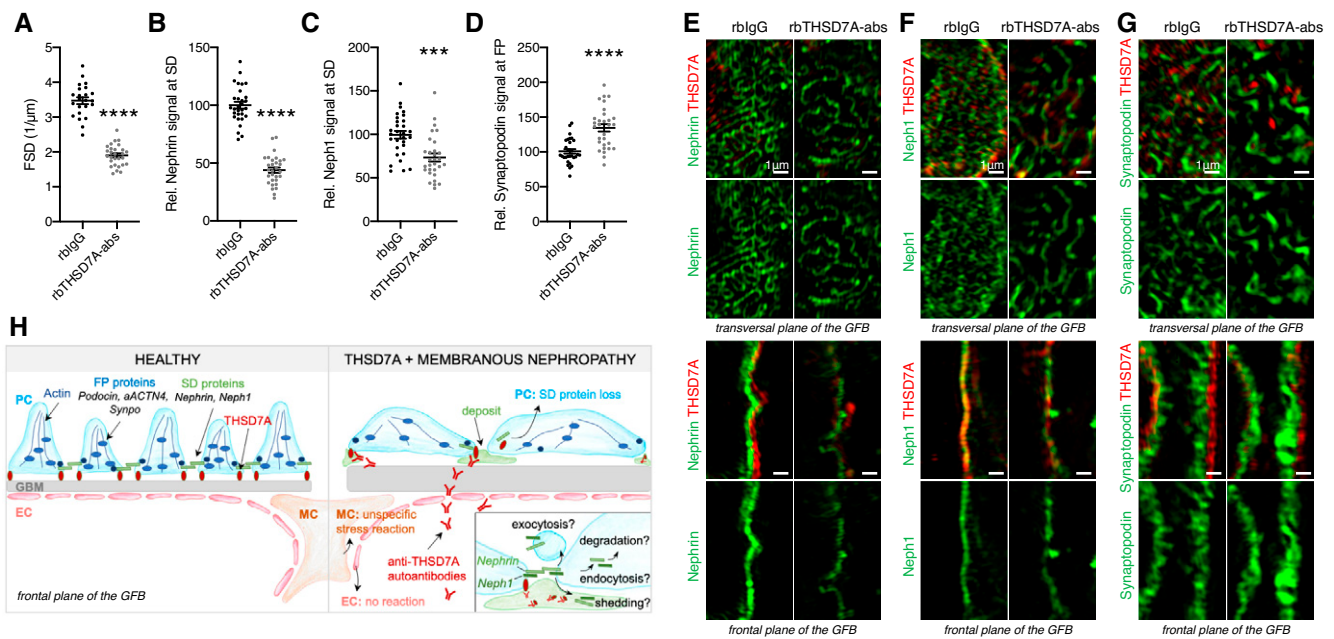


Figure 8. TimMEP unravels selective loss of slit diaphragm proteins as a pathogenic factor in THSD7A-MN. Experimental THSD7A-associated MN was induced in male BALB/c mice by injection of podocyte-targeting rbTHSD7A-abs or nonspecific control rblgG. Glomeruli were analyzed on day 7 by super-resolution structured illumination microscopy (SR-SIM). (A) Quantification of filtration slit density (FSD) by podocyte exact morphology measurement procedure demonstrates extensive foot process effacement of rbTHSD7A-abs-injected mice. $n \geq 23$ regions of interest. (B–D) Quantification of Neph1, Neph1, and Synaptopodin abundance at the frontal plane of the GFB using FIJI. $n = 30$ regions of interest. (E–G) SR-SIM high-resolution micrographs of double immunostainings for THSD7A (red) with Neph1, or Neph1, or Synaptopodin (all green) using guinea pig or goat secondary antibodies to prevent the detection of the bound rbTHSD7A-abs. (H) Scheme of proposed pathogenic process in THSD7A-associated MN: THSD7A-autoantibodies traverse the GBM and bind to THSD7A localized at the slit diaphragm (SD) in close proximity to Neph1 and Neph1. Binding of autoantibodies induces the selective removal/degradation of the SD proteins Neph1 and Neph1, whereas most foot process (FP) proteins are not lost. *** $P < 0.001$, **** $P < 0.0001$, Mann–Whitney U test. Rel., relative. EC, endothelial cell; MC, mesangial cell; PC, podocyte.

C57BL/6 background, BALB/c females, and—as a control—mT/mG female mice that were subjected to the original protocol. To test the generalizability of the method from FACS-sorted cells, and to test the purity of the preparations, we generated proteomics profiles from three different cell types by single-shot proteomics from the cell fractions from a single mouse. An overview of the dataset revealed very clear separations of three distinct cell types, suggesting the identity of these cells is in fact different (Figure 4A). We again determined which proteins were specifically enriched in the different glomerular cell types, and found novel cell type markers by comparing our results with the Human Protein Atlas (Figure 4B, Supplemental Figures 8–10). To the best of our knowledge, we identified 12 new podocyte-enriched proteins, 16 new mesangial cell-enriched proteins, and 22 new glomerular endothelial cell-specific proteins on the basis of strict criteria (see *Methods*). In addition, the clear presence of mesangial cells in this protocol is remarkable, because the molecular protein composition of these cells has not yet been described. In confirmation of our proteomic data, qPCR and immunofluorescence validation experiments found that expression of integrin $\beta 3$ and its ligand,

fibronectin, was restricted to glomerular endothelial cells (Supplemental Figure 11). We next analyzed which protein classes had high variance between the four mouse strains (Figure 4C). Podocyte proteins had the largest variance (highest SD) between the proteins among all three cell types, which may be due to the disruptive isolation method used in this protocol. Through the high sensitivity of the assay, we also observed that the mesangial cell populations had minimal contamination by podocytes with the initial gating strategy (Supplemental Figures 1A, 2B and 2C), which we estimated to be around 2%, as compared with the mT/mG-derived mesangial cells. In reaction to this observation, we improved the gating strategy for all other investigations (Figure 1D, Supplemental Figure 1B). The UMAP analysis demonstrates the removal of the contaminating podocytes in the mesangial cell population by using these adjustments (Supplemental Figure 2, B and C).

Glomerular Endothelial Cells Exhibit Proteomic Differences between Mouse Strains

We performed deeper proteomic bioinformatic analysis of the population with the highest homogeneity: the

glomerular endothelial cells. PCA of the glomerular endothelial cell proteomes derived from four different mouse strains (female C57BL/6, male C57BL/6, BALB/c, and mT/mG mice) was performed. Data revealed a separation by strain, with male and female C57BL/6 mice being similar, and mT/mG mice being the most different from the others (Figure 5A). The proteins with the most significant differences in this dataset were UCH-L1 (a major neuronal deubiquitinase of the degradative ubiquitin proteasome system³⁵) and Gvin1 (GTPase, very large IFN inducible 1, which contributes to the cellular response to both type I and type II IFNs³⁶) (Figure 5B), suggesting that reporter-dependent artifacts in the proteome must be considered when using fluorescent reporter systems. Volcano plot analysis revealed a >16-fold difference of these proteins in the mT/mG endothelial cells as compared with C57BL/6 cells (Figure 5C). In fact, the differences in endothelial expression of UCH-L1 could be confirmed using confocal microscopy of C57BL/6 and mT/mG glomeruli (Figure 5D). We also performed unbiased analysis of differentially expressed proteins within the four strains (Figure 5E), using an ANOVA with FDR<0.01. Clustering analysis revealed there was a significant alteration in stress-response proteins in mT/mG mice, compared with the other strains, and an alteration of immunity and cell adhesion proteins in BALB/c females, compared with C57BL/6 females (Figure 5F).

Glomerular Cell Types Resolve Specific Reactions in Anti-THSD7A MN

We then determined whether our glomerular cell isolation technique was also suitable for the separation of glomerular cell types in the setting of glomerular damage and inflammation. For this purpose, we induced defined glomerular injury through injection of rabbit antibodies that specifically target the podocyte foot process antigen THSD7A.³⁷ This immunologic model of THSD7A-associated MN⁹ leads to selective podocyte injury with massive proteinuria within days, and mimics the pathophysiology of human THSD7A-associated MN.³⁸ CD45, as an additional marker, was added to the FACS protocol to remove potential leukocytes adhering to the endothelium of the perfused glomeruli in inflammation (Supplemental Figure 12). A UMAP demonstrated separation of CD45-positive cells from all other cells (Supplemental Figure 2D). No significant infiltration and adherence of leukocytes could be detected in this GN model (Supplemental Figure 13, A and B). Further, the cell-sort marker expression of Podoplanin, CD31, and CD73 was mostly preserved in day 7 glomeruli of highly proteinuric mice (Supplemental Figure 13C), a predisposition for the successful isolation of podocytes, glomerular endothelial cells, and mesangial cells. Glomerular cell types were analyzed for a stress response by qPCR on day 1 after antibody binding, before development of proteinuria, and on day 7, when severe podocyte injury and nephrotic syndrome were

established (Figure 6, A and B). The qPCR analyses demonstrated significant changes in podocyte gene transcription as early as day 1 for (1) genes involved in GBM remodeling (*Agrin*, a major proteoglycan of the GBM,³⁹ laminin chain β 1 [*Lamb1*], laminin chain of the immature/injury remodeled GBM⁴⁰; Figure 6C); (2) for genes involved in an oxidative stress response (vascular endothelial growth factor a [*Vegfa*], involved in angiogenesis and maintenance of the glomerular endothelium⁴¹, and *Sod1*, detoxifies reactive oxygen radicals⁴²; Figure 6D); and (3) for genes of key metabolic enzymes (pyruvate kinase [*Pkm*], key enzyme of glycolysis⁴³; acyl-CoA dehydrogenase, long chain [*Acadl*], a key enzyme in β -oxidation of fatty acids⁴⁴; Figure 6E) in mice exposed to rabbit THSD7A antibodies (rbTHSD7A-abs) in comparison with control rabbit IgG (rbIgG). Importantly, these changes in gene transcription were not visible upon analyses of isolated bulk glomeruli on day 1 and day 7, demonstrating the enhanced sensitivity obtained when performing glomerular cell type-based analyses. Mesangial and glomerular endothelial cells showed no major alterations in the evaluated transcription levels on day 1 or 7. Strikingly, the observed gene induction on day 1 was no longer apparent on day 7 in rbTHSD7A-abs-injected mice. On day 7, all analyzed transcript levels were repressed in rbTHSD7A-MN podocytes in comparison to day 1, and were only slightly elevated in comparison to day 7 rbIgG-injected control mice (data not shown), suggesting a specific and acute reaction to rbTHSD7A-abs on day 1.

We then analyzed the proteome of all three cell types at day 7 of the rbTHSD7A-MN model. At this time point, mice were proteinuric and transcriptional differences were minimal between rbIgG and rbTHSD7A-MN podocytes. PCA analyses demonstrated a successful separation of the three glomerular cell types in control and rbTHSD7A-injected mice (Figure 7A). In podocytes, 10.8% of all identified proteins were significantly regulated, with 7.2% in mesangial cells and only 0.6% in glomerular endothelial cells (Figure 7B). Volcano plot analyses also demonstrated regulated proteins in the mesangial cells (Figure 7C), whereas endothelial cells (Figure 7D) did not demonstrate a significant reaction to the podocyte-bound rbTHSD7A-abs. In contrast, podocytes depicted a differential loss of the slit diaphragm proteins Neph1 (Kirrel) and, to a lesser extent, Nephin, whereas foot process proteins remained unchanged in rbTHSD7A-abs-treated mice (Figure 7E). Western blot validation in isolated glomeruli confirmed the specific and significant loss of THSD7A, Nephin, and Neph1, whereas the foot process proteins α -Actinin 4 and Synaptopodin remained unchanged in rbTHSD7A-abs-treated mice in comparison with rbIgG control mice. Podocin exhibited a slight, but not significant, reduction in abundance (Figure 7F). Because THSD7A was described to localize beneath Nephin at foot process subdomains, in close proximity to the slit diaphragm,³⁷ we asked whether THSD7A interacted with Neph1, located basally from Nephin at the slit

diaphragm.⁴⁵ Super-resolution structured illumination microscopy showed THSD7A was in close proximity to Neph1 and Neph1r at the human, pig, and murine healthy GFB (Figure 7G, Supplemental Figure 14A). However, we were not able to show a direct interaction of the three proteins in unchallenged conditions (Supplemental Figure 14B). In the setting of experimental murine THSD7A-MN, the differential loss of Neph1r and Neph1 protein was not solely attributable to a decrease of slit diaphragm density upon rbTHSD7A-*abs* binding to THSD7A (Figure 8A). Notably, signal intensity of the slit diaphragm marker was disrupted and decreased in Neph1r and Neph1 immunostainings, whereas the signal for Synaptopodin was preserved, and even enhanced, at the GFB (Figure 8, B–F, Supplemental Figure 15). Together, these findings suggest the decreased Neph1r and Neph1 protein levels in rbTHSD7A-MN originate from a local loss/degradation of both proteins from the slit diaphragm upon rbTHSD7A autoantibody binding, possibly representing one pathogenic mechanism in THSD7A-associated MN (summarized in Figure 8H).

DISCUSSION

The complicated architecture of the kidney hampers the direct access of susceptible cell types in kidney diseases for further functional analysis. Here, we established a generalizable method for generating molecular reference profiles of all kidney glomerular cell types in health and disease. This FACS-based method, which we propose to name timMEP, results in the precise isolation of the three glomerular cell types, as extensively validated by qPCR, proteomic, immunoblot, and immunofluorescence analyses. timMEP does not require the extensive breeding of transgenic reporter mouse models for subsequent isolation of glomerular cell types, which saves time, animals, and animal housing costs. Therefore, timMEP is theoretically amenable to any existing mouse model and will facilitate and sharpen investigations of glomerular cell biology in a cell type-specific, cost-effective, and timely manner. timMEP not only allows the quantification of transcript and protein levels per bulk transcriptomic, proteomic, and Western blot approaches, but also allows for the biologically relevant assessment of enzymatic activities and of post-translational modifications of selected proteins. This enables a glomerular cell type-specific analysis of regulatory events involved in driving glomerular cell injury.

As a proof of principle, we applied timMEP in the experimental model of THSD7A-associated MN and demonstrated the advantage of this method in detecting early cell type-specific changes in mRNA, which were not discernable upon analysis of whole glomeruli. Further, we used timMEP in severely nephrotic THSD7A-MN mice to perform cell type-specific proteomic analyses. These analyses revealed that endothelial cells were not affected in a murine model of

MN, whereas mesangial cells exhibited a nonspecific stress reaction to the podocyte-bound autoantibodies, which requires further investigation. Importantly, bulk proteomes from timMEP-isolated podocytes helped discern a specific reaction of podocytes to the bound THSD7A antibody, a reaction encompassing the selective loss/degradation of slit diaphragm proteins, whereas the foot process proteins we analyzed remained mostly unaffected. To this end, a close proximity, but no direct interaction, of THSD7A with Neph1r and Neph1 could be detected in the healthy setting, a situation that could potentially change after autoantibody binding to THSD7A, because this antibody-antigen reaction has been shown to localize at the slit diaphragm in early disease.³⁷ The precise mechanisms underlying the selective loss of the slit diaphragm proteins upon THSD7A autoantibody binding will be studied in future investigations.

Despite multiple advantages, timMEP has limitations. It depends on (1) successful isolation of glomeruli using magnetic beads, (2) successful single-cell suspensions, (3) binding of the fluorescent-labeled antibodies to glomerular proteins, and (4) flow sorting. Most of these experimental factors need to be considered for any kind of single-cell isolation/sample-generating procedure and can be mitigated by adequate controls and experimental design.⁴⁶ Of particular concern for this method are any potential changes in the binding of the marker antibody. Frequently, glomerular cells change their proteome and, thereby, their cell type marker expression in the setting of stress,^{6,47} a process often reflecting a dedifferentiation (especially of podocytes) or inflammatory activation (especially within endothelial and mesangial cells) of glomerular cells.⁴⁸ In addition, proteolysis occurs extracellularly to a large extent.⁴⁹ Therefore, we carefully selected glomerular cell type markers, which were relatively stably expressed by the glomerular cell types in health and disease. We found that, despite massive proteinuria and inflammation and a decreased signal for Podoplanin in immunofluorescence, sorting was still successful. We currently do not have evidence that the expression of these sorting markers is sex dependent. For instance, CD73 was not different between mesangial cells isolated from male (mean \pm SD normalized expression, 4.50 ± 0.30) versus female (mean \pm SEM normalized expression, 4.5338245 ± 0.25) C75BL/6 mice, and we found no observable differences in immunostaining for these markers. Further, the numbers of isolated cell types were not sex dependent using these sorting markers. As a potential alternative strategy, we also provide other cell type markers that could be used for modified FACS analysis (Supplemental Table 5).

As for any detection technique, there are limits to the detection of transcripts and proteins in timMEP-isolated glomerular cell types. The number of isolated podocytes, mesangial cells, and glomerular endothelial cells per mouse using timMEP is sufficient for routine qPCR, transcriptomic, and proteomic analyses. However, protein analyses of less abundant proteins will, in some cases, require pooling of

isolated glomerular cell types from two to four mice to reach a sufficient protein concentration for the analyses. The efficiency of timMEP is best in mice aged 6–20 weeks, thereafter, the number of isolated podocytes, mesangial cells, and glomerular endothelial cells decreases. This might partly be due to the fact that the efficiency of glomerular isolation decreases with age, and that the number of glomerular cells (especially of podocytes) decreases with age.⁴

Using timMEP, the presented dataset provides, for the first time, a reference for the proteomes of the three cell types in the glomerulus. Although we already described the podocyte proteome,¹⁴ this dataset now also covers cell types that are not easily amenable to single-cell dissociation, such as mesangial cells. Single-cell transcriptomic data generally have a large under-representation of mesangial cell capture, as compared with what is expected on the basis of morphometry.⁵⁰ Analysis of several single-cell datasets revealed that mesangial cells are not “easily accessible,” given their common renin lineage (and thus the high chance of misclassification). Our dataset, in contrast, now provides unambiguous mRNA and protein-based markers, several of which are novel markers. These data are also benchmarked against single-cell transcriptomics datasets derived from glomerular populations.³⁰

Further, our analyses unraveled a strain- and transgene-dependent expression of proteins among glomerular cell types, offering insights into protein machineries among strains and, possibly, an explanation for the differential susceptibility of different mouse strains to glomerular disease models.^{9,10,51} These observations expand descriptions of strain-dependent composition of the GBM.⁵² Moreover, these findings also support the presence of reporter-associated artifacts in transgenic reporter mice, because the expression of fluorescent reporters, such as eGFP, constitutes up to 6% of the proteome,¹⁴ a fact that could affect distinct cellular pathways, such as degradation pathways. In line with this, UCH-L1, a major deubiquitinating enzyme of the neuronal proteasomal degradation system, was one of the most differentially regulated proteins between the endothelia of mT/mG and C57BL/6 mice. Further, one should note that different isolation and analysis techniques might result in differences in mRNA and protein expression patterns between glomerular cell types. For example, we identified integrin $\beta 3$ and its ligand, fibronectin, to be highly expressed in glomerular endothelial cells by proteomics, data carefully validated by qPCR and immunofluorescence in our mouse strains, whereas other publications suggest an integrin $\beta 3$ protein expression in cultured podocytes^{53–56} or *in vivo*.^{57–59} Conflicting evidence also exists on single-cell RNA sequencing data. One study identified the highest level of *Itgb3* in mesangial cells, and none in epithelial cells of C57BL/6 mice,⁶⁰ whereas others found it in endothelial cells of C57BL/6 mice,⁶¹ consistent with our study. The exact explanation for these conflicting expression data shown for integrin $\beta 3$ remains to be elucidated, but could be related to

strain differences. Also, podocyte-expressed *Itgb3* could have escaped proteomic detection.

The added value, however, is the gain of functional information that cannot be gleaned by transcriptomic approaches. Protein levels do not always reflect transcript abundances.⁶² At a complex barrier system such as the filtration barrier, additional insights can be gained. Here, for instance, we discovered a loss of Neph/1 protein in a model of THSD7A-associated MN. In addition, our results offered a glimpse into the phosphoproteome. These data revealed acidophilic phosphorylation motifs in podocytes, with preference for casein kinases, consistent with previously reported phosphoproteomics data at the slit diaphragm. The phosphorylation motif preference, however, was different in the other cells. As a caveat, we acknowledge that phosphatase inhibitors were not included in the initial dissociation steps of the samples. When increasing depth or proteomic profiling, ligand-protein interactions, governing glomerular crosstalk, could be monitored; here, we found heterogeneous expression of the Ephrin receptor system.

In summary, we present a generalizable and effective method to isolate native glomerular cell types, which will enable a widespread and detailed glomerular cell type-resolved transcriptional and protein-biochemical analysis to deepen our future understanding of glomerular cell biology in health and disease.

DISCLOSURES

T.B. Huber reports receiving research funding from Amicus Therapeutics, Fresenius Medical Care; having consultancy agreements with AstraZeneca, Bayer, Boehringer-Ingelheim, DaVita, Deerfield, Fresenius Medical Care, GoldfinchBio, Mantrabio, Novartis, and Retrophin; serving on the editorial board for *Kidney International*, and the advisory board for *Nature Review Nephrology*. M. Rinschen reports being a member of the renal editorial board for the *American Journal of Physiology*, and being an associate editor for *JASN*. Therefore, he was not involved in the peer-review process for this manuscript; a guest editor oversaw the peer-review and decision-making process for this manuscript. All remaining authors have nothing to disclose.

FUNDING

This work was supported by the Deutsche Forschungsgemeinschaft grants SFB1192 (Graduiertenkolleg to S. Skuza and C. Kosub), project B3 (to C. Meyer-Schwesinger), project B2 (to N.M. Tomas), project B8 (to T.B. Huber), Ri2811/1, and Ri2811/2 (to M.M. Rinschen); and Else Kröner-Fresenius-Stiftung (Else Kröner-Promotionskolleg Hamburg-Translationale Entzündungsforschung) and iPRIME to U. Wedekind. Work in M.M. Rinschen's laboratory is supported by the Novo Nordisk Young Investigator Award, grant number NNF19OC0056043.

ACKNOWLEDGMENTS

We are grateful to the staff of the FACS Sorting Core Unit for excellent technical assistance. We thank the Advanced Light and Fluorescence

Microscopy facility at the Centre for Structural Systems Biology, in particular, Dr. Roland Thünauer for support with light microscopy/image recording/image analysis, and Ruth Herzog and the Cologne proteomics facility (head Dr. Jan-Wilm Lackmann) for excellent technical assistance. F.A. Hatje, U. Wedekind, J. Reichelt, L. Heintz, and S. Skuza developed the glomerular cell isolation technique, performed the experiments, and analyzed the data; D. Loreth performed the super-resolution structured illumination microscopy; C. Kosub performed the coimmunoprecipitations; S. Skuza performed the primary cell culture experiments; M.M. Rinschen and F. Demir performed the proteomic analyses; W. Sachs and M. Sachs performed the immunoblot and qPCR analyses; T.B. Huber provided the mT/mG mice; C. Meyer-Schwesinger developed the glomerular cell isolation technique, performed immunofluorescence and confocal microscopy, and analyzed the data; and F.A. Hatje, U. Wedekind, M.M. Rinschen, and C. Meyer-Schwesinger wrote the manuscript.

DATA SHARING STATEMENT

The raw data of the files are available at PRIDE/ProteomeXchange at <https://www.ebi.ac.uk/pride/archive/login> using the following tokens^{63,64}: dataset, mT/mG dataset; project name, analysis of mouse glomerular cells; project accession, PXD016238; project DOI, not applicable; username, reviewer50821@ebi.ac.uk; password, UHUYumfS; dataset, different strains; project name, FACS-sorted podocytes, mesangial cells; project accession, PXD016237; project DOI, not applicable; username, reviewer27484@ebi.ac.uk; password, kQUh8pJC.

SUPPLEMENTAL MATERIAL

This article contains the following supplemental material online at <http://jasn.asnjournals.org/lookup/suppl/doi:10.1681/ASN.2020091346/-/DCSupplemental>.

Supplemental Appendix 1. Supplemental methods.

Supplemental Table 1. Antibodies and dyes used in the study for FACS sort.

Supplemental Table 2. Primers used in the study.

Supplemental Table 3. Podocyte-specific, endothelia specific and mesangial specific proteins that were significantly enriched over the other cell types in mt/mg mice.

Supplemental Table 4. Podocyte-specific, endothelia specific and mesangial specific proteins that were significantly enriched age, sex, and species in wildtype mice.

Supplemental Table 5. Alternative membrane proteins potentially useful for TimMEP in diseased glomeruli.

Supplemental Figure 1. Comparison of old and new gating strategy.

Supplemental Figure 2. UMAP analysis of FACS sorted glomerular cells.

Supplemental Figure 3. Non-labeled FACS sorted glomerular cells express nephron mRNA.

Supplemental Figure 4. Counts of isolated cells were comparable in between gender, species but not age

Supplemental Figure 5. Comparison of FACS-sort between mt/mg mice and wildtype mice.

Supplemental Figure 6. FACS-sorted glomerular cells are not contaminated with parietal epithelial or tubular cells.

Supplemental Figure 7. Tripartite cell type isolation and proteomic analysis from mt/mg mice.

Supplemental Figure 8. Identification of new podocyte enriched proteins.

Supplemental Figure 9. Identification of new mesangial cell enriched proteins.

Supplemental Figure 10. Identification of new glomerular endothelial cell enriched proteins.

Supplemental Figure 11. Integrin-b3 and its ligand fibronectin 1 are predominantly expressed on glomerular endothelial cells.

Supplemental Figure 12. Gating strategy used for the separation of glomerular cell types in the mouse model of anti-THSD7A membranous nephropathy.

Supplemental Figure 13. Leukocytes are not increased in glomeruli in the setting of experimental THSD7A-associated membranous nephropathy.

Supplemental Figure 14. THSD7A localizes closely to the slit diaphragm proteins Neph1 and nephrin.

Supplemental Figure 15. Differential loss of podocyte proteins in experimental THSD7A-associated membranous nephropathy.

REFERENCES

- Pavenstädt H, Kriz W, Kretzler M: Cell biology of the glomerular podocyte. *Physiol Rev* 83: 253–307, 2003
- Dimke H, Maezawa Y, Quaggin SE: Crosstalk in glomerular injury and repair. *Curr Opin Nephrol Hypertens* 24: 231–238, 2015
- Takemoto M, Asker N, Gerhardt H, Lundkvist A, Johansson BR, Saito Y, et al.: A new method for large scale isolation of kidney glomeruli from mice. *Am J Pathol* 161: 799–805, 2002
- Wanner N, Hartleben B, Herbach N, Goedel M, Stickel N, Zeiser R, et al.: Unraveling the role of podocyte turnover in glomerular aging and injury. *J Am Soc Nephrol* 25: 707–716, 2014
- Boerries M, Grahmmer F, Eiselein S, Buck M, Meyer C, Goedel M, et al.: Molecular fingerprinting of the podocyte reveals novel gene and protein regulatory networks. *Kidney Int* 83: 1052–1064, 2013
- Koehler S, Kuczkowski A, Kuehne L, Jüngst C, Hoehne M, Grahmmer F, et al.: Proteome analysis of isolated podocytes reveals stress responses in glomerular sclerosis. *J Am Soc Nephrol* 31: 544–559, 2020
- Muzumdar MD, Tasic B, Miyamichi K, Li L, Luo L: A global double-fluorescent Cre reporter mouse. *Genesis* 45: 593–605, 2007
- Koehler S, Brähler S, Braun F, Hagmann H, Rinschen MM, Späth MR, et al.: Construction of a viral T2A-peptide based knock-in mouse model for enhanced Cre recombinase activity and fluorescent labeling of podocytes. *Kidney Int* 91: 1510–1517, 2017
- Tomas NM, Meyer-Schwesinger C, von Spiegel H, Kotb AM, Zahner G, Hoxha E, et al.: A heterologous model of thrombospondin type 1 domain-containing 7A-associated membranous nephropathy. *J Am Soc Nephrol* 28: 3262–3277, 2017
- Meyer TN, Schwesinger C, Wahlefeld J, Dehde S, Kerjaschki D, Becker JU, et al.: A new mouse model of immune-mediated podocyte injury. *Kidney Int* 72: 841–852, 2007
- Höhne M, Frese CK, Grahmmer F, Dafinger C, Ciarimboli G, Butt L, et al.: Single-nephron proteomes connect morphology and function in proteinuric kidney disease. *Kidney Int* 93: 1308–1319, 2018
- Rinschen MM: Single glomerular proteomics: A novel tool for translational glomerular cell biology. *Methods Cell Biol* 154: 1–14, 2019
- Hughes CS, Moggridge S, Müller T, Sorensen PH, Morin GB, Krijgsveld J: Single-pot, solid-phase-enhanced sample preparation for proteomics experiments. *Nat Protoc* 14: 68–85, 2019
- Rinschen MM, Gödel M, Grahmmer F, Zschiedrich S, Helmstädter M, Kretz O, et al.: A multi-layered quantitative in vivo expression atlas of the podocyte unravels kidney disease candidate genes. *Cell Rep* 23: 2495–2508, 2018
- Cox J, Mann M: MaxQuant enables high peptide identification rates, individualized p.p.b.-range mass accuracies and proteome-wide protein quantification. *Nat Biotechnol* 26: 1367–1372, 2008
- Cox J, Hein MY, Luber CA, Paron I, Nagaraj N, Mann M: Accurate proteome-wide label-free quantification by delayed normalization and maximal peptide ratio extraction, termed MaxLFQ. *Mol Cell Proteomics* 13: 2513–2526, 2014
- Tyanova S, Temu T, Sinitcyn P, Carlson A, Hein MY, Geiger T, et al.: The Perseus computational platform for comprehensive analysis of (prote)omics data. *Nat Methods* 13: 731–740, 2016

18. Szklarczyk D, Morris JH, Cook H, Kuhn M, Wyder S, Simonovic M, et al.: The STRING database in 2017: quality-controlled protein-protein association networks, made broadly accessible. *Nucleic Acids Res* 45: D362–D368, 2017
19. Shannon P, Markiel A, Ozier O, Baliga NS, Wang JT, Ramage D, et al.: Cytoscape: A software environment for integrated models of biomolecular interaction networks. *Genome Res* 13: 2498–2504, 2003
20. Rinschen MM, Palygin O, Guijas C, Palermo A, Palacio-Escat N, Domingo-Almenara X, et al.: Metabolic rewiring of the hypertensive kidney. *Sci Signal* 12: eaax9760, 2019
21. Thomsen MC, Nielsen M: Seq2Logo: A method for construction and visualization of amino acid binding motifs and sequence profiles including sequence weighting, pseudo counts and two-sided representation of amino acid enrichment and depletion. *Nucleic Acids Res* 40: W281–W287, 2012
22. Panzer U, Steinmetz OM, Reinking RR, Meyer TN, Fehr S, Schneider A, et al.: Compartment-specific expression and function of the chemokine IP-10/CXCL10 in a model of renal endothelial microvascular injury. *J Am Soc Nephrol* 17: 454–464, 2006
23. Abramoff MMP, Ram SJ: Image Processing with ImageJ. *Biophotonics Int* 11: 36–42, 2004
24. Sosna J, Voigt S, Mathieu S, Kabelitz D, Trad A, Janssen O, et al.: The proteases HtrA2/Omi and UCH-L1 regulate TNF-induced necroptosis. *Cell Commun Signal* 11: 76, 2013
25. Artelt N, Siegerist F, Ritter AM, Grisk O, Schlüter R, Endlich K, et al.: Comparative Analysis of podocyte foot process morphology in three species by 3D super-resolution microscopy. *Front Med (Lausanne)* 5: 292, 2018
26. Siegerist F, Ribback S, Dombrowski F, Amann K, Zimmermann U, Endlich K, et al.: Structured illumination microscopy and automated image processing as a rapid diagnostic tool for podocyte effacement. *Sci Rep* 7: 11473, 2017
27. Kabgani N, Grigoleit T, Schulte K, Sechi A, Sauer-Lehnen S, Tag C, et al.: Primary cultures of glomerular parietal epithelial cells or podocytes with proven origin. *PLoS One* 7: e34907, 2012
28. Lertkiatmongkol P, Liao D, Mei H, Hu Y, Newman PJ: Endothelial functions of platelet/endothelial cell adhesion molecule-1 (CD31). *Curr Opin Hematol* 23: 253–259, 2016
29. Castrop H, Huang Y, Hashimoto S, Mizel D, Hansen P, Theilig F, et al.: Impairment of tubuloglomerular feedback regulation of GFR in ecto-5'-nucleotidase/CD73-deficient mice. *J Clin Invest* 114: 634–642, 2004
30. Karaiskos N, Rahmatollahi M, Boltengagen A, Liu H, Hoehne M, Rinschen M, et al.: A single-cell transcriptome atlas of the mouse glomerulus. *J Am Soc Nephrol* 29: 2060–2068, 2018
31. Bierzynska A, Soderquest K, Koziell A: Genes and podocytes - new insights into mechanisms of podocytopathy. *Front Endocrinol (Lausanne)* 5: 226, 2015
32. Rinschen MM, Wu X, König T, Pisitkun T, Hagmann H, Pahmeyer C, et al.: Phosphoproteomic analysis reveals regulatory mechanisms at the kidney filtration barrier. *J Am Soc Nephrol* 25: 1509–1522, 2014
33. Rinschen MM, Pahmeyer C, Pisitkun T, Schnell N, Wu X, Maaß M, et al.: Comparative phosphoproteomic analysis of mammalian glomeruli reveals conserved podocin C-terminal phosphorylation as a determinant of slit diaphragm complex architecture. *Proteomics* 15: 1326–1331, 2015
34. Cerami E, Demir E, Schultz N, Taylor BS, Sander C: Automated network analysis identifies core pathways in glioblastoma. *PLoS One* 5: e8918, 2010
35. Bishop P, Rubin P, Thomson AR, Rocca D, Henley JM: The ubiquitin C-terminal hydrolase L1 (UCH-L1) C terminus plays a key role in protein stability, but its farnesylation is not required for membrane association in primary neurons. *J Biol Chem* 289: 36140–36149, 2014
36. Klamp T, Boehm U, Schenk D, Pfeffer K, Howard JC: A giant GTPase, very large inducible GTPase-1, is inducible by IFNs. *J Immunol* 171: 1255–1265, 2003
37. Herwig J, Skuza S, Sachs W, Sachs M, Failla AV, Rune G, et al.: Thrombospondin type 1 domain-containing 7A localizes to the slit diaphragm and stabilizes membrane dynamics of fully differentiated podocytes. *J Am Soc Nephrol* 30: 824–839, 2019
38. Tomas NM, Beck LH Jr, Meyer-Schwesinger C, Seitz-Polski B, Ma H, Zahner G, et al.: Thrombospondin type-1 domain-containing 7A in idiopathic membranous nephropathy. *N Engl J Med* 371: 2277–2287, 2014
39. Groffen AJ, Ruegg MA, Dijkman H, van de Velden TJ, Buskens CA, van den Born J, et al.: Agrin is a major heparan sulfate proteoglycan in the human glomerular basement membrane. *J Histochem Cytochem* 46: 19–27, 1998
40. Abrahamson DR, Prettyman AC, Robert B, St John PL: Laminin-1 reexpression in Alport mouse glomerular basement membranes. *Kidney Int* 63: 826–834, 2003
41. Eremina V, Baelde HJ, Quaggin SE: Role of the VEGF-a signaling pathway in the glomerulus: evidence for crosstalk between components of the glomerular filtration barrier. *Nephron, Physiol* 106: 32–37, 2007
42. Sea K, Sohn SH, Durazo A, Sheng Y, Shaw BF, Cao X, et al.: Insights into the role of the unusual disulfide bond in copper-zinc superoxide dismutase. *J Biol Chem* 290: 2405–2418, 2015
43. Gupta V, Bamezai RN: Human pyruvate kinase M2: A multifunctional protein. *Protein Sci* 19: 2031–2044, 2010
44. Chegary M, Brinke H, Ruitter JP, Wijburg FA, Stoll MS, Minkler PE, et al.: Mitochondrial long chain fatty acid beta-oxidation in man and mouse. *Biochim Biophys Acta* 1791: 806–815, 2009
45. Grahammer F, Wigge C, Schell C, Kretz O, Patrakka J, Schneider S, et al.: A flexible, multilayered protein scaffold maintains the slit in between glomerular podocytes. *JCI Insight* 1: e86177, 2016
46. Kuppe C, Perales-Patón J, Saez-Rodriguez J, Kramann R: Experimental and computational technologies to dissect the kidney at the single-cell level [published online ahead of print December 17, 2020]. *Nephrol Dial Transplant*
47. Meyer-Schwesinger C, Meyer TN, Münster S, Klug P, Saleem M, Helmchen U, et al.: A new role for the neuronal ubiquitin C-terminal hydrolase-L1 (UCH-L1) in podocyte process formation and podocyte injury in human glomerulopathies. *J Pathol* 217: 452–464, 2009
48. Guhr SS, Sachs M, Wegner A, Becker JU, Meyer TN, Kietzmann L, et al.: The expression of podocyte-specific proteins in parietal epithelial cells is regulated by protein degradation. *Kidney Int* 84: 532–544, 2013
49. Rinschen MM, Huesgen PF, Koch RE: The podocyte protease web: Uncovering the gatekeepers of glomerular disease. *Am J Physiol Renal Physiol* 315: F1812–F1816, 2018
50. Clark JZ, Chen L, Chou CL, Jung HJ, Lee JW, Knepper MA: Representation and relative abundance of cell-type selective markers in whole-kidney RNA-Seq data. *Kidney Int* 95: 787–796, 2019
51. Meyer-Schwesinger C, Dehde S, Klug P, Becker JU, Mathey S, Arefi K, et al.: Nephrotic syndrome and subepithelial deposits in a mouse model of immune-mediated anti-podocyte glomerulonephritis. *J Immunol* 187: 3218–3229, 2011
52. Randles MJ, Woolf AS, Huang JL, Byron A, Humphries JD, Price KL, et al.: Genetic background is a key determinant of glomerular extracellular matrix composition and organization. *J Am Soc Nephrol* 26: 3021–3034, 2015
53. Raval N, Jogi H, Gondaliya P, Kalia K, Tekade RK: Cyclo-RGD truncated polymeric nanoconstruct with dendrimeric templates for targeted HDAC4 gene silencing in a diabetic nephropathy mouse model. *Mol Pharm* 18: 641–666, 2021

54. Wu J, Zheng C, Wang X, Yun S, Zhao Y, Liu L, et al.: MicroRNA-30 family members regulate calcium/calcineurin signaling in podocytes. *J Clin Invest* 125: 4091–4106, 2015
55. Rinschen MM, Schroeter CB, Koehler S, Ising C, Schermer B, Kann M, et al.: Quantitative deep mapping of the cultured podocyte proteome uncovers shifts in proteostatic mechanisms during differentiation. *Am J Physiol Cell Physiol* 311: C404–C417, 2016
56. Schroeter CB, Koehler S, Kann M, Schermer B, Benzing T, Brinkkoetter PT, et al.: Protein half-life determines expression of proteostatic networks in podocyte differentiation. *FASEB J* 32: 4696–4713, 2018
57. Kliewe F, Kaling S, Löttsch H, Artelt N, Schindler M, Rogge H, et al.: Fibronectin is up-regulated in podocytes by mechanical stress. *FASEB J* 33: 14450–14460, 2019
58. Wei C, El Hindi S, Li J, Fornoni A, Goes N, Sageshima J, et al.: Circulating urokinase receptor as a cause of focal segmental glomerulosclerosis. *Nat Med* 17: 952–960, 2011
59. Wei C, Möller CC, Altintas MM, Li J, Schwarz K, Zacchigna S, et al.: Modification of kidney barrier function by the urokinase receptor. *Nat Med* 14: 55–63, 2008
60. Wu H, Kirita Y, Donnelly EL, Humphreys BD: Advantages of single-nucleus over single-cell RNA sequencing of adult kidney: Rare cell types and novel cell states revealed in fibrosis. *J Am Soc Nephrol* 30: 23–32, 2019
61. Park J, Shrestha R, Qiu C, Kondo A, Huang S, Werth M, et al.: Single-cell transcriptomics of the mouse kidney reveals potential cellular targets of kidney disease. *Science* 360: 758–763, 2018
62. Rinschen MM, Saez-Rodriguez J: The tissue proteome in the multi-omic landscape of kidney disease. *Nat Rev Nephrol* 17: 205–219, 2021
63. Perez-Riverol Y, Csordas A, Bai J, Bernal-Llinares M, Hewapathirana S, Kundu DJ, et al.: The PRIDE database and related tools and resources in 2019: Improving support for quantification data. *Nucleic Acids Res* 47: D442–D450, 2019
64. Vizcaíno JA, Csordas A, Del-Toro N, Dienes JA, Griss J, Lavidas I, et al.: 2016 update of the PRIDE database and its related tools [published correction appears in *Nucleic Acid Res* 44: 11033, 2016 10.1093/nar/gkw880]. *Nucleic Acids Res* 44: D447–D456, 2016

AFFILIATIONS

¹Institute of Cellular and Integrative Physiology, University Medical Center Hamburg-Eppendorf, Hamburg, Germany

²Department of Biomedicine, Aarhus University, Aarhus, Denmark

³III Department of Medicine, University Medical Center Hamburg-Eppendorf, Hamburg, Germany

⁴Department II of Internal Medicine, Center for Molecular Medicine Cologne, University of Cologne, Cologne, Germany

Supplemental table 1: Antibodies and dyes used in the study for FACS sort.

Supplemental table 2: Primers used in the study.

Supplemental table 3: Podocyte-specific, endothelia specific and mesangial specific proteins that were significantly enriched over the other cell types in mT/mG mice.

Supplemental table 4: Podocyte-specific, endothelia specific and mesangial specific proteins that were significantly enriched age, sex, and species in wildtype mice.

Supplemental table 5: Alternative membrane proteins potentially useful for timMEP in diseased glomeruli.

Supplemental figure 1: Comparison of old and new gating strategy.

Supplemental figure 2: UMAP analysis of FACS sorted glomerular cells.

Supplemental figure 3: Non-labeled FACS sorted glomerular cells express nephron mRNA.

Supplemental figure 4: Counts of isolated cells were comparable in between gender, species but not age.

Supplemental figure 5: Comparison of FACS-sort between mT/mG mice and wildtype mice.

Supplemental figure 6: FACS-sorted glomerular cells are not contaminated with parietal epithelial or tubular cells.

Supplemental figure 7: Tripartite cell type isolation and proteomic analysis from mT/mG mice.

Supplemental figure 8: Identification of new podocyte enriched proteins.

Supplemental figure 9: Identification of new mesangial cell enriched proteins.

Supplemental figure 10: Identification of new glomerular endothelial cell enriched proteins.

Supplemental Figure 11: Integrin- β 3 and its ligand Fibronectin 1 are predominantly expressed on glomerular endothelial cells.

Supplemental figure 12: Gating strategy used for the separation of glomerular cell types in the mouse model of anti-THSD7A membranous nephropathy.

Supplemental figure 13: Leukocytes are not increased in glomeruli in the setting of experimental THSD7A-associated membranous nephropathy.

Supplemental figure 14: THSD7A localizes closely to the slit diaphragm proteins Neph1 and Nephrin.

Supplemental figure 15: Differential loss of podocyte proteins in experimental THSD7A-associated membranous nephropathy.

Reporter transgene	Cell type	Ex [λ] / Em [λ]
GFP	podocytes	488/509
tdTomato	all other cells	554/581

Antibody Target	Fluorescent Agent	Clone	Company	Dilution	Laser	Filter
Podoplanin	Phycoerythrin (PE)	8.1.1	BioLegend	1:200	561nm	582/15
CD73	Alexa Fluor 647	TY/11.8	BioLegend	1:2000	640nm	670/30
CD31	Brilliant Violet 421	MEC 13.3	BD OptiBuild	1:800	405nm	450/50
CD45	Alexa Fluor 700	30-F11	BioLegend	1:100	640nm	730/45

Dye	Company	Dilution	Laser	Filter
Near-IR fluorescent reactive dye	Invitrogen	1:4000	640nm	780/60

Supplemental table 1: Transgenic reporters, antibodies, and dyes used in the study for FACS-sort.

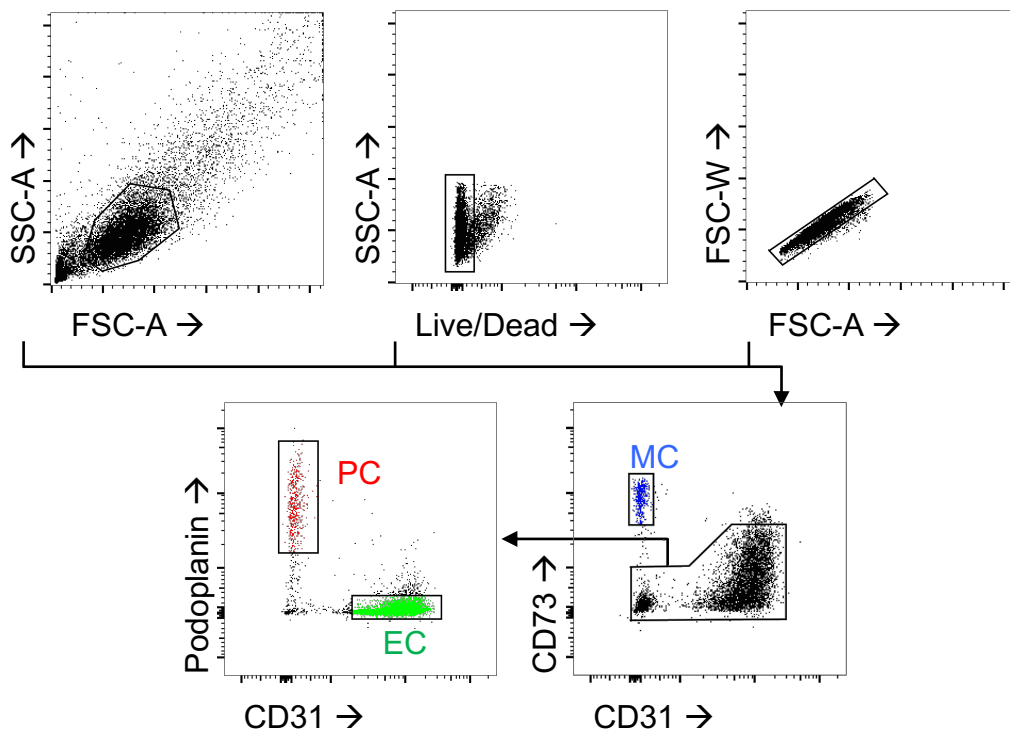
Target	Forward Primer Sequence 5' – 3'	Reverse Primer Sequence 5' – 3'
<i>Agrn</i>	CTAGGGGAATCTCCGGTCCC	GGCCTCTTAGAGACACCAGC
<i>Aqp4</i>	CCCGCAGTTATCATGGGAAAC	GAAGGCTTCCTTAAGGCGACG
<i>Cdh5</i>	CGTTGGACTTGATCTTTCCC	CGCCAAAAGAGAGACTGGAT
<i>Fn1</i>	CTTGACGATGATATGGAGA	AGCTGAACACTGGGTGCTAT
<i>Hk1</i>	CGGAATGGGGAGCCTTTGG	GCCTTCCTTATCCGTTTCAATGG
<i>Itgb3</i>	GCGCGCGGCGTGAAG	CACGCCTCGTGTGGTACAGAT
<i>Lad1</i>	CACAGCCATCCAGAGGTCAG	TCAAAGAGGTGTCGCTTGCT
<i>Lamb1</i>	TCCCCGCTACCTCTCCAGAA	CCATAGGGCTAGGACACCAA
<i>Nphs2</i>	TGACGTTCCCTTTTTCCATC	AGGAAGCAGATGTCCCAGT
<i>Nt5e</i>	GCAGCATTCTGAAGATGCG	CTCCCGAGTTCCTGGGTAGA
<i>Pdgrfb</i>	TGGTATCACTCCTGGAAGCC	AACAGAAGACAGCGAGGTGG
<i>Pdpn</i>	GGGATGAAACGCAGACAACAG	TTTAGGGCGAGAACCTTCCAG
<i>Pecam1</i>	AGCCAACAGCCATTACGGTTA	AGCCTTCCGTTCTCTTGGTG
<i>Pkm</i>	GCCGCCTGGACATTGACTC	CCATGAGAGAAATTCAGCCGAG
<i>Scin</i>	CCAGAATTGTGGAGGTTGACG	GCCATTGTTTTCGTGGCAGTT
<i>Slc12a3</i>	CGGGATAATGGCAAGGTCAAGTCG	GGAATTCTGATGCGGATGTCATTGATGG
<i>Slc5a2</i>	CGGGATCCACGTAGAGGCAGGCTCTGA	GGAATTCACCTTGCTGCACCAGTCCC
<i>Slc12a1</i>	GGCCATGGCAGTGCGGCAGCCG	GCACTCCTGATTCCCAGGCCTAAAGCTG
<i>Scnn1a</i>	CGGGATCCCGGCATGATGTACTGGCAG	GGAATTCGCCTGGCGAGTGTAGGAAG
<i>Sod1</i>	GGAACCATCCACTTCGAGCA	CTGCACTGGTACAGCCTTGT
<i>Vegfa</i>	AATGCTTTCTCCGCTCTGAA	GCTTCCTACAGCACAGCAGA

Supplemental table 2: Primers used in the study.

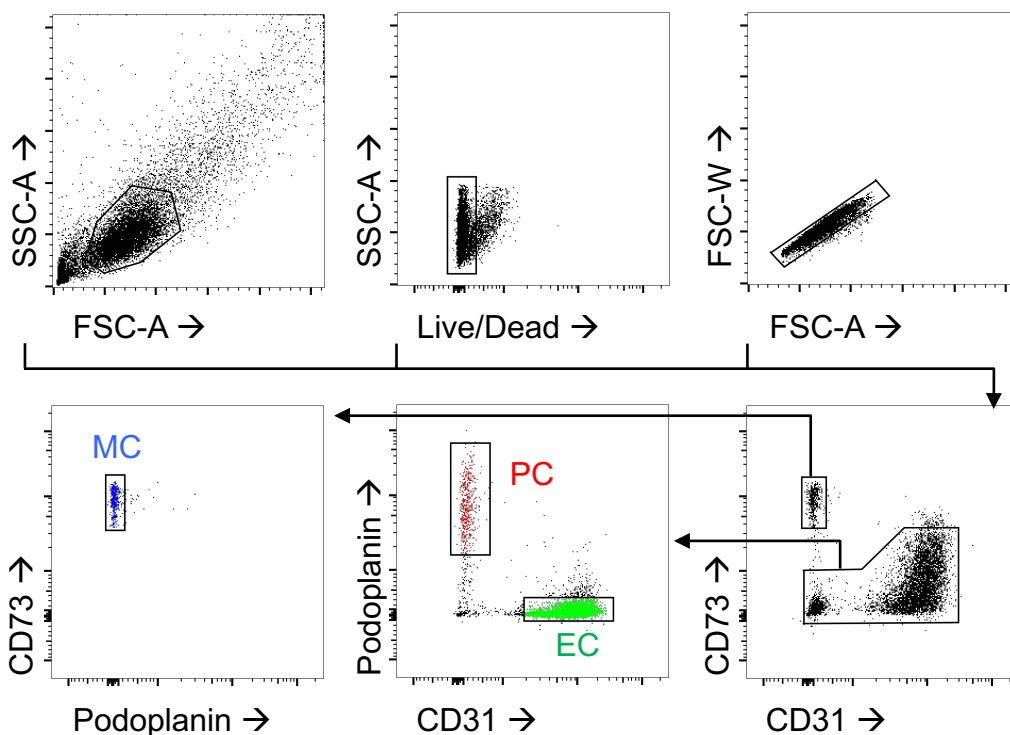
Enriched in podocytes	Enriched in mesangial cells	Enriched in glomerular endothelial cells
Kirrel1	Itga8	Dysf
Enpep	Gja5	Emcn
Ptpro	Lrp1	Tmem2
Cxadr	Mcam	Gimap1
Galnt10	Cspg4	Slc43a3
Sdc4		Kdr
Crb2		Tspan7
Itgb5		Ece1
Itm2b		Ppap2a
Cldn5		Lpcat1

Supplemental table 5: Alternative membrane proteins potentially useful for timMEP in diseased glomeruli. The used FACS-sort markers presented here for timMEP (Podoplanin, CD73 and CD31) might be altered in specific glomerular disease models. Therefore, we analyzed our proteomic data for possible alternatives. The presented proteins are enriched in the respective glomerular cell type and have been annotated to reside on the cellular membrane. Cell type-specific expression has been verified in the Human Protein Atlas. If an alternative to our standard targets is needed, this list may serve as a starting point.

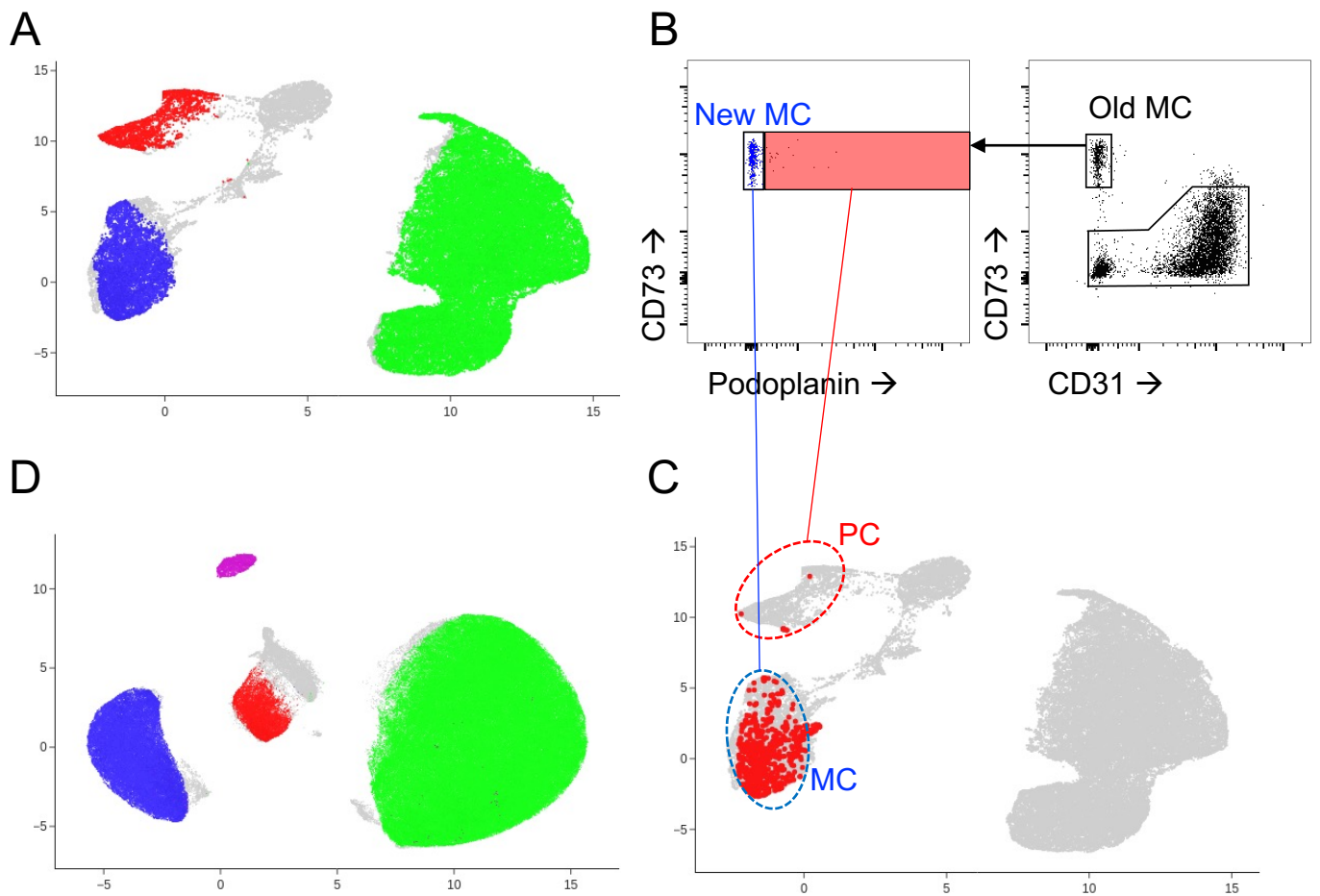
A INITIAL gating strategy used for individual mouse glomerular cell type proteomes of Figures 3, 4, 5), in which the mesangial cell population exhibited a minor contamination with podocytes. The endothelial and podocyte populations were free of contaminants.



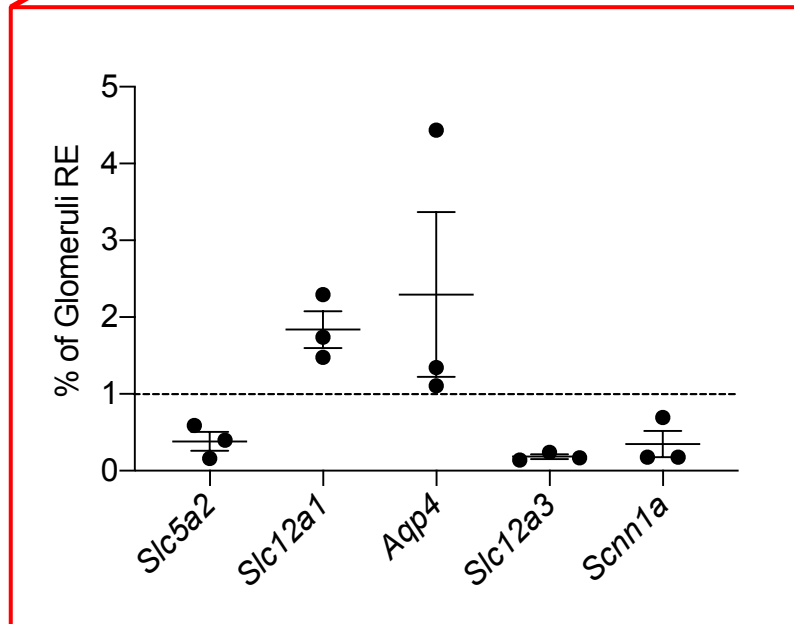
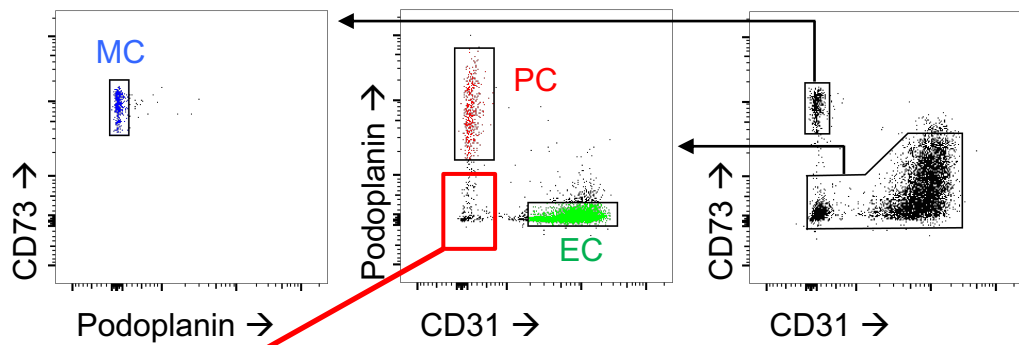
B NEW gating strategy for all experiments, with pure mesangial, endothelial and podocyte populations



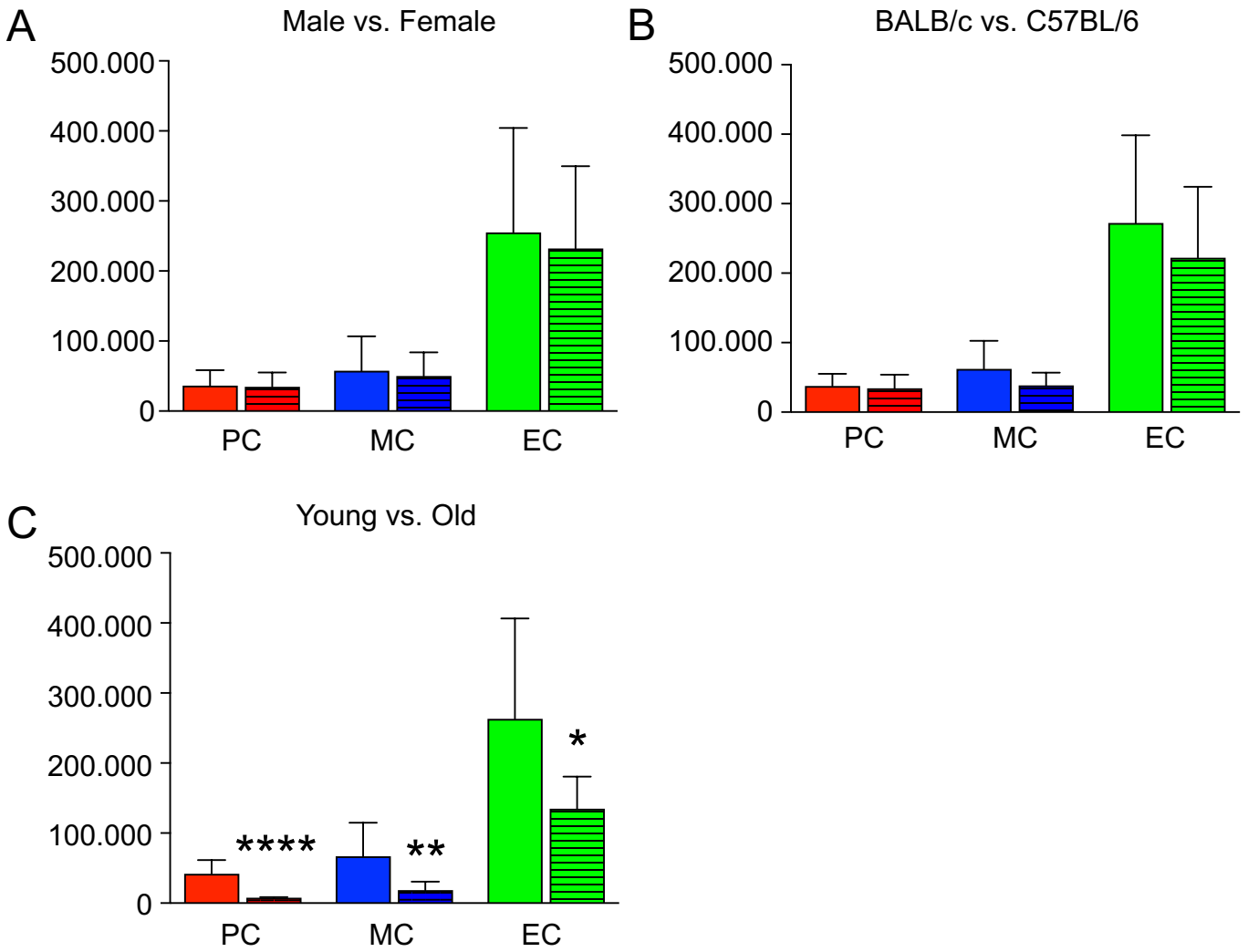
Supplemental figure 1: Comparison of old and new gating strategy. (A) Gating strategy used for individual mouse proteome investigations in Figures 3, 4, 5 and **(B)** improved gating strategy removing podocyte contamination of mesangial cells used for all subsequent experiments.



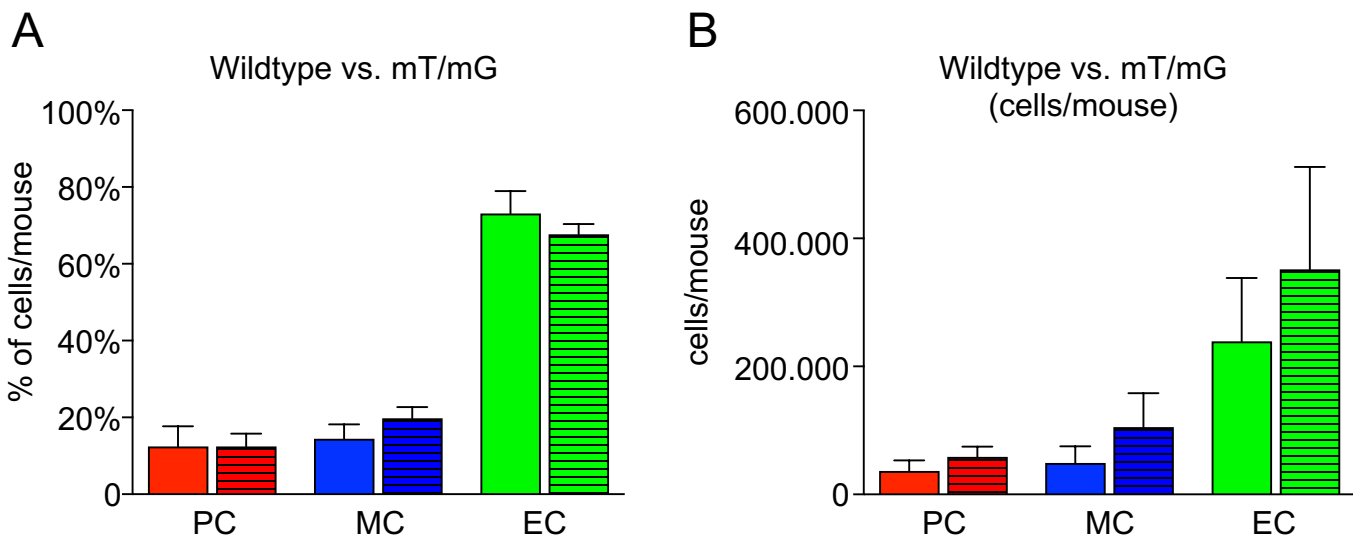
Supplemental figure 2: UMAP analysis of FACS-sorted glomerular cells. (A) UMAP plot of cytometry data recorded during sorting of wildtype cells used for proteomic analyses in this paper. The plot demonstrates clear clustering of podocytes (PC, red), mesangial (MC, blue) and endothelial cells (green), respectively. (B) Modified snippet taken from Fig. 1D demonstrating the differences between the earlier and revised gating strategy. Highlighted in the light red box are cells that might have caused a slight podocyte contamination in the mesangial cell population. (C) To further investigate actual contamination, we overlaid these cells (light red box in B) in red on to the UMAP shown in A. Interestingly, most of those cells reside inside the mesangial cell cluster (blue dotted ellipse; previously correctly classified as mesangials) with only very few cells residing in the podocyte cell cluster (red dotted ellipse in A; previously misclassified as mesangials). Furthermore, the improved gating strategy removed the contamination as there are no mesangials (blue dots) in the podocyte cluster (red dots) in A. (D) UMAP of cytometry data with additional CD45 gating to visualize immune cells (violet cluster).



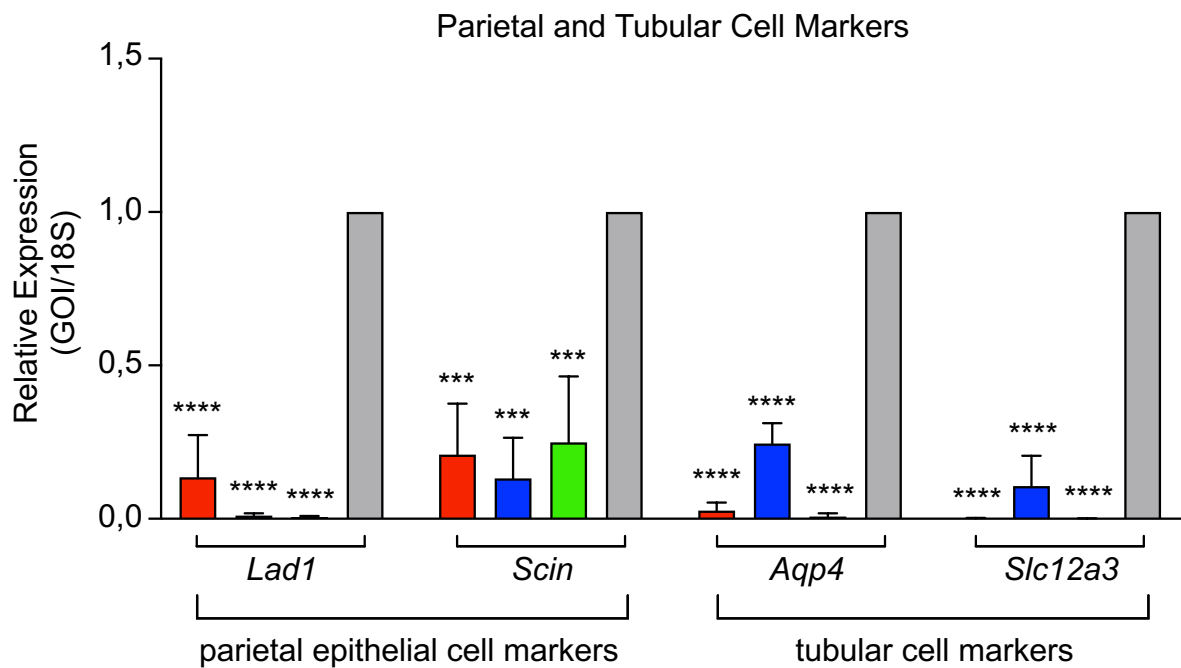
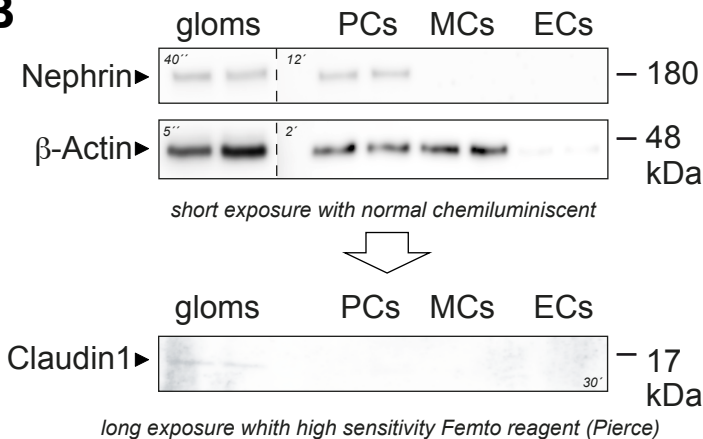
Supplemental figure 3: Non-labeled FACS sorted glomerular cells express nephron markers. mRNA was isolated from the non-labeled FACS-sort population (red emboxed Podoplanin⁻ /CD31⁻ /CD73⁻ cells). Real-time qPCR analysis of this rest cell population for *Slc5a2* (encodes for SGLT2), *Slc12a1* (encodes for NKCC2), *Aqp4* (encodes for Aquaporin 4), *Slc12a3* (encodes for NCC), and *Scnn1a* (encodes for ENaC) exhibits the expression of genes specific for tubular cells, thereby representing cells originating from the few tubuli that contaminated the isolated glomeruli, which are however discarded in the timMEP gating strategy. Δ CT values were calculated using 18S as home keeper. $\Delta\Delta$ CT values were calculated as difference between glomerular and non-labeled FACS-sorted cell Δ CT. Displayed is the relative expression (RE, $2^{(\Delta\Delta CT)}$) of non-labeled FACS-sorted cell types in percent of the glomerular RE, n = 3 individual mice.



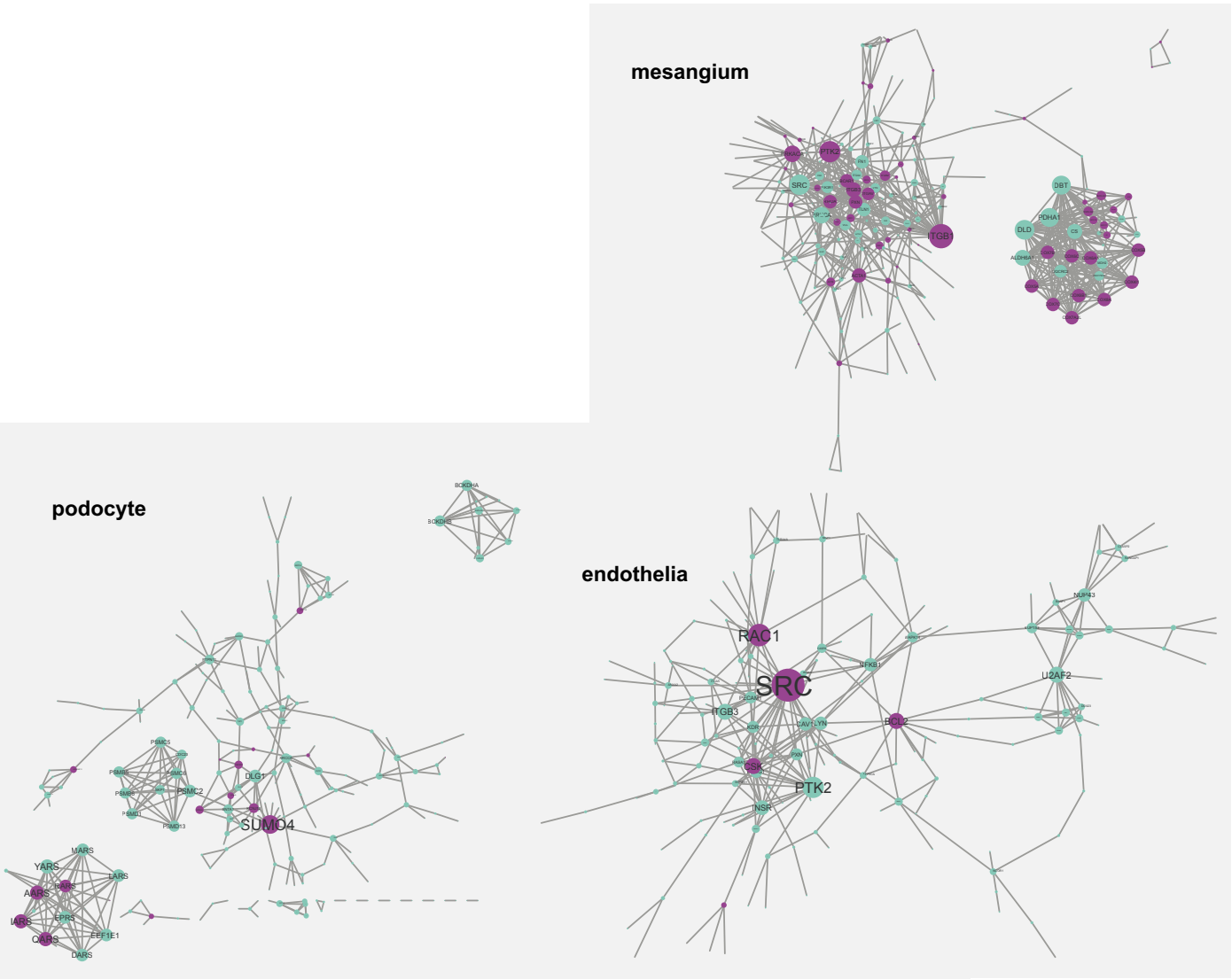
Supplemental figure 4 Counts of isolated cells were comparable in between gender, species but not age. Absolute number of podocytes (PC), mesangial (MC), and endothelial cells (EC) FACS-sorted from the isolated glomerular cells per mouse, mean +/- SEM, n=5-74, pooled data from 18 independent experiments. **(A)** Empty bars represent cell counts from male C57BL/6 mice, striped bars from female C57BL/6 mice, all aged 11-14 weeks. **(B)** Empty bars represent cell counts from female BALB/c mice, striped bars from female C57BL/6 mice, all aged 11-14 weeks. **(C)** Empty bars represent cell counts from young male C57BL/6 mice 11-14 weeks of age, striped bars from old male C57BL/6 mice aged 61-69 weeks. Mean +/- SD; * $p < 0.05$, ** $p < 0.01$, **** $p < 0.0001$ to young male mice, Mann Whitney U test. Upon ageing, the percentage loss was 49% for endothelials, 72% for mesangials and 82% for podocytes.



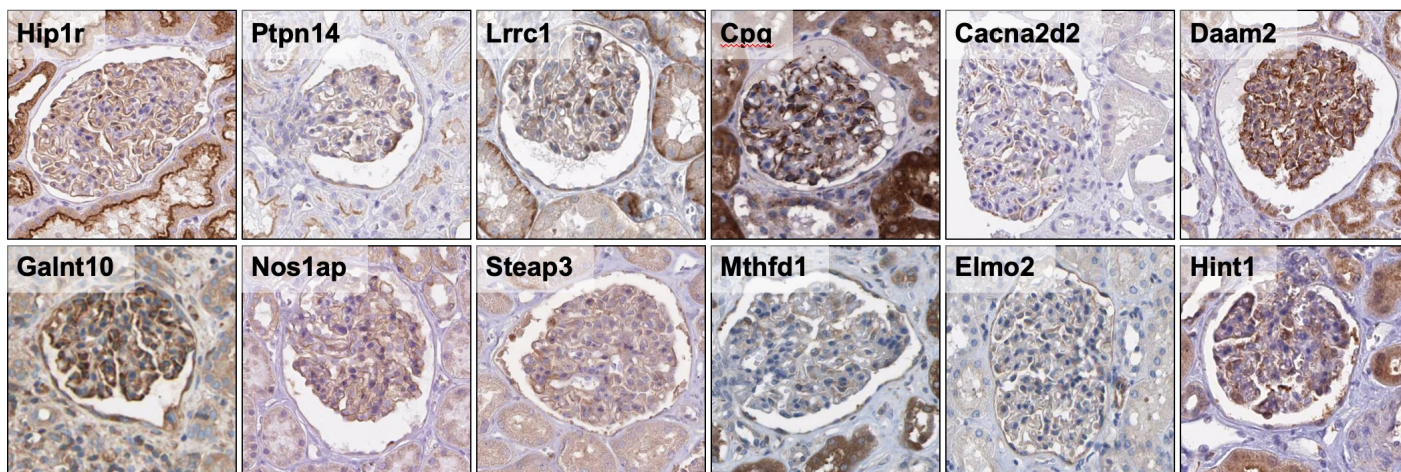
Supplemental figure 5: Comparison of FACS sort between mT/mG mice and wildtype mice. (A) Percentage of podocytes, mesangial, and endothelial cells FACS-sorted from the isolated glomerular cells per mouse and **(B)** Absolute number of podocytes, mesangial, and endothelial cells FACS-sorted from the isolated glomerular cells per mouse, mean \pm SD, $n \geq 23$, pooled data from 18 independent experiments. Empty bars represent wildtype mice, striped bars mT/mG mice.

A**B**

Supplemental figure 6: FACS sorted glomerular cells are not contaminated with parietal epithelial cells or tubular cells. (A) Real-time qPCR analysis exhibiting the expression of genes of interest (GOI) specific for parietal epithelial cells: *Lad1* (encodes for Ladinin) and *Scin* (encodes for Scinderin); and specific of tubular cells: *Aqp4* (encodes for Aquaporin 4) and *Slc12a3* (encodes for sodium chloride channel NCC). mRNA was isolated from FACS-sorted podocytes (red bars), mesangial cells (blue bars), endothelial cells (green bars), and from isolated glomeruli (grey bars) derived from the same individual. Δ CT values were calculated using 18S as home keeper. $\Delta\Delta$ CT values were calculated as difference between glomerular and FACS-sorted cell type Δ CT. Displayed is the relative expression (RE, $2^{-(\Delta\Delta CT)}$) of FACS-sorted cell types in percent of the glomerular RE. Note the significant decrease of cell-specific transcripts in the FACS sorted cell-types compared to the glomerulus, mean \pm SEM, *** p <0.005; **** p <0.0001, $n=4$, tested for statistical significance with ordinary one-way ANOVA and Bonferroni's multiple comparisons test. (B) Glomerular cells from naïve BALB/c mice were separated by timMEP, loaded in a cell number-adapted manner and analyzed for Claudin1 and Nephrin levels by Western blot. β -Actin served as a loading control, isolated glomeruli from the same mice were loaded as positive control. Gloms = glomeruli, PCs = podocytes, MCs = mesangial cells, ECs = endothelial cells. The dotted line separates two different exposure times (indicated in the figure i.e., as 40'' = 40 seconds, 12' = 12 minutes) of the same membrane as the signal for Nephrin and β -Actin in isolated glomeruli required a shorter exposure than in timMEP isolated cell types due to the higher protein abundance. Note the very late occurrence of Claudin1 signal in the glomerular preparations (in relation to Nephrin) since glomeruli were mostly decapsulated and note the absence of Claudin1 in timMEP isolated podocytes.

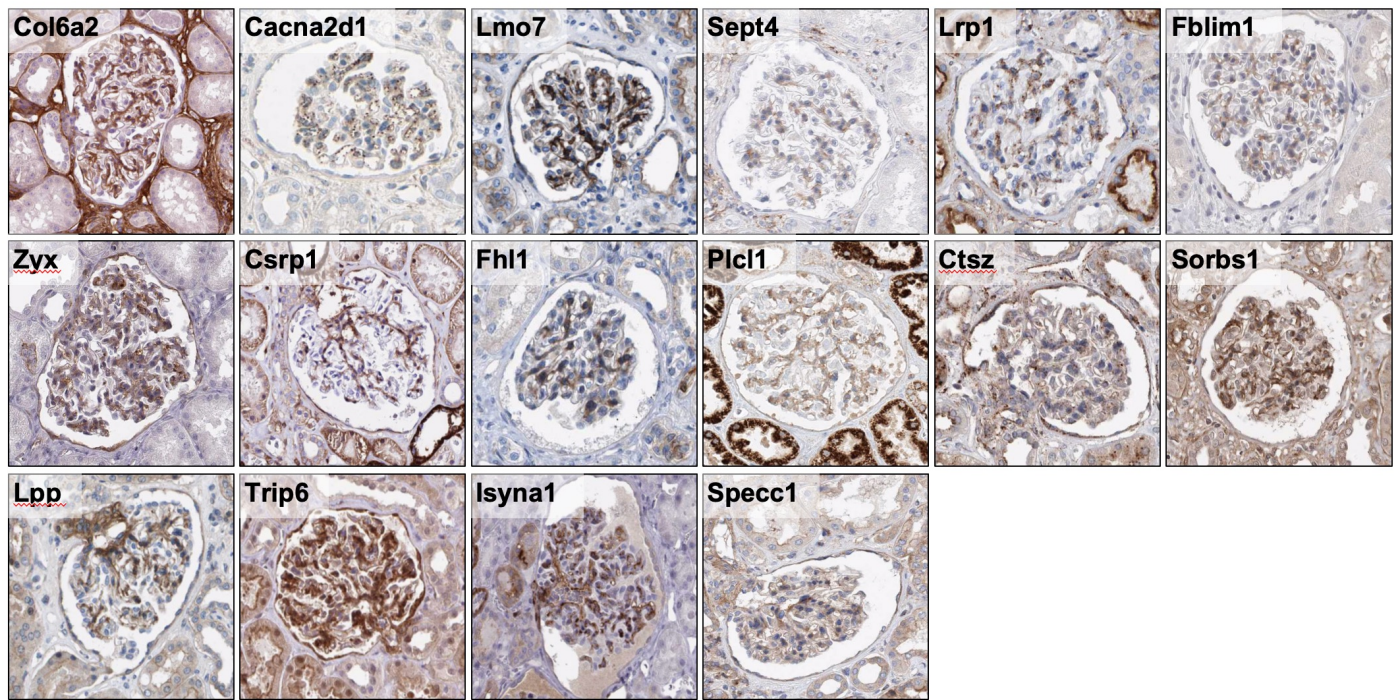


Supplemental figure 7: Tripartite cell type isolation and proteomic analysis from mT/mG mice. Visualization of significant protein-protein interaction networks in original (green) and linker (violet) proteins.



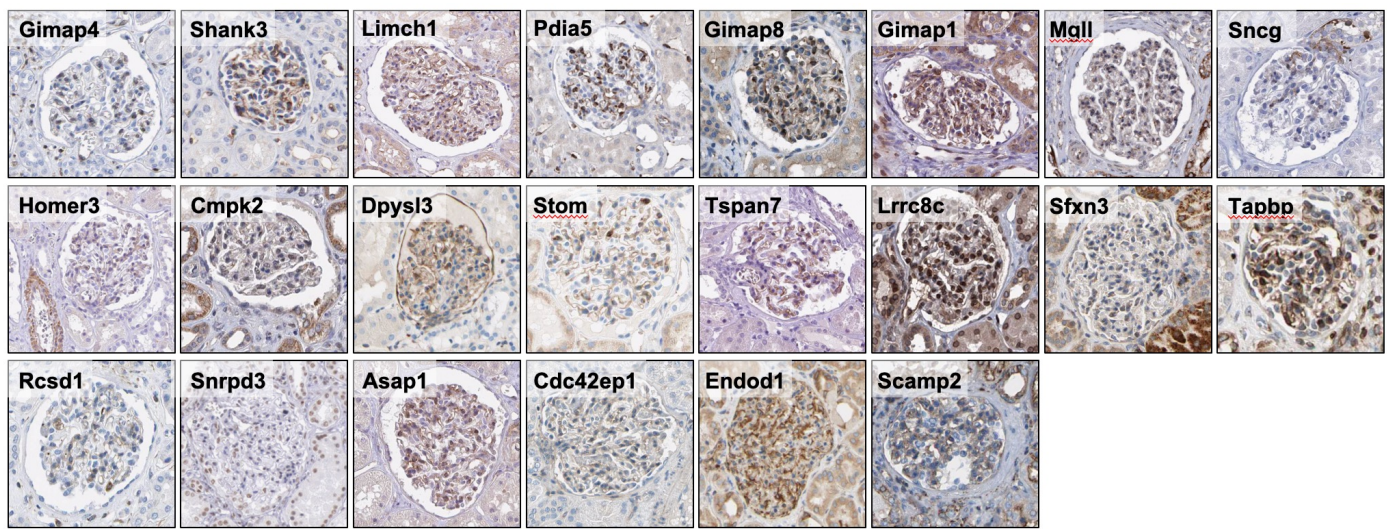
Protein	Protein ID	Function (PMID)
Hip1r	Q9JKY5	<i>Huntingtin-interacting protein 1-related protein</i> ; Actin binding protein involved in clathrin mediated endocytosis (10613908); Isolog of huntingtin interacting protein (9852681)
Ptpn14	Q62130	<i>Protein tyrosine phosphatase, nonreceptor-type 14</i> ; Coimmunoprecipitates with VEGFR3 (136352)
Lrrc1	Q80VQ1	<i>Leucine-rich repeat-containing protein 1</i> ; Interacts with DLG1 (601014) and PSD95 (602887)
Cpq	Q9WVJ3	<i>Carboxypeptidase Q</i> ; Has significant glutamate carboxypeptidase activity (10206990)
Cacna2d2	Q6PHS9	<i>Calcium channel, voltage-dependent, alpha 2/ delta subunit 2</i> ; Confers modulation of presynaptic function (22678293)
Daam2	Q80U19	<i>Dishevelled-associated activator of morphogenesis 2</i> ; Member of the formin family, regulates actin and cytoskeletal dynamics and cell elongation (22275430)
Galnt10	Q6P9S7	<i>Membrane-bound polypeptide N-acetylgalactosaminyltransferase</i> ; Catalyzes the first step in mucin-type O-glycosylation of peptides in the Golgi (20977886)
Flot2	Q60634	<i>Flotillin 2</i> ; Human epidermal surface antigen-1, copurifies with Caveolin-1 (601047)
Nos1ap	Q9D3A8	<i>Nitric oxide synthasae 1 (neuronal) adaptor protein</i> ; Inhibition of L-type calcium channels (114205); Regulation of dendrite number (19553464)
Steap3	A0A0R4J1G9	<i>Six-transmembrane epithelial antigen of prostate 3/Tsap6</i> ; Involved in exosome secretion (18617898)
Mthfd1	Q922D8	<i>Methylenetetrahydrofolate dehydrogenase 1</i> ; Mutations associated with combined immunodeficiency and megaloblastic anemia (27707659) and neuronal tube defects (12384833)
Elmo2	Q8BHL5	<i>Engulfment and cell motility gene 2</i> ; Phagocytosis and cell migration (11595183)
Hint1	P70349	<i>Histidine triad nucleotide binding protein 1/PKCI1</i> ; Interacts with PKC-beta, Mutations associated with axonal neuropathy and neuromyotonia (22961002)

Supplemental figure 8: Identification of new podocyte enriched proteins. To identify new podocyte enriched proteins, glomerular cell types proteome lists of individual mice were compared. For the comparisons we defined 1) a Student t-test difference cut-off of log2-fold change of 2 between podocytes and non-podocytes, 2) a negative search result in pubmed (<https://www.ncbi.nlm.nih.gov/pubmed>; i.e., with the keywords “protein of interest” and “podocyte”) and 3) a validated podocyte expression pattern in the human protein atlas (<https://www.proteinatlas.org/search>), from which the histological micrographs are taken from. The table very briefly summarizes what is known for the identified proteins in other non-glomerular cell types, PMID = pub med identification number.



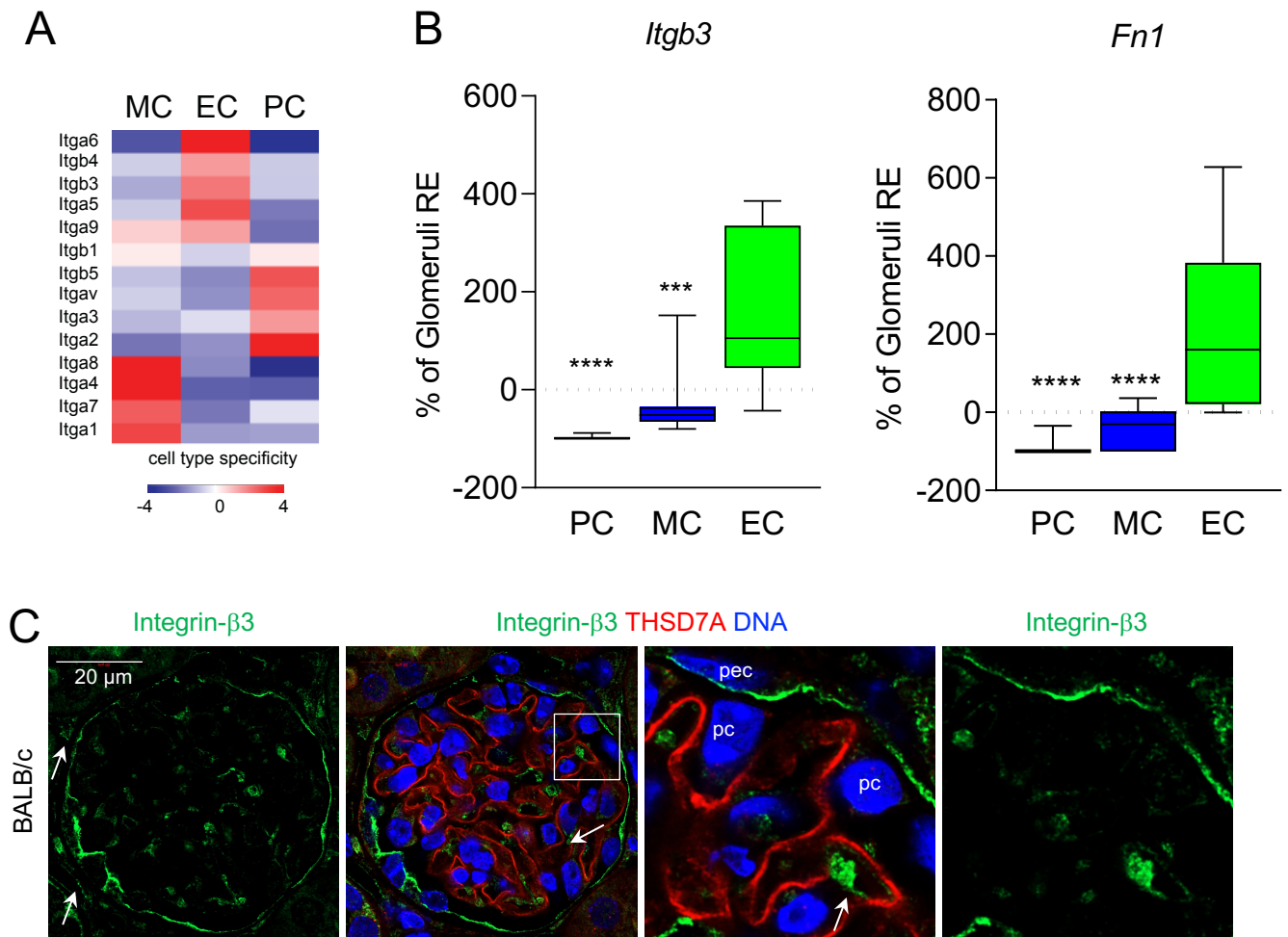
Protein	Protein ID	Function (PMID)
Col6a2	Q02788	<i>Collagen, type VI, alpha 2</i> ; Integrity of muscle fibres (9817932); Mutations associated with muscle dystrophy (12840783) and myopathy (8782832)
Cacna2d1	O08532	<i>Calcium channel, voltage-dependent, alpha 2/ delta subunit 1</i> ; Alters properties of the pore-forming alpha 1 subunit of voltage gated calcium channels (10534405, 17088553)
Lmo7	F6VG99	<i>Lim domain only 7</i> ; Involved in protein-protein interactions, shuttles between cytoplasm and nucleus (17067998)
Sept4	P28661	<i>Septin 4</i> ; Polymerizing GTP-binding protine that scaffolds molecules beneath the plasma membrane; Colocalizes with alpha-synuclein in Lewy bodies (15737930; 17296554)
Lrp1	A0A0R4J0I9	<i>Low density lipoprotein receptor related protein 1</i> ; Interacts and traffics with APP (15749709)
Fblim1	Q71FD7	<i>Filamin-binding LIM protein 1</i> ; Localizes to cell-ECM adhesions, associates with actin filaments and is essential for cell shape modulation (12679033)
Zyx	Q62523	<i>Zyxin</i> ; Phosphoprotein concentrated at adhesion plaques and along actin filament bundles near where they insert at the adhesion plaques (8940160)
Csrp1	P97315	<i>Cysteine- and glycine-rich protein 1</i> ; Highly conserved, cell cycle regulated gene induced in the immediate early response to serum replation in serum-starved noncycling cells (1385304)
Fhl1	A2AEX8	<i>Four-and-a-half LIM domains 1</i> ; Mutations associated with faciocardiomusculoskeletal syndrome (11102932), X-linked myopathy (18274675)
Plcl1	Q3USB7	<i>Phospholipase C-like 1</i> ; Negative regulation of bone formation (21757756)
Ctsz	Q9WUU7	<i>Cathepsin Z</i> ; member of papain family of cystein proteinases (9642240)
Sorbs1	Q62417	<i>Sorbin and SH3-domains containing protein 1</i> ; Required for insulin-stimulated GLUT4 translocation (11309621)
Lpp	Q8BFW7	<i>LIM domain -containing preferred translocation partner in lipoma</i> ; Most frequent translocation partner of HMGA2 in a subgroup of lipomas (15755872)
Trip6	Q9Z1Y4	<i>Thyroid hormone receptor interactor 6</i> ; Contains 2 LIM domains (601329) and is similar to zyxin (602002)
Isyna1	Q9JHU9	<i>Inositol -3-phosphate synthase 1</i> ; Component of plasma membrane phospholipids and functions as a cell signaling molecule
Specc1	A0A0J9YTU3	<i>Sperm antigen with calponin homology and coiled-coil domains 1</i> ; Function in head and neck tumors (22170762)

Supplemental figure 9: Identification of new mesangial cell enriched proteins. To identify new mesangial cell enriched proteins, glomerular cell types proteome lists of individual mice were compared. For the comparisons we defined 1) a Student t-test difference cut-off of log2-fold change of 2 between mesangial cells and non-mesangial cells, 2) a negative search result in pubmed (<https://www.ncbi.nlm.nih.gov/pubmed>; i.e., with the keywords “protein of interest” and “mesangial”) and 3) a validated mesangial expression pattern in the human protein atlas (<https://www.proteinatlas.org/search>), from which the histological micrographs are taken from. The table very briefly summarizes what is known for the identified proteins in other non-glomerular cell types, PMID = pub med identification number.

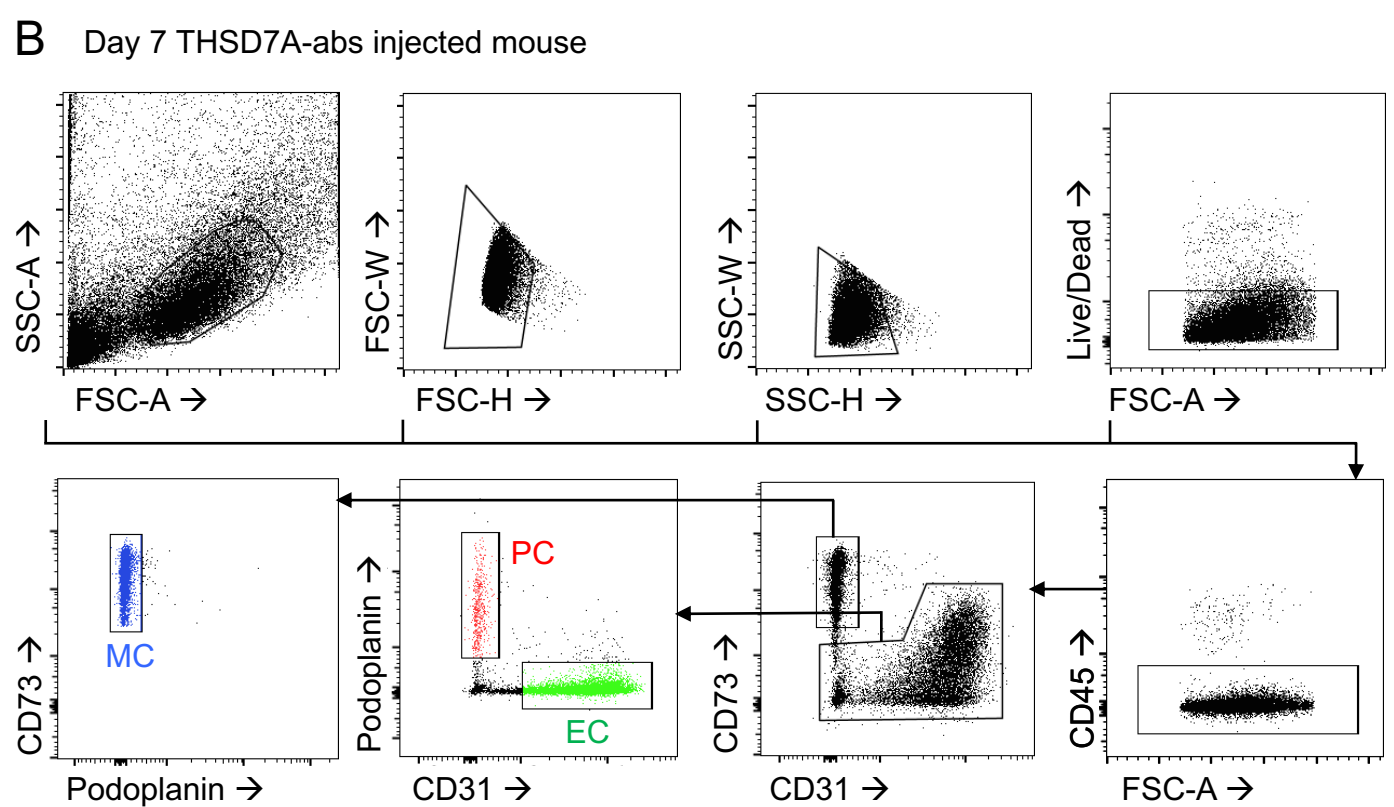
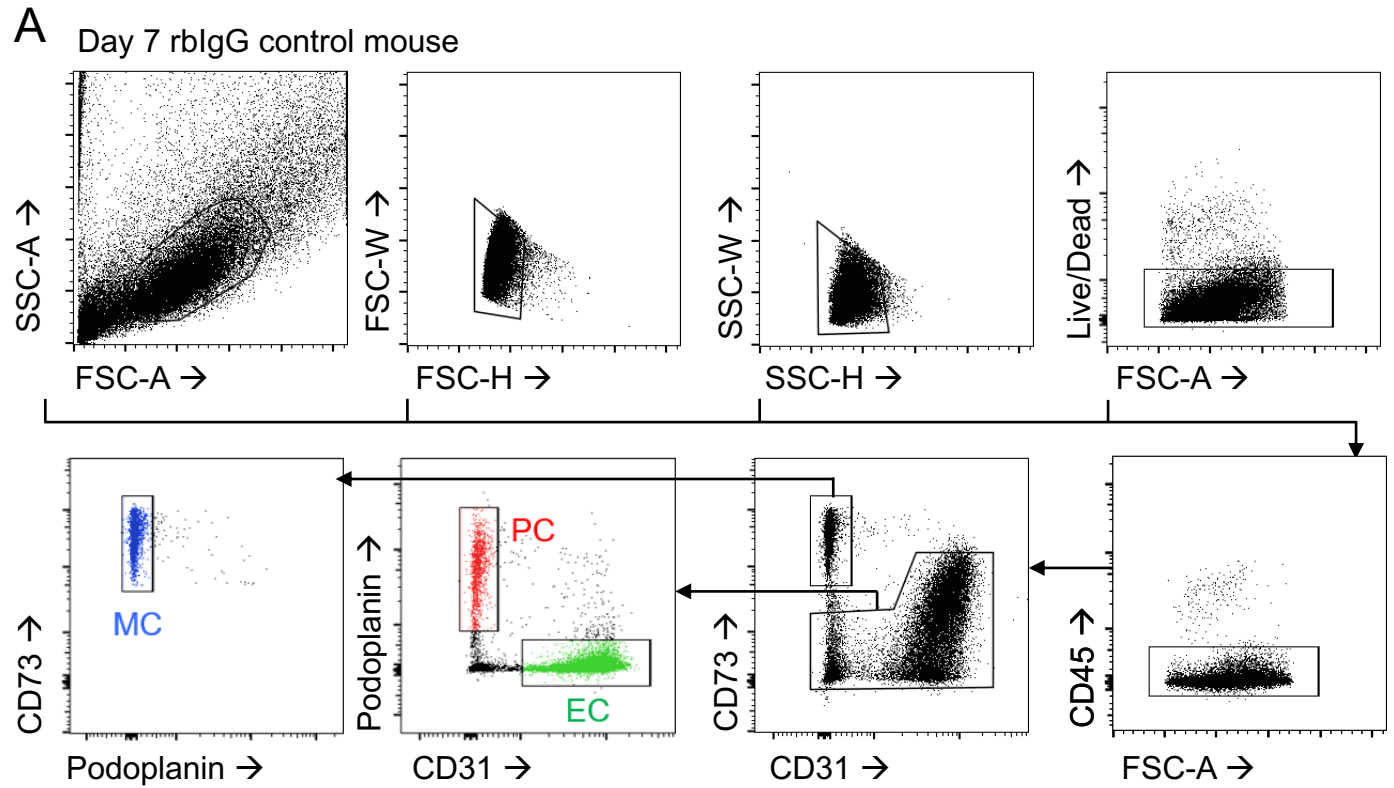


Protein	Protein ID	Function (PMID)
Gimap4	Q99JY3	<i>GTPase, Immunity-associated protein 4</i> ; IFN γ secretion regulation from T cells (25287446), regulation of T cell survival (16569770)
Shank3	Q4ACU6	<i>SH3 and multiple ankyrin repeat domains 3</i> ; Scaffolding protein enriched in postsynaptic densities of excitatory synapses (26966193)
Limch1	Q3UH68	<i>LIM and calponin homology domains-containing protein 1</i> ; Actin stress fibre-associated protein that regulates nonmuscle myosin II (MYH9) activity (28338547)
Pdia5	Q921X9	<i>Protein disulfide isomerase family A, member 5</i> ; ER-resident protein that catalyzes oxidation, reduction, and isomerization of protein disulfide bonds which accelerates protein folding (24636989)
Gimap8	Q75N62	<i>GTPase, Immunity-associated protein 8</i> ; Regulator of lymphocyte survival and homeostasis (23454188)
Gimap1	Q3TFI6	<i>GTPase, Immunity-associated protein 1</i> ; Survival of peripheral T cells (287792288) and B cells (26621859)
Mgl1	E9Q3B9	<i>Monoglyceride lipase</i> ; Functions together with hormone sensitive lipase to hydrolyze intracellular triglyceride stores to fatty acids and glycerol (11470505)
Sncg	Q9Z0F7	<i>Synuclein gamma</i> ; Highly expressed in neurons, correlation of overexpression and breast cancer progression (10813729)
Homer3	Q99JP6	<i>Homer scaffold protein 3</i> ; Cytoplasmic scaffolding protein that binds to metabotropic glutamate receptors (9069287) and interacts with Shank (19345194)
Cmpk2	Q3U5Q7	<i>Cytidine monophosphate kinase 2</i> ; Mitochondrial UMP-CMP kinase component of the salvage pathway for nucleotide synthesis (17999954)
Dpysl3	E9PWE8	<i>Dihydropyrimidinase-like 3</i> ; Role in neurite and axonal outgrowth (23568759), modulates mitosis migration and epithelial to mesenchymal transition (30498031)
Stom	P54116	<i>Stomatin</i> ; Modulates activity of anion exchanger 1 (28387307), tumor suppressor (31949395) and enhancer of cell fusion when associated with lipid rafts (27663861)
Tspan7	Q3UHG5	<i>Tetraspanin 7</i> ; Contributes to molecular complexes that include β 1-integrin (10655063), TSPN7 autoantibodies in diabetes type 1 (27221092)
Lrrc8c	Q8R502	<i>Leucine-rich repeat-containing protein 8C</i> ; B cell development (15094057) and adipocyte differentiation (15184384)
Sfxn3	Q91V61	<i>Sideroflexin 3</i> ; Mitochondrial serine transporter (30442778), α -synuclein dependent that regulates synaptic morphology (28049716)
Tapbp	Q3TCU5	<i>Tap-binding protein</i> ; Type 1 transmembrane protein encoded by an MHC-linked gene (8769474) in the ER, edits peptide loading onto MHC1 (32167472)
Rcsd1	Q3UZA1	<i>RCSD domain-containing protein 1</i> ; Interacts with F-actin capping protein Capz (601580)
Snrpd3	P62320	<i>Small nuclear ribonucleoprotein polypeptide D3</i> ; Part of snRNP core
Asap1	H3BL41	<i>ARF GTPase-activating protein with SH3 domain, ankyrin repeat and PH domain 1</i> ; Coordinates actin and membrane remodeling (25774636)
Cdc42ep1	Q91W92	<i>CDC42 effector protein 1</i> ; Mediates actin cytoskeletal reorganization at the plasma membrane (10430899)
Endod1	Q8C522	<i>Endonuclease domain-containing 1</i> ; Tumor suppressor in prostate cancer (28532481)
Scamp2	Q9ERN0	<i>Secretory carrier membrane protein 2</i> ; Regulates cell membrane targeting of NHE5 (19276089) and NKCC2 (21205824), role in granule exocytosis (12475951)
Gimap4	Q99JY3	<i>GTPase, Immunity-associated protein 4</i> ; IFN γ secretion regulation from T cells (25287446), regulation of T cell survival (16569770)

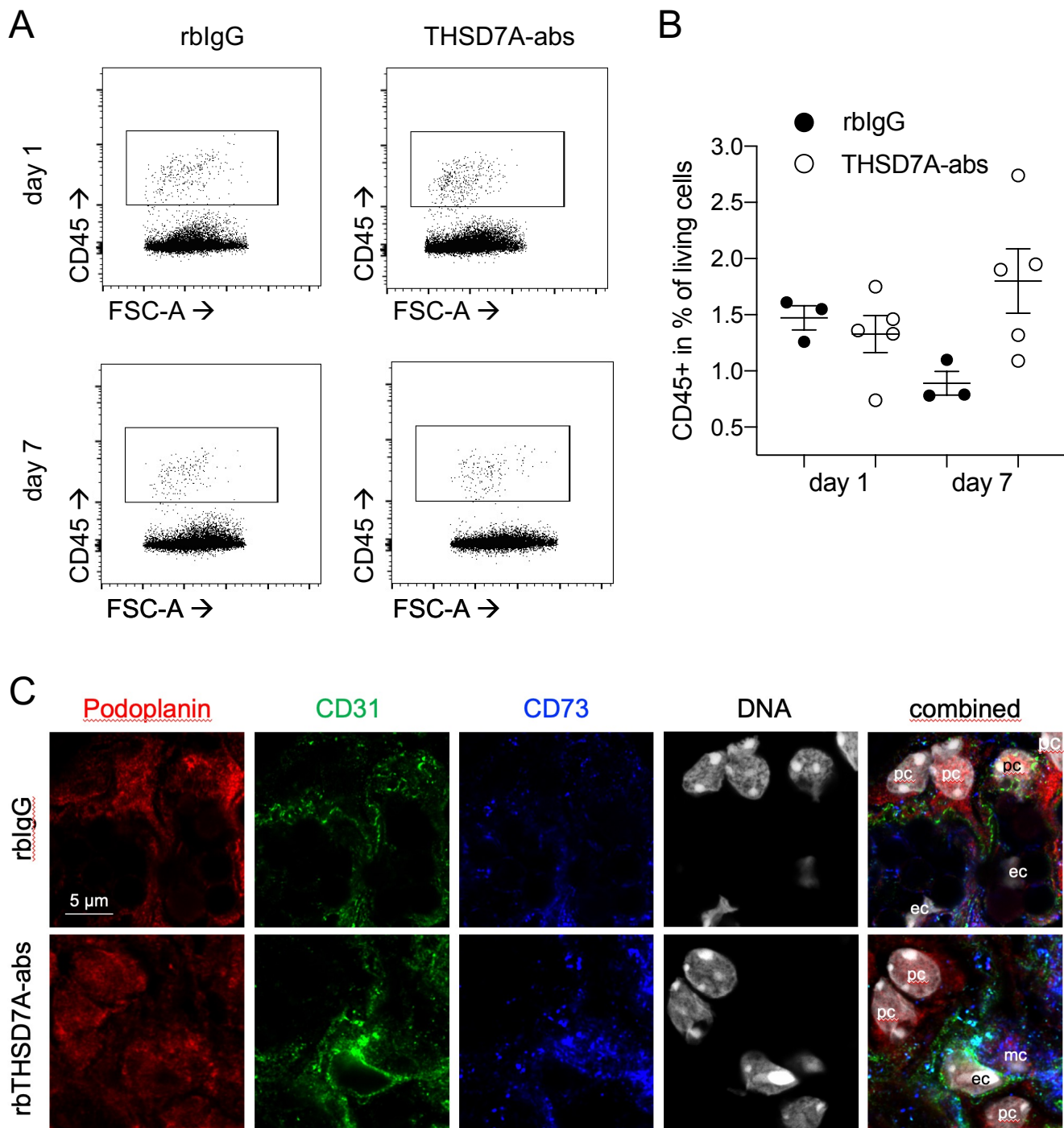
Supplemental figure 10: Identification of new glomerular endothelial cell enriched proteins. To identify new glomerular endothelial cell enriched proteins, glomerular cell types proteome lists of individual mice were compared. For the comparisons we defined 1 a Student t-test difference cut-off of log₂-fold change of 2 between endothelial cells and non-endothelial cells, 2) a negative search result in pubmed (<https://www.ncbi.nlm.nih.gov/pubmed>; i.e., with the keywords “protein of interest” and “endothelial”) and 3) a validated glomerular endothelial expression pattern in the human protein atlas (<https://www.proteinatlas.org/search>), from which the histological micrographs are taken from. The table very briefly summarizes what is known for the identified proteins in other non-glomerular cell types, PMID = pub med identification number.



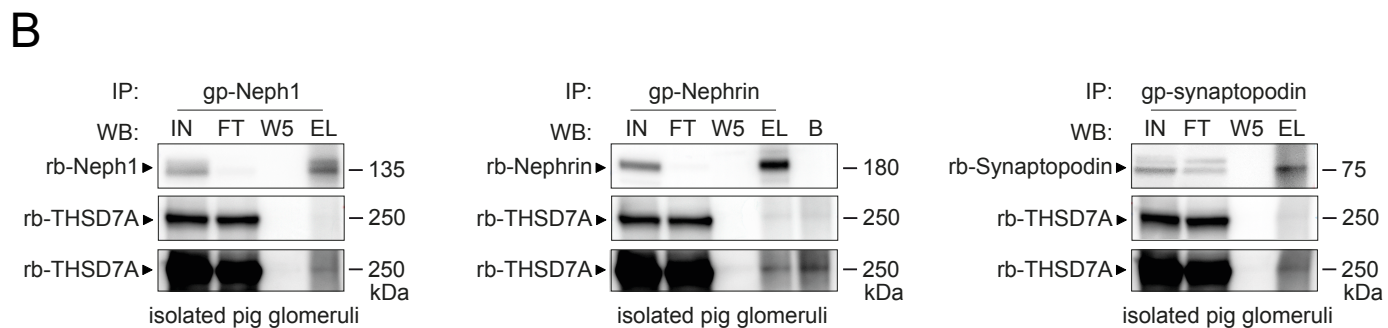
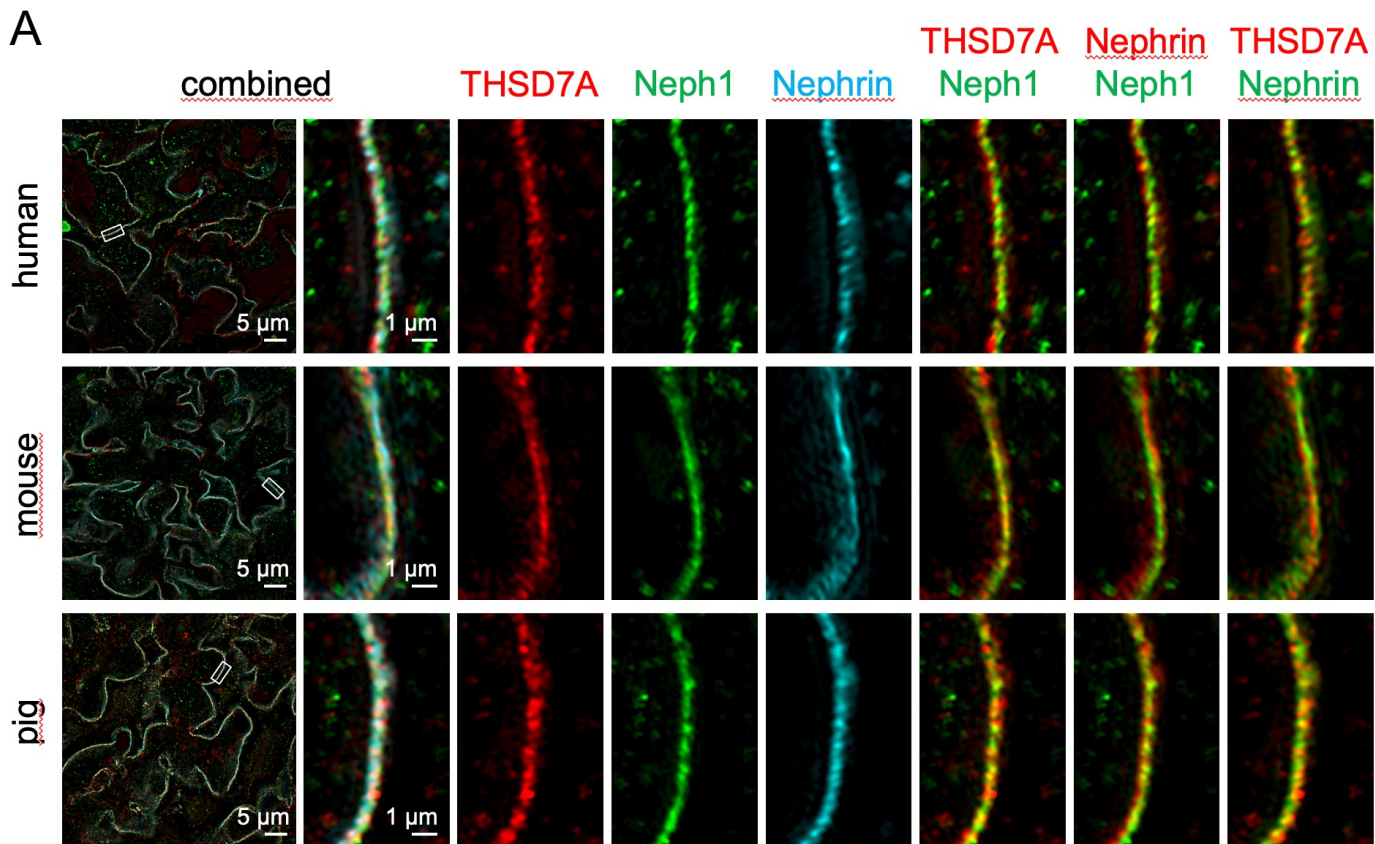
Supplemental Figure 11: Integrin- β 3 and its ligand Fibronectin 1 are predominantly expressed on glomerular endothelial cells. (A) Heatmap showing euclidean distance clustering of single-mouse single shot proteomics results of Integrins in timMEP isolated glomerular cell-types of mT/mG mice. (B) Integrin- β 3 (*Itgb3*) and Fibronectin (*Fn1*) transcript levels were quantified in FACS sorted glomerular cells relative to total glomeruli transcript levels in untreated BALB/c mice. Values are expressed as mean \pm SEM, N = 10 per group, *** p <0.001 and **** p <0.0001 to podocytes (PC), One Way ANOVA, Bonferroni's multiple comparison test. MC = mesangial cells, EC = glomerular endothelial cells. (C) Representative high-resolution confocal microscopy of Integrin- β 3 (green) expression in a BALB/c glomerulus in combination with THSD7A (red) to demarcate the podocyte foot processes and DNA (blue). Arrows point towards Integrin- β 3 expression in endothelial cells, pc = podocyte, pec = parietal epithelial cell.



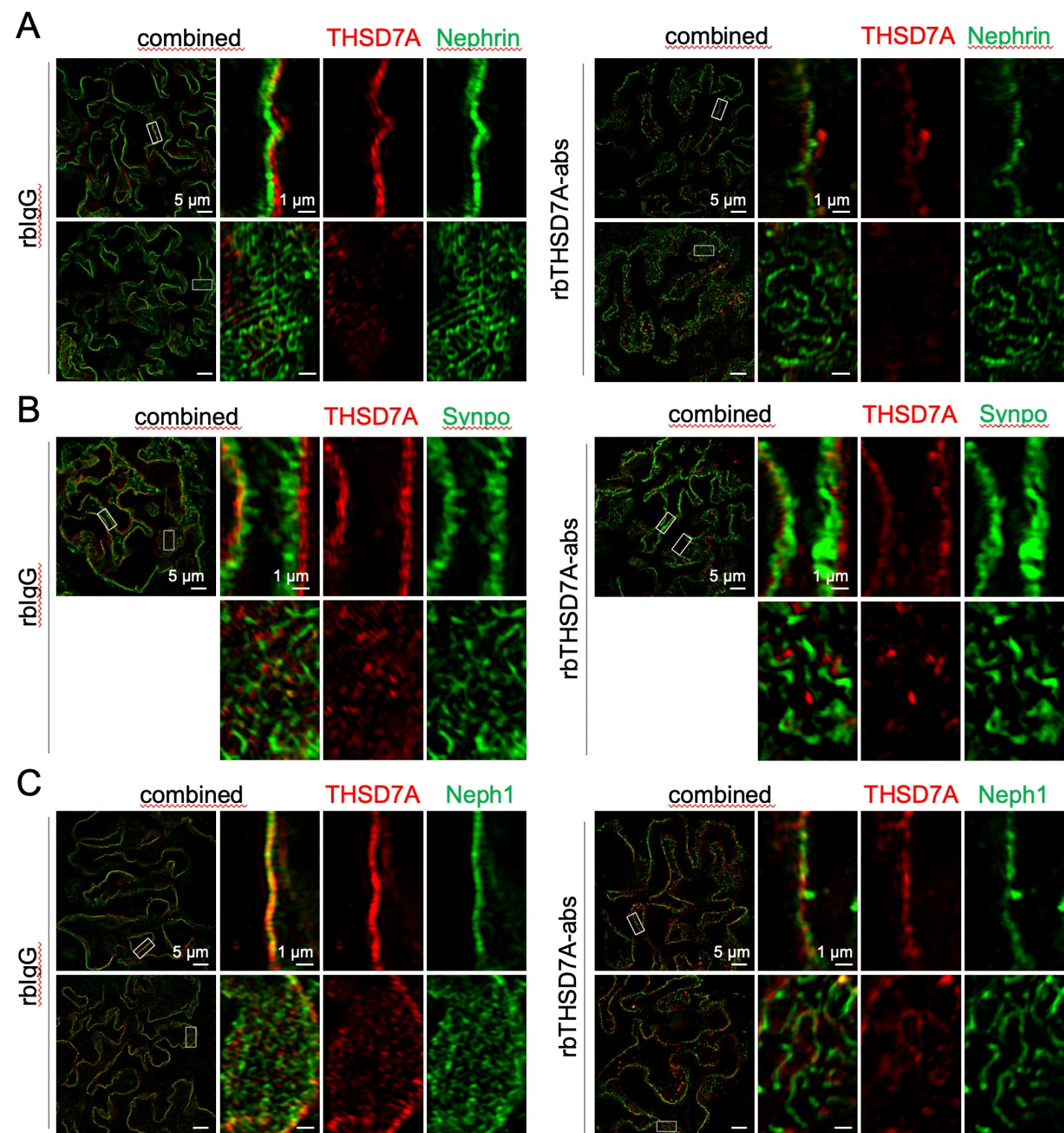
Supplemental figure 12: Gating strategy used for the separation of glomerular cell types in the mouse model of anti-THSD7A membranous nephropathy. Individual mouse FACS plots are shown of a (A) unspecific rabbit IgG injected control mouse on day 7 and (B) a nephrotic anti-THSD7A-antibody injected mouse on day 7. CD45 was added to the FACS panel to remove potential contaminating leukocytes in the setting of glomerulonephritis.



Supplemental figure 13: Leukocytes are not increased in glomeruli in the setting of experimental THSD7A-associated membranous nephropathy. Experimental THSD7A membranous nephropathy was induced by injection of rabbit-anti-THSD7A antibodies or unspecific control rabbit IgG to male BALB/c mice and analyzed on day 1 and 7. **(A)** Representative FACS plots for CD45 at day 1 and day 7. **(B)** Quantification of CD45+ leukocytes in % of all living glomerular single cells on day 1 and day 7. **(C)** Confocal micrographs depicting labeled podocytes (Podoplanin, red), endothelial cells (CD31, green) and mesangial cells (CD73, blue) in a 4% PFA fixed frozen section of a murine kidney, DNA was visualized using Hoechst, pc = podocyte, mc = mesangial cell, ec = endothelial cell.



Supplemental figure 14: THSD7A localizes closely to the slit diaphragm proteins Neph1 and Nephrin but does not directly interact under native conditions. (A) Paraffin sections from healthy human, mouse, and pig kidneys were stained for THSD7A (gt-Cy3), Neph1 (rb-Cy2), and Nephrin (gp-Cy5) and analyzed for proximity by SR-SIM high-resolution microscopy. Note the close proximity of all three proteins in the frontal plane of the glomerular filtration barrier. (B) Glomeruli were isolated from native pig kidneys by sieving. Guinea pig (gp)-Nephrin, gp-Neph1 and gp-Synaptopodin (as negative control) antibodies were used for immunoprecipitation. Western blot detection was performed with rabbit (rb)-THSD7A, rb-Nephrin, rb-Neph1 and rb-Synaptopodin antibodies; two exposure times are shown for THSD7A (middle panel: short exposure time, lower panel: long exposure time); IN = input, FT = flow through, W5 = wash 5, EL = elution, B = beads only as an additional negative control. Note the successful immunoprecipitation of Neph1, Nephrin and Synaptopodin from pig glomeruli. A band at 250 kDa at the height of THSD7A is seen in all three elutions, however also in the bead only control and in the presumable Synaptopodin negative control, suggesting a non-specific co-precipitation of THSD7A.



Supplemental figure 15: Differential loss of podocyte proteins in experimental THSD7A-associated membranous nephropathy. Experimental THSD7A membranous nephropathy was induced by injection of rabbit-anti-THSD7A antibodies or unspecific control rabbit IgG to male BALB/c mice and analyzed on day 7 by SR-SIM high-resolution microscopy. **(A)** Co-staining of Nephrin (green) and THSD7A (red), **(B)** co-staining of Synaptopodin (green) and THSD7A (red), **(C)** co-staining of Neph1 (green) and THSD7A (red).

2. Dissertation

2.1. Einleitung

2.1.1. Anatomie der Niere und des Nierenkörperchens

Die Niere ist ein zentrales Organ des Menschen mit einer Fülle an Aufgaben, darunter die Regulierung des Blutdruckes und die Filtration des Blutes. Makroskopisch unterteilt sich die Niere in die Rinde, das Mark und das Nierenbeckenkelchsystem. Die kleinste funktionelle Einheit der Niere ist das Nephron. Das Nephron setzt sich aus dem Nierenkörperchen und dem Nierentubulus zusammen. Das Nierenkörperchen liegt in der Nierenrinde und besteht aus zwei Bestandteilen: einer Kapillarschlinge, Glomerulus genannt, und der sie umgebenden Bowman-Kapsel.(Deetjen and Alzheimer, 2005, p. 516; Klink et al., 2010, p. 330).

Die Filtration des Blutes findet in zwei Phasen statt: der Bildung von Primärharn in den Glomeruli sowie der Resorption von Wasser und Elektrolyten und damit der gleichzeitigen Aufkonzentrierung des Harns im tubulären System. Innerhalb der Glomeruli findet die Primärfiltration des Blutes an einer einzigartigen anatomischen Struktur statt - der glomerulären Filtrationsbarriere.(Klink et al., 2010, p. 340)

Die glomeruläre Filtrationsbarriere setzt sich aus drei Schichten zusammen: dem Endothel der Kapillaren, der Basalmembran und der Schlitzmembran. Das Endothel ist fenestriert, das heißt es formt Aussparungen zwischen den Zellen die Poren bilden, durch die das Blutplasma, nicht aber die korpuskulären Anteile des Blutes hindurchtreten können.(Klink et al., 2010, p. 340) Darauf folgend liegt zwischen dem Endothel und den Podozyten eine Basalmembran, welche durch ihre negative Ladung den größten Teil der Eiweiße zurückhält.(Klink et al., 2010, p. 343) Die letzte Schicht formt die von den Podozyten gebildete Schlitzmembran,(Herwig et al., 2019; Kocylowski et al., 2022) bevor der nun proteinarme Primärharn in den Bowman-Kapselraum und kurz darauf in das tubuläre System weiterströmt.

Das Glomerulus besteht aus einem Kapillarknäuel des bereits erwähnten fenestrierten Endothels und den Podozyten, welche als hochdifferenzierte viszerale Epithelzellen die Gegenseite des Kapillarknäuels und damit die Innenseite des Bowman-Kapselraumes auskleiden. Zwischen den Schlingen der Kapillaren befinden sich die Mesangialzellen.(Deetjen and Alzheimer, 2005, p. 516; Klink et al., 2010, p. 330)

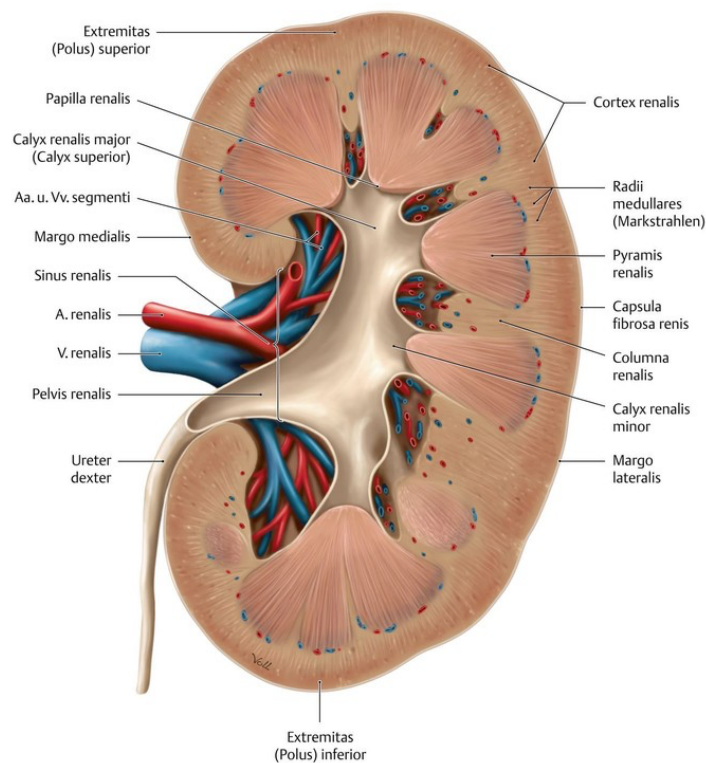


Abbildung 1: Längsschnitt einer menschlichen Niere. Die Filtration des Primärharns erfolgt in den Nierenkörperchen, welche sich im Nierenkortex befinden.

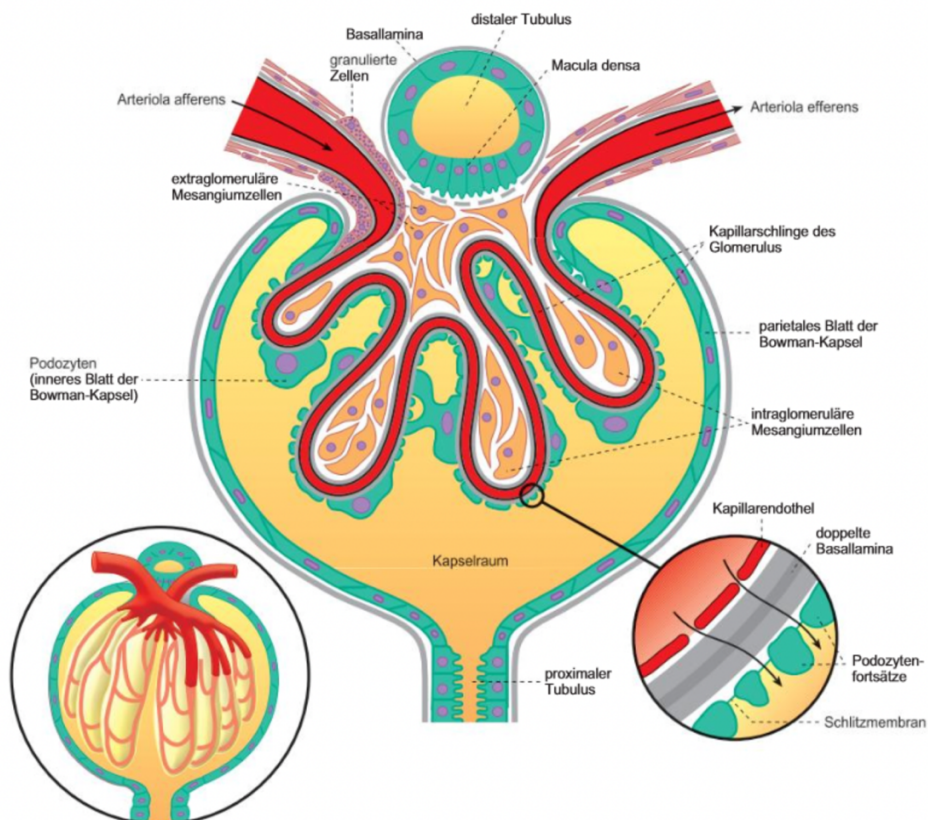


Abbildung 2: Schematische Darstellung eines Nierenkörperchens. **Links:** Blick auf das Nierenkörperchen. **Mitte:** Längsschnitt durch das Nierenkörperchen mit Darstellung der räumlichen Beziehung von Mesangium, Endothel und Podozyten.

Rechts: Filtrationsbarriere bestehend aus dem Endothel und den Podozyten und der dazwischenliegenden glomerulären Basalmembran.

2.1.2. Die Zellen des Glomerulus

2.1.2.1. Podozyten

Die Podozyten bilden das viszerale Blatt der Bowman-Kapsel und spannen sich über den kompletten primärharnseitigen Glomerulus. Sie besitzen eine charakteristische morphologische Struktur: Aus dem Zellkörper gehen Primärfortsätze hervor, aus denen wiederum Sekundärfortsätze (Fußfortsätze) entspringen, welche sich mit den Sekundärfortsätzen benachbarter Podozyten verzahnen. Dabei lassen sie eine Lücke von circa 30 - 40 Nanometer, wodurch ein physikalischer Filter entsteht. Im Interzellularraum zwischen den Fortsätzen befindet sich eine zweischichtig organisierte Struktur: die Schlitzmembran. Sie wird durch verschiedene Proteine gebildet, unter anderem Nephrin und Podocin, die auf bzw. an der Extrazellulärmembran der Fußfortsätze lokalisiert sind und dem jeweils gegenüberliegenden Fußfortsatz entgegenragen. Die Schlitzmembran erfüllt mehrere Aufgaben: Sie ist ein makromolekularer Filter, sie dient als Anker des Filters in der Basalmembran und ist darüber hinaus auch ein Signalkomplex, der die Plastizität der Fußfortsätze reguliert. (Butt et al., 2020; Kocylowski et al., 2022)

2.1.2.2. Mesangialzellen

Der Raum zwischen den Kapillaren wird von Mesangialzellen und ihrer Extrazellulärmatrix ausgefüllt. Durch Kontraktion und Relaxation sind diese Zellen in der Lage, die strukturelle Integrität des Kapillarknäuels aufrecht zu erhalten und können darüber hinaus die Wandspannung der Kapillaren regulieren. (Kurihara and Sakai, 2017; Welsch and Sobotta, 2009, p. 456)

2.1.2.3. Endothelzellen

Endothelzellen bilden die Gefäßwände im gesamten Körper aus. Die Endothelzellen des Kapillarknäuels des Glomerulus gehören einer besonderen Unterart an: dem fenestrierten Endothel. Die Zellen bilden unvollständige Zell-zu-Zell-Verbindungen aus, wodurch Poren in den Gefäßwänden entstehen. Die Poren des Endothels messen zirka 70-100 Nanometer und sind zu klein für den Durchtritt der zellulären Bestandteile des Blutes. (Welsch and Sobotta, 2009, p. 456)

2.1.3. Podozyten, Mesangial- und Endothelzellen im Kontext glomerulärer Pathologien

Der Funktionsverlust eines einzigen dieser Zelltypen kann in dem Verlust der Filtration des Glomerulus resultieren, was sich durch Proteinurie äußert. Sind zu viele Glomeruli der Nieren betroffen, resultiert klinisch das nephrotische Syndrom.

Die Feststellung, dass bereits der Verlust einer Zellart genügt, um Proteinurie zu verursachen, führte zu der Hypothese, dass die glomerulären Zellarten untereinander kommunizieren. (Dimke et al., 2015) In-silico Auswertungen von transcriptomics Studien unterstreichen die Hypothese einer interzellulären Kommunikation im

Glomerulus, welche jedoch bisher experimentell nur schwer evaluiert werden konnte. Ursächlich dafür ist eine für proteinbiochemische Untersuchungen benötigte große Zellzahl der glomerulären Zellarten.

Daher müsste ein umfassenderer Ansatz die Gewinnung von großen Mengen an glomerulären Zellen aus demselben Individuum ermöglichen, die für beliebige weiterführende molekularbiologische Untersuchungen genutzt werden können.

Die Entwicklung der beads-gestützten Glomerulusisolation durch Takemoto et al. ermöglichte die Erforschung glomerulärer Erkrankungen in bis dato unerreichtem Maßstab.(Takemoto et al., 2002) Diese Methodik wurde soweit verfeinert, dass die Isolation von Podozyten aus Glomeruli möglich wurde, solange dafür bestimmte transgene Mäuse genutzt wurden.(Boerries et al., 2013; Wanner et al., 2014) Diese Reporter-mäuse exprimieren zellspezifisch die fluoreszenten Proteine tandem-dimer-tomato (tdTomato) und enhanced green-fluorescent protein (eGFP), die es ermöglichen, die Zellen in einem fluorescence-activated cell sorter (FACS) voneinander zu trennen. Der Gruppe um Wanner et al. gelang es mithilfe dieser mT/mG (membrane-targeted tdTomato/membrane-targeted eGFP) Mäuse (Muzumdar et al., 2007), die eGFP-exprimierenden Podozyten von allen restlichen tdTomato-exprimierenden Zellen nach der Herauslösung aus den Glomeruli in einem FACS zu sortieren. Erstmals konnten hoch aufgelöste transkriptomik-Studien an Podozyten durchgeführt werden.(Wanner et al., 2014)

Die Anwendbarkeit dieser Methode ist jedoch begrenzt. Sie ist von der Nutzung transgener Tiere abhängig, die allein durch die Expression der fluoreszenten Proteine zwangsläufig ein verändertes Proteom besitzen. Ferner erlaubt sie nur die Unterscheidung zwischen Podozyten und Nicht-Podozyten, sodass sich Effekte zwischen Mesangial- und Endothelzellen nachfolgenden Untersuchungen entziehen. Um diese Zellen gezielt untersuchen zu können, müssten Mäuse neu gekreuzt und gezüchtet werden, ein teurer und zeitaufwendiger Prozess.

2.1.4. Das Ziel meiner Arbeit

Das Ziel meiner Arbeit war die Entwicklung einer universellen Methode zur Isolation muriner glomerulärer Zellarten aus beliebigen Mäusen. Mit der Methode sollten Zellarten in großer Zahl gewonnen werden können, um beliebige weiterführende Untersuchungen durchführen zu können. Ein Gelingen würde Untersuchungen von Podozyten, Mesangial- und Endothelzellen beliebiger Mausmodelle in einem bisher unerreichten Detailgrad erlauben.

2.2. Ergebnisse

2.2.1. Arbeitshypothese

Die zentrale Technologie zum Trennen verschiedener Zelltypen in Zellsuspensionen ist das FACS, mit dem fluoreszierende Zellen voneinander unterschieden und sortiert werden können. In Wildtyp Mäusen exprimiert jedoch kein glomerulärer Zelltyp Fluorochrome, sodass die Zellen manuell anhand Fluorochrom-gekoppelter Antikörper markiert werden müssen. Wir nutzen fluorochrom-gekoppelte spezifische Antikörper gegen spezifische Oberflächenproteine der drei Zelltypen, um sie in

Einzelzellsuspensionen gezielt markieren und mit Hilfe des FACS effektiv voneinander trennen zu können.

Auf Grundlage dieser Hypothese haben wir den Versuchsaufbau wie folgt erarbeitet:

1. Entnahme frischer Mäusenieren und Perfusion dieser mit magnetischen Beads.
2. Isolation der größtmöglichen Zahl an Glomeruli unter Nutzung magnetischer Beads.
3. Auflösung der Glomeruli durch Trennung der Zellen voneinander, um eine Einzelzellsuspension zu schaffen.
4. Markierung der Zellen in der Suspension mit zelltyp-spezifischen fluoreszenzgekoppelten Antikörpern.
5. Sortierung der Zellen in drei reine Zellsuspensionen durch Nutzung eines FACS.

Die Methode wurde von uns „tripartite isolation method for murine mesangial and endothelial cells and podocytes“, kurz timMEP, getauft.

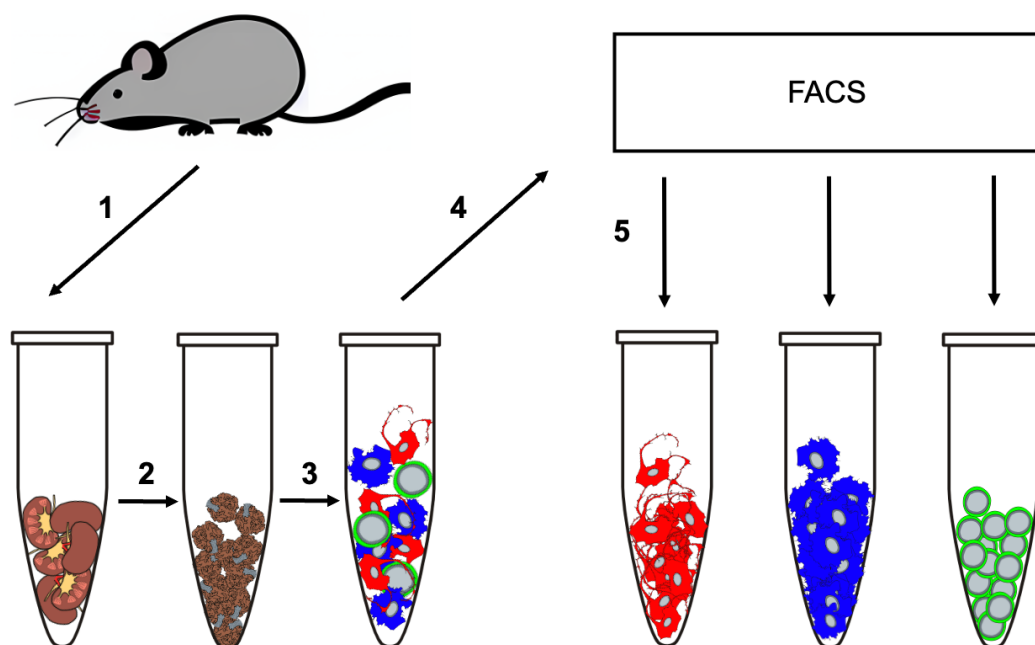


Abbildung 3: Schematischer Ablauf von timMEP. Illustrative Darstellung von Nieren, Glomeruli, Podozyten (rot), Mesangialzellen (blau) und Endothelzellen (grün) **1)** Entnahme frischer Mäusenieren. **2)** Glomeruläre Isolation aus den Nieren. **3)** Auftrennung der Glomeruli in die zellulären Bestandteile. **4)** Markierung der Zellen mit zelltyp-spezifischen fluoreszenzgekoppelten Antikörpern. **5)** Trennung der Zellen in einem FACS.

2.2.2. Tiere

Eines der Ziele meiner Arbeit ist es, die Methode universell an beliebigen Mäusen anwenden zu können, vom gesunden Wildtyp, über transgene Reportermause, bis hin zu kranken Tieren. Um den Fortschritt meiner Experimente besser beurteilen zu können und Vergleichbarkeit zu schaffen, nutzten wir neben Wildtypmausstämmen

BALB/c und C57BL/6 auch die bereits beschriebenen transgenen mT/mG Mäuse. Der Zellisoliationsprozess ist für die drei Mausspezies gleich, jedoch unterscheiden sich die genutzten Fluorochrome und Gatingstrategien, da nur die mT/mG Mäuse eigene Fluorochrome exprimieren, die als Marker genutzt werden können. Das erlaubt es, die aus den Experimenten resultierenden Zellen auch ohne erfolgreiche Markierung mit Antikörpern in einem Durchflusszytometer analysieren zu können.

2.2.3. Isolation von Glomeruli

Die Isolation muriner Glomeruli war bereits bei meiner Ankunft im Labor von Professorin Catherine Meyer-Schwesinger eine fest etablierte, verfeinerte Version der von Takemoto eingeführten, beads-gestützten Extraktion. Bei Beads handelt es sich um kleinste, magnetisierbare Metallkugeln. Die Tiere wurden euthanasiert, ihre Nieren entnommen und mit einer Feinnadel arteriell mit magnetischen Beads perfundiert. Die Beads sind klein genug, um bis in die Kapillarschlingen der Glomeruli zu gelangen, gleichzeitig jedoch zu groß, um diese passieren zu können, sodass sie sich in den Glomeruli anreichern. Danach folgt die mechanische Zerkleinerung der Nieren, eine Inkubation in Kollagenase 1A und DNase 1 und eine weitere mechanische Zerkleinerung durch Siebe. Schließlich werden die Proben an einem Magneten wiederholt gewaschen, bis nur noch die mit Beads angereicherten und damit magnetisierten Glomeruli am Magneten verbleiben. Während der Isolation geht die Bowmankapsel verloren, sodass nur der Verband des Kapillarknäuels, bestehend aus den Podozyten, Mesangialzellen und Endothelzellen, verbleibt.

2.2.4. Entwicklung eines Protokolls zur Lösung glomerulärer Zellen aus ihrem Verband

Eine signifikante Hürde ergab sich aus der Feststellung, dass der enzymatische Verdau zum Herauslösen der Zellen, wie sie Boerries et al. und Wanner et al. verwendeten, für unseren Ansatz nicht nutzbar war. (Boerries et al., 2013; Wanner et al., 2014) Wir entdeckten schnell, dass die Pronase E (Sigma P6911), die von den Autoren genutzt wurde, membranständige Proteine - und damit potenzielle Ziele für die Markierung mit Antikörpern - entfernte. Ein Großteil meiner Arbeit verbrachte ich damit, Proteine zu recherchieren, die zwischen den drei Zelltypen einzigartig und extrazellulär membranständig waren. Gleichzeitig führte ich systematische Experimente diverser proteolytischer Enzyme in verschiedenen Kombinationen, Konzentrationen und Inkubationsprotokollen durch, um einen Weg zu finden, die größtmögliche Menge an Zellen aus Glomeruli herauszulösen, ohne ihre spezifischen Oberflächenmoleküle zu entfernen. Letztendlich erwies sich die Kombination aus dem Präparat Liberase TL von Sigma Aldrich Fine Chemicals Biosciences sowie DNase 1 und den Oberflächenmolekülen Podoplanin, CD73 und CD31 als erfolgreich.

2.2.4.1. Podoplanin

Podoplanin ist ein 43 Kilodalton schweres und aus 162 Aminosäuren bestehendes membranständiges Glykoprotein. Es findet sich auf Endothelzellen lymphatischer Gefäße, auf Typ-1 Pneumozyten, sowie in Nierenkörperchen auf Podozyten und parietal-epithelialen Zellen der Bowman-Kapsel. (Breiteneder-Geleff et al., 1997; Ugorski et al., 2016) Über die physiologische Funktion des Proteins ist wenig bekannt, jedoch wurden abnormale embryonale Entwicklungen von Herz und Lunge in Knock-out Mäusen festgestellt. In Podozyten wird eine Regulierung der Form der

Fußfortsätze durch Podoplanin vermutet.(Ugorski et al., 2016) Auf der Membran der Podozyten ist Podoplanin in etwa zu 90% auf der luminalen Seite lokalisiert, also nicht in direkter räumlicher Beziehung zur Basalmembran.(Breiteneder-Geleff et al., 1997) Durch seine kräftige Expression auf der Podozytenmembran und der Tatsache, dass die Bowmankapsel und damit die andere podoplanintragende Zellgruppe im Nierenkörperchen während der Isolation der Glomeruli verloren geht, bietet es sich als Ziel für die spezifische Färbung der Podozyten an.

2.2.4.2. CD73

Die ecto-5'-nucleosidase ist ein extrazelluläres, an der Membran lokalisiertes Enzym, welches Adenosinmonophosphat hydrolysiert und die extrazelluläre Konzentration von Adenosin reguliert.(Scaletti et al., 2021) Innerhalb des Glomerulus kommt es nur auf der Oberfläche von Mesangialzellen vor, daher eignet es sich als Ziel für eine spezifische Färbung.

2.2.4.3. CD31

Das 130 Kilodalton schwere Platelet/endothelial cell adhesion molecule-1 (PECAM-1) wurde in den 1980er Jahren von mehreren Gruppen unter verschiedenen Namen entdeckt und beschrieben. Heute wird es als PECAM-1 oder CD31 bezeichnet. Neben seiner Expression auf Leukozyten und Thrombozyten findet sich CD31 konzentriert an den Zell-Zell-Verbindungen von Endothelzellen und ist an der Regulation der Gefäßpermeabilität beteiligt.(Lertkiatmongkol et al., 2016) Bereits als zuverlässiger Marker für Endothelzellen etabliert, eignet es sich auch zur gezielten Färbung der glomerulären Endothelzellen.

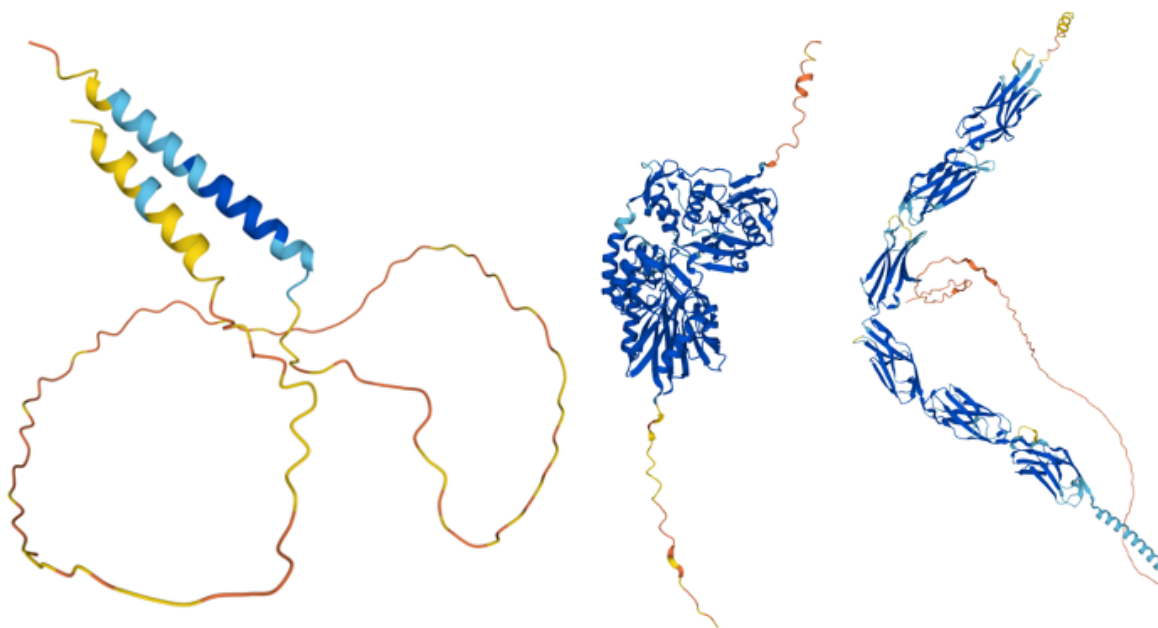


Abbildung 4: Illustration der vorgeschlagenen Strukturen der murinen Proteine (v.l.n.r.) Podoplanin, CD73 und CD31 durch AlphaFold2 (Jumper et al., 2021). Diese Proteine sind die Antigene, die für die zellspezifische Markierung mit fluorochrom-gekoppelten Antikörpern genutzt werden. Podoplanin wird von den drei Zelltypen spezifisch von Podozyten exprimiert, sowie CD73 von Mesangialzellen und CD31 von Endothelzellen.

2.2.5. Zellen sortieren

Nachdem ein Inkubationsprotokoll gefunden war, mit dem sich glomeruläre Zellen in ausreichender Zahl mit intaktem molekularem Oberflächenbesatz isolieren ließen, war es im Weiteren unkompliziert, die Konzentrationen der Antikörper für die Färbung zu optimieren. Genutzt werden jeweils eine spezifische Farbe pro Zelltyp sowie ein Marker für tote Zellen, sodass schließlich vier verschiedene Farbspektren zum Einsatz kommen. Eine Variation findet sich hier für die mT/mG Zellen, die keine dedizierte Podozytenfärbung benötigten. Zusammen mit dem Forward- und Sidewardscattering wurde sichergestellt, dass nur lebendige Einzelzellen sortiert wurden. Tote oder nicht vollständig getrennte Zellen wurden von der Sortierung ausgeschlossen.

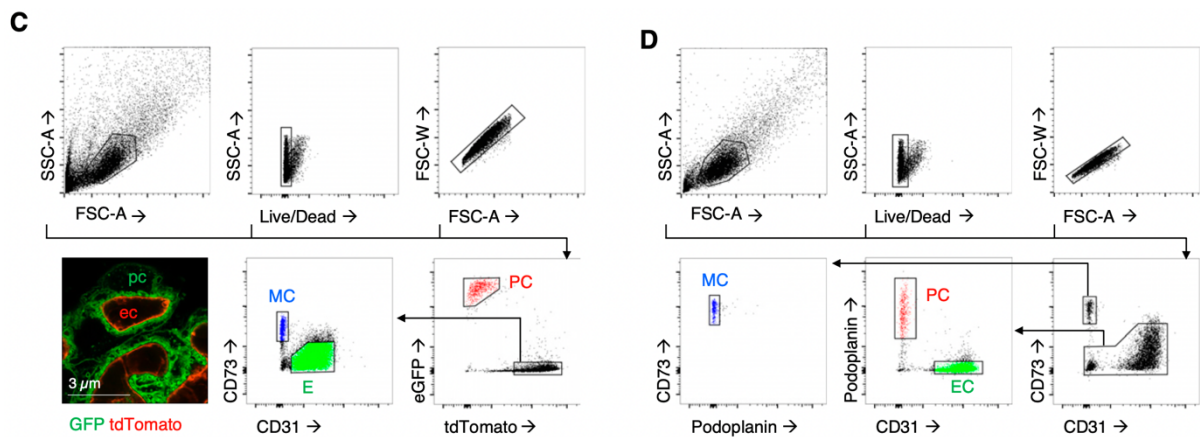


Abbildung 5: Gatingstrategien für die Sortierung glomerulärer Zellen für mT/mG Mäuse (C) und Wildtyp Mäuse (D). Die obere Reihe enthält jeweils die Sequenz an Gates, die nur lebendige Einzelzellen für die weitere Sortierung zulässt. C: Die Podozyten (PC) der mT/mG Mäuse exprimieren eGFP und können direkt identifiziert werden. Über Markierung der Mesangialzellen (MC) und Endothelzellen (E) mit spezifischen Antikörpern können diese in einem weiteren Schritt voneinander getrennt werden. D: Alle 3 Zelltypen werden mit jeweils spezifischen Antikörpern markiert und gegeneinander gated, sodass nur Zellen sortiert werden, die positiv für genau einen Marker sind.

2.2.6. Reinheit isolierter Zellpopulationen

Die Reinheit der isolierten Zellpopulationen wurde vielfach mit folgenden Methoden überprüft.

2.2.6.1. Konfokale Mikroskopie

Um die isolierten Zellen bildlich darstellen zu können, haben wir Zellen ausgesät, kultiviert, fixiert, Zellstrukturen (Glykokalyx mit Wheat Germ Agglutinin, Aktin Filamente mit Phalloidin und Zellkerne mit Hoechst) gefärbt und in einem konfokalen Mikroskop betrachtet (siehe Abbildung 6). In der Podozytenpopulation ließen sich Zellen mit typischen Primär- und Sekundärfortsätzen sowie kortikal betontem Aktin-Zytoskelett darstellen. In der Mesangialzellpopulation fanden wir Zellen mit vielen kleinen, radiär ausstrahlenden Fortsätzen, vereinbar mit einer Zelle, die die Struktur ihrer Umgebung durch gezielte Kontraktion und Relaxation reguliert. Die Endothelzellen hingegen zeigten sich als kleine, zytosolarme, rundliche Zellen ohne

besondere Merkmale, was ebenfalls Sinn ergab, da sich ihre fenestrierte Struktur erst im Verbund mit anderen Zellen ergeben kann.

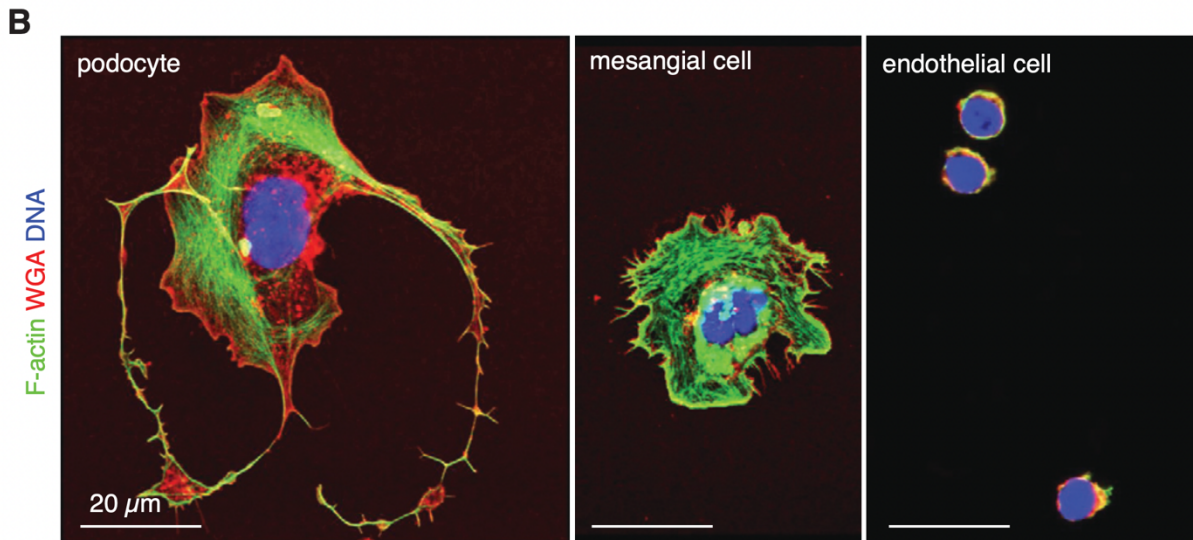


Abbildung 6: Konfokale Mikroskopien isolierter, sortierter und kultivierter (v.l.n.r.) Podozyten, Mesangialzellen und Endothelzellen.

2.2.6.2. Quantitative polymerase chain reaction

Um die Reinheit der Zellpopulationen quantitativ erfassen zu können, habe ich die mRNA der Zellen isoliert, in cDNA umgeschrieben und die Transkription zellspezifischer Proteine aller Zelltypen in allen Proben in der qPCR quantifiziert. Die Gene *Nphs2* und *Pdpr*, kodierend für die Proteine Podocin und Podoplanin, wurden als Marker für Podozyten genutzt. Die Marker für Mesangialzellen waren *Pdgfrb* und *Cd73*, kodierend für die gleichnamigen Proteine. Letztlich wurden die Gene *Cdh5* und *Pecam1* als Marker für Endothelzellen genutzt, welche die Proteine VE-Cadherin und CD31 kodieren. Die qPCR zeigte eine deutliche Anreicherung der Proteine in ihren jeweiligen spezifischen sortierten Zellpopulationen. Zusätzlich habe ich die Proben auf eine mögliche Kontamination durch parietale epitheliale Zellen und Tubuluszellen überprüft und konnte diese ausschließen. (Hatje et al., 2021, supplement 6)

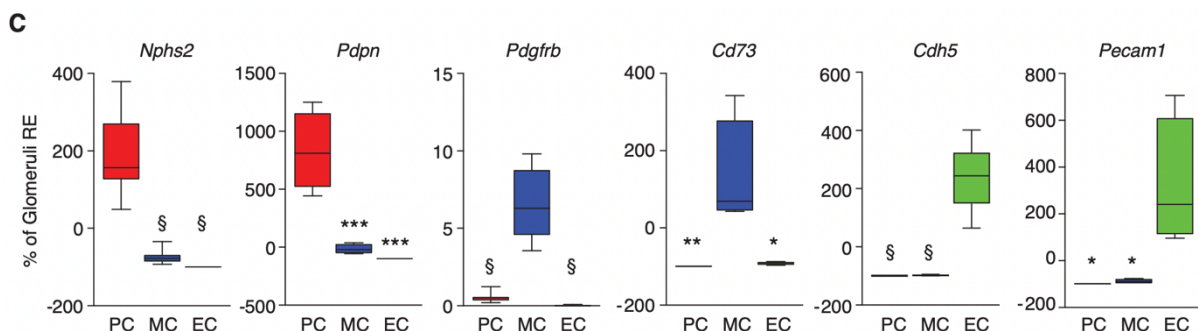


Abbildung 7: qPCR von jeweils zwei zelltyp-spezifischen Genen der sortierten Zellen. Hier zeigt sich eine vermehrte Expression der Markergene innerhalb der entsprechenden Zellpopulationen.

2.2.6.3. Western Blot

Die Western Blots, mit denen wir die von lysierten sortierten Zellen gewonnenen Proteine sichtbar machen und quantifizieren konnten, wurden von meiner Kollegin Wiebke Sachs durchgeführt. Nephrin, ein podozytäres Protein der Schlitzmembran wurde als Marker für Podozyten gewählt, PDGFR-beta als Marker für Mesangialzellen und VE-Cadherin als Marker für Endothelzellen. Die Ergebnisse ihrer Untersuchungen decken sich mit den Ergebnissen der qPCR und demonstrieren die Reinheit der sortierten Zellen.

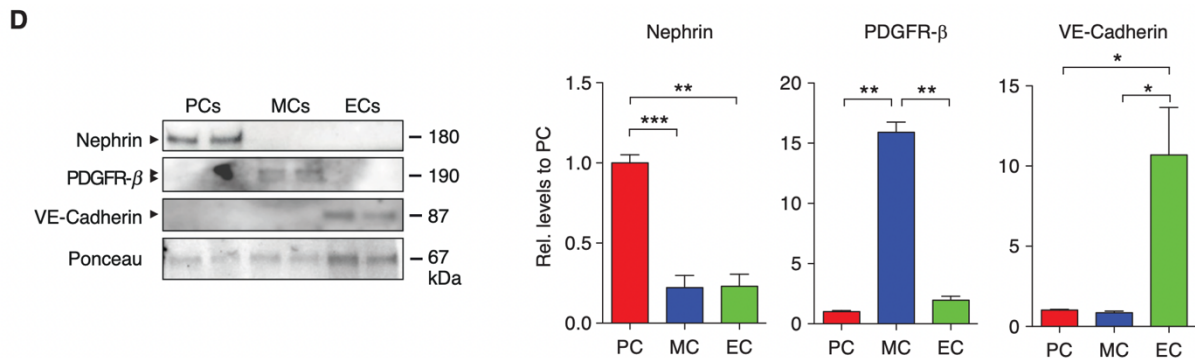


Abbildung 8: Western Blots zelltyp-spezifischer Proteine. Die Proteine sind signifikant in den Proben des jeweiligen Zelltyps angereichtert.

2.2.6.4. Proteomics

Große, aus mehreren Mäusen zusammengestellte Proben wurden an Markus Rinschen geschickt, der diese mit einem Massenspektrometer analysiert hat. Hier zeigte sich im ersten Batch eine geringfügige Verunreinigung der Mesangialzellpopulation durch Podozyten, welche den vorangegangenen Tests entgangen war. Nach akribischer Suche fand sich schließlich ein kleiner Fehler in der Gatingstrategie des Sortierens. Nach der entsprechenden Korrektur schickten wir einen zweiten Batch, welcher schließlich die erwartete Reinheit aufwies.

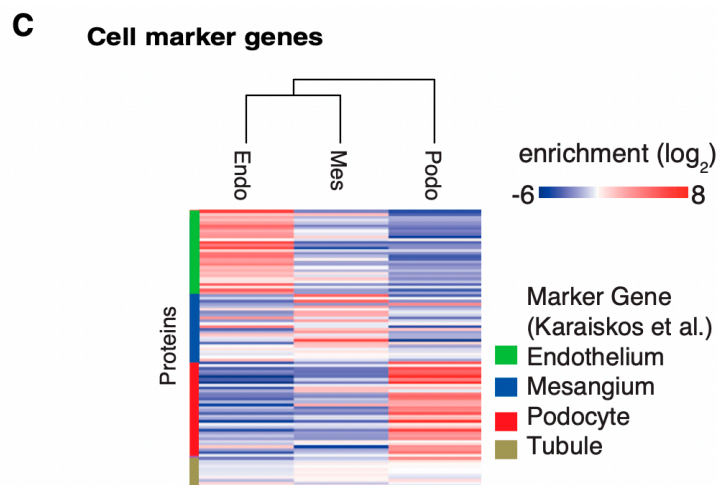


Abbildung 9: Proteomics-Analyse mit Darstellung der Anreicherung zelltyp-spezifischer Proteine (Karaiskos et al., 2018), innerhalb der sortierten Zellpopulationen. Hier zeigt sich eine deutliche Anreicherung der Proteine der Zellmarkergene innerhalb ihrer entsprechenden Zellpopulation. Zusätzlich zeigt sich

eine deutliche schwächere und gleichmäßige Expression tubulärer Proteine in den Zellpopulationen.

2.2.7. Weiterführende Untersuchungen

Nach dem Abschluss der Entwicklungsphase von timMEP haben wir damit begonnen, verschiedene weiterführende Experimente durchzuführen.

2.2.7.1. Angereicherte Proteine in den Zellpopulationen

Nach den Proteomicsanalysen erhielten wir von Markus Rinschen einen Datensatz aller identifizierten Proteine. Eine weiterführende Auswertung der Daten resultierte in 12 podozytenspezifischen, 16 mesangialzellspezifischen und 22 endothelzellspezifischen Proteinen, die bisher nicht als solche beschrieben wurden. (Hatje et al., 2021, fig. 4B)

2.2.7.2. Ergebnisse proteomischer Untersuchungen sortierter Zellpopulationen

Zusätzlich zu der Darstellung der erfolgreichen Auftrennung glomerulärer Zellen, konnten wir weiterführende Analysen der gewonnenen Proteomicsdaten durchführen. Wir konnten zeigen, dass signifikante Unterschiede des Proteoms auch zwischen den gleichen Zelltypen unterschiedlicher Mausstämme darstellbar sind. Die größten Differenzen ergaben sich zwischen den Wildtyp-Proteomen und den mT/mG-Proteomen, hinweisend auf die Verfälschung bzw. Artefaktbildung, die in den Proteomen von Reportermausen entstehen kann.

2.2.7.3. Spezifische Reaktionen glomerulärer Zellen im Mausmodell der anti-THSD7A membranösen Glomerulonephritis

Nach erfolgreicher Darstellung signifikanter Unterschiede zwischen den von uns genutzten Mausstämmen im Gesunden, wollten wir die Applikation von timMEP mit kranken Tieren überprüfen. Dafür haben wir Wildtyp-Mäuse mit anti-THSD7A Antikörpern behandelt, um das Mausmodell der anti-THSD7A membranösen Glomerulonephritis zu induzieren (Tomas et al., 2017). THSD7A ist ein in der Schlitzmembran der Podozyten lokalisiertes Protein und ein Ziel für Autoantikörper, die im Menschen bei Bindung die membranöse Glomerulonephritis auslösen. (Herwig et al., 2019; Tomas et al., 2014) Isolation der Zellen erfolgte 1 Tag und 7 Tage nach Injektion der Antikörper. Eine Kontrollgruppe erhielt unspezifisches Kaninchen IgG. Auswertungen von qPCR-Experimenten zeigten signifikante Transkriptionsunterschiede in Podozyten zwischen dem 1. und 7. Tag nach Injektion. Diese Effekte waren in Proben kompletter Glomeruli nicht nachweisbar, hinweisend auf die genauere Auflösbarkeit zellulärer Effekte in Mausmodellen mit timMEP.

2.3. Diskussion

2.3.1. Der Verlust von Antigenen

timMEP birgt das Potenzial, die nächste Etappe in der Erforschung glomerulärer Erkrankungen zu katalysieren. Umso wichtiger ist es sich ihrer Grenzen klar zu sein. Die Sortierbarkeit der Zellen fundiert vollständig auf der Markierung der Zelltypen mit

Fluorochromen. Wir setzen mit der Methode auf die Bindung fluorochrom-gekoppelter Antikörper an extrazelluläre, membranständige, für ihren Zelltyp spezifische Proteine. Können diese nicht gebunden werden, können die Zellen im FACS nicht sortiert werden.

Für die Erforschung von Erkrankungen sind vergleichbare Mausmodelle von großem Wert. Es besteht jedoch keine Garantie, dass eine in der Maus induzierte Erkrankung nicht zu einem Verlust der Oberflächenmoleküle führt. Die Podozyten einer Maus, die beispielsweise ihr Podoplanin vollständig verliert, können nicht mit unserer Methode isoliert werden.

Aus der Überlegung des Verlustes von Antigenen auf kranken Zellen resultiert eine weitere Schlussfolgerung. Wenn kranke Zellen weniger gut markiert und sortiert werden können, besteht die Möglichkeit einer Verzerrung der nachfolgenden Untersuchungen. Durch das Wegfallen kranker Zellen beim Sortieren resultiert eine ungleich höhere Gewinnung gesunder Zellen, die nicht der Verteilung von kranken und gesunden Zellen in-vivo entspricht.

Es müssen jedoch nicht zwingend die drei Markermoleküle Podoplanin, CD73 und CD31 genutzt werden. Sollten die Moleküle in einem Mausmodell nicht zuverlässig markierbar sein, können alternative Markerproteine getestet werden. Eine Auswahl an möglichen potenziellen Oberflächenmarkern haben wir in unserer Veröffentlichung mitangefügt.(Hatje et al., 2021, Supplemental table 5) Außerdem wäre es möglich timMEP zu modifizieren, indem beispielsweise nach der Zellisolation intrazelluläre Moleküle markiert werden. Diese Möglichkeit habe ich während der Entwicklung der Methode zwar in Betracht gezogen, aber nicht weiterverfolgt, da sie zum Tod aller Zellen führt. Je nach Ziel des Experimentes könnte dieser Umstand jedoch akzeptabel sein.

2.3.2. Die membranöse Glomerulonephritis

Die Niere ist als zentrales Organ für die Gesundheit des Menschen unerlässlich. Als hochkomplexe Funktionseinheit besitzt sie zahllose Stellschrauben, an denen Funktionsverluste zu umfangreichen klinischen Syndromen eskalieren können. Einer dieser Symptomkomplexe ist das nephrotische Syndrom, das sich durch Proteinurie, Ödeme, Hypalbuminämie und Hypertriglycerinämie auszeichnet.(Ronco and Debiec, 2020) Ursächlich für diesen Symptomkomplex ist der Verlust von Bluteiweißen durch einen Funktionsverlust der glomerulären Filtration. Die häufigste mit dem nephrotischen Syndrom einhergehende Erkrankung des Erwachsenen ist die membranöse Glomerulonephritis.(Medawar et al., 1990; Ronco and Debiec, 2020) Pathophysiologisch entsteht sie durch die autoimmune Bildung von anti-PLA2-Rezeptor Antikörpern (Beck et al., 2009) oder anti-THSD7A-Antikörpern (Tomas et al., 2014), welche durch die Bindung mit ihren Antigenen Immunkomplexe bilden, die sich wiederum an der Basalmembran ablagern. Dies führt zu einer Schädigung glomerulärer Strukturen durch die Aktivierung des Komplementsystems. Ist der Schaden von den Podozyten nicht mehr kompensierbar, zeigt sich das Verstreichen der podozytären Fußfortsätze mit Funktionsverlust der Schlitzmembran und der glomerulären Basalmembran.(Butt et al., 2020; Nagata, 2016; Ronco and Debiec, 2020) Resultierend verliert der glomeruläre Filter seine Fähigkeit, das Ausschwemmen von Plasmaproteinen in den Primärharn zu verhindern.

2.3.3. Relevanz von timMEP im Kontext medizinischer Grundlagenforschung

Moderne Grundlagenforschung wendet zunehmend komplexere Instrumente zum Erlangen neuer Erkenntnisse an. Auch timMEP ist im Vergleich zu vorangegangenen Methoden komplexer und aufwendiger geworden. Wir haben jedoch zeigen können, dass sich die Arbeit überproportional auszahlt, da sie die Gewinnung großer Mengen an Probenmaterial erlaubt. Entscheidend ist auch die Tatsache, dass es nun möglich ist, große Proben aller 3 Zelltypen aus einer einzigen Maus zu gewinnen. Dies erlaubt den direkten Vergleich zwischen den Zellen und gewährt einen Weg zu zunehmend detaillierten Untersuchungen des interzellulären Crosstalks im gesunden und kranken Glomerulus.

3. Zusammenfassung

3.1. Deutsch

Der Glomerulus der Niere besteht aus 3 zellulären Hauptbestandteilen: Podozyten, Mesangialzellen und Endothelzellen. Gemeinsam sind sie für die Bildung und Aufrechterhaltung der glomerulären Filtrationsbarriere verantwortlich, ein Funktionsverlust dieser Struktur resultiert im nephrotischen Syndrom. Die Erforschung des Glomerulus stellt daher eine fundamentale Voraussetzung für das Erlangen pathogenetischen Verständnisses glomerulärer Erkrankungen sowie die Entwicklung effektiver Therapien dar. Ziel dieser Arbeit war es, eine Methodik zu entwickeln, die es erlaubt alle 3 Zelltypen aus einer Wildtyp-Maus zu isolieren und für beliebige nachfolgende Analysen nutzbar zu machen, genannt timMEP. timMEP verläuft in 5 Schritten: Entnahme muriner Nieren, Isolation der Glomeruli, Herauslösen der Zellen aus den Glomeruli, Markierung der Zellen mit zelltypspezifischen fluoreszenzgekoppelten Antikörpern und Sortierung der Zellen in einem FACS. Die Reinheit der erhaltenen Zellpopulationen wurde unter Nutzung konfokaler Mikroskopie, qPCR, Western Blots und Proteomics bestätigt. timMEP erlaubt es Untersuchungen an den 3 Hauptzellbestandteilen eines Individuums durchzuführen und ebnet somit den Weg für Experimente mit glomerulären Zellen in einem bisher unerreichtem Detailgrad.

3.2. Englisch

The kidney's glomerulus consists of 3 main cellular components: podocytes, mesangial cells and endothelial cells. Together they are responsible for the formation and maintenance of the glomerular filtration barrier, a loss of function of this structure results in the nephrotic syndrome. Consequently, the investigation of the glomerulus is a fundamental prerequisite for gaining a pathogenetic understanding of glomerular diseases and the development of effective therapies. The aim of this work was to develop a protocol that enables the isolation of all 3 cell types from the same individual. We call this method timMEP. timMEP consists of 5 steps: harvest of murine kidneys, isolation of the glomeruli, extraction of the cellular components, labeling the cells with cell-type-specific fluorescence-coupled antibodies and fluorescence-activated cell sorting. The purity of the obtained cell populations was confirmed using confocal microscopy, qPCR, Western blots and proteomics. timMEP enables glomerular cell type-resolved investigations in unprecedented detail.

4. Abkürzungsverzeichnis

timMEP	tripartite isolation method for murine mesangial and endothelial cells and podocytes
THSD7a	Thrombospondin Type 1 Domain-Containing 7A
FACS	fluorescence-activated cell sorting
eGFP	enhanced green-fluorescent protein
tdTomato	tandem-dimer-tomato
mT/mG	membrane-targeted tdTomato/membrane-targeted eGFP
PECAM-1	Platelet/endothelial cell adhesion molecule-1
CD31	Cluster of Differentiation 31
CD73	Cluster of Differentiation 73
qPCR	quantitative polymerase chain reaction
mRNA	messenger ribonucleic acid
cDNA	complementary desoxyribonucleic acid

5. Abbildungsverzeichnis

Abbildung 1: Schünke et al., 2005, p. 230

Abbildung 2: Welsch and Sobotta, 2009, p. 454

Abbildung 3: Die Grafik wurde vom Autor angefertigt.

Abbildung 4: Zusammenstellung von Bildschirmfotos durch den Autor, aufgenommen am 13.04.2022, von links nach rechts:
<https://www.uniprot.org/uniprot/Q62011>
<https://www.uniprot.org/uniprot/Q61503>
<https://www.uniprot.org/uniprot/Q08481>

Abbildung 5: Hatje et al., 2021, fig. 1C,D

Abbildung 6: Hatje et al., 2021, fig. 2B

Abbildung 7: Hatje et al., 2021, fig. 2C

Abbildung 8: Hatje et al., 2021, fig. 2D

Abbildung 9: Hatje et al., 2021, fig. 3C

6. Literaturverzeichnis

- Beck, L.H., Bonegio, R.G.B., Lambeau, G., Beck, D.M., Powell, D.W., Cummins, T.D., Klein, J.B., Salant, D.J., 2009. M-type phospholipase A2 receptor as target antigen in idiopathic membranous nephropathy. *N. Engl. J. Med.* 361, 11–21. <https://doi.org/10.1056/NEJMoa0810457>
- Boerries, M., Grahammer, F., Eiselein, S., Buck, M., Meyer, C., Goedel, M., Bechtel, W., Zschiedrich, S., Pfeifer, D., Laloë, D., Arrondel, C., Gonçalves, S., Krüger, M., Harvey, S.J., Busch, H., Dengjel, J., Huber, T.B., 2013. Molecular fingerprinting of the podocyte reveals novel gene and protein regulatory networks. *Kidney Int.* 83, 1052–1064. <https://doi.org/10.1038/ki.2012.487>
- Breiteneder-Geleff, S., Matsui, K., Soleiman, A., Meraner, P., Poczewski, H., Kalt, R., Schaffner, G., Kerjaschki, D., 1997. Podoplanin, novel 43-kd membrane protein of glomerular epithelial cells, is down-regulated in puromycin nephrosis. *Am. J. Pathol.* 151, 1141–1152.

- Butt, L., Unnersjö-Jess, D., Höhne, M., Edwards, A., Binz-Lotter, J., Reilly, D., Hahnfeldt, R., Ziegler, V., Fremter, K., Rinschen, M.M., Helmstädter, M., Ebert, L.K., Castrop, H., Hackl, M.J., Walz, G., Brinkkoetter, P.T., Liebau, M.C., Tory, K., Hoyer, P.F., Beck, B.B., Brismar, H., Blom, H., Schermer, B., Benzing, T., 2020. A molecular mechanism explaining albuminuria in kidney disease. *Nat. Metab.* 2, 461–474. <https://doi.org/10.1038/s42255-020-0204-y>
- Deetjen, P., Alzheimer, C. (Eds.), 2005. *Physiologie: mit 88 Tabellen ; plus CD-ROM mit Prüfungsfragen und allen Abbildungen ; [Lern-Tipp: nach neuer AO], 4., vollst. überarb. Aufl. ed. Urban & Fischer, München Jena.*
- Dimke, H., Maezawa, Y., Quaggin, S.E., 2015. Crosstalk in glomerular injury and repair. *Curr. Opin. Nephrol. Hypertens.* 24, 231–238. <https://doi.org/10.1097/MNH.0000000000000117>
- Hatje, F.A., Wedekind, U., Sachs, W., Loreth, D., Reichelt, J., Demir, F., Kosub, C., Heintz, L., Tomas, N.M., Huber, T.B., Skuza, S., Sachs, M., Zielinski, S., Rinschen, M.M., Meyer-Schwesinger, C., 2021. Tripartite Separation of Glomerular Cell Types and Proteomes from Reporter-Free Mice. *J. Am. Soc. Nephrol. JASN* 32, 2175–2193. <https://doi.org/10.1681/ASN.2020091346>
- Herwig, J., Skuza, S., Sachs, W., Sachs, M., Failla, A.V., Rune, G., Meyer, T.N., Fester, L., Meyer-Schwesinger, C., 2019. Thrombospondin Type 1 Domain-Containing 7A Localizes to the Slit Diaphragm and Stabilizes Membrane Dynamics of Fully Differentiated Podocytes. *J. Am. Soc. Nephrol. JASN* 30, 824–839. <https://doi.org/10.1681/ASN.2018090941>
- Jumper, J., Evans, R., Pritzel, A., Green, T., Figurnov, M., Ronneberger, O., Tunyasuvunakool, K., Bates, R., Žídek, A., Potapenko, A., Bridgland, A., Meyer, C., Kohl, S.A.A., Ballard, A.J., Cowie, A., Romera-Paredes, B., Nikolov, S., Jain, R., Adler, J., Back, T., Petersen, S., Reiman, D., Clancy, E., Zielinski, M., Steinegger, M., Pacholska, M., Berghammer, T., Bodenstein, S., Silver, D., Vinyals, O., Senior, A.W., Kavukcuoglu, K., Kohli, P., Hassabis, D., 2021. Highly accurate protein structure prediction with AlphaFold. *Nature* 596, 583–589. <https://doi.org/10.1038/s41586-021-03819-2>
- Karaiskos, N., Rahmatollahi, M., Boltengagen, A., Liu, H., Hoehne, M., Rinschen, M., Schermer, B., Benzing, T., Rajewsky, N., Kocks, C., Kann, M., Müller, R.-U., 2018. A Single-Cell Transcriptome Atlas of the Mouse Glomerulus. *J. Am. Soc. Nephrol. JASN* 29, 2060–2068. <https://doi.org/10.1681/ASN.2018030238>
- Klinke, R., Pape, H.-C., Kurtz, A., Silbernagl, S., Baumann, R., Brenner, B., Gay, R., Rothenburger, A. (Eds.), 2010. *Physiologie, 6., vollst. überarb. Aufl. ed. Thieme, Stuttgart.*
- Kocylowski, M.K., Aypek, H., Bildl, W., Helmstädter, M., Trachte, P., Dumoulin, B., Wittösch, S., Kühne, L., Aukschun, U., Teetzen, C., Kretz, O., Gaal, B., Kulik, A., Antignac, C., Mollet, G., Köttgen, A., Göcmen, B., Schwenk, J., Schulte, U., Huber, T.B., Fakler, B., Grahammer, F., 2022. A slit-diaphragm-associated protein network for dynamic control of renal filtration. *Nat. Commun.* 13, 6446. <https://doi.org/10.1038/s41467-022-33748-1>
- Kurihara, H., Sakai, T., 2017. Cell biology of mesangial cells: the third cell that maintains the glomerular capillary. *Anat. Sci. Int.* 92, 173–186. <https://doi.org/10.1007/s12565-016-0334-1>
- Lertkiatmongkol, P., Liao, D., Mei, H., Hu, Y., Newman, P.J., 2016. Endothelial functions of platelet/endothelial cell adhesion molecule-1 (CD31). *Curr. Opin. Hematol.* 23, 253–259. <https://doi.org/10.1097/MOH.0000000000000239>

- Medawar, W., Green, A., Campbell, E., Carmody, M., Donohoe, J., Doyle, G., Walshe, J.J., 1990. Clinical and histopathologic findings in adults with the nephrotic syndrome. *Ir. J. Med. Sci.* 159, 137–140. <https://doi.org/10.1007/BF02937405>
- Muzumdar, M.D., Tasic, B., Miyamichi, K., Li, L., Luo, L., 2007. A global double-fluorescent Cre reporter mouse. *Genes.* N. Y. N 2000 45, 593–605. <https://doi.org/10.1002/dvg.20335>
- Nagata, M., 2016. Podocyte injury and its consequences. *Kidney Int.* 89, 1221–1230. <https://doi.org/10.1016/j.kint.2016.01.012>
- Ronco, P., Debiec, H., 2020. Molecular Pathogenesis of Membranous Nephropathy. *Annu. Rev. Pathol.* 15, 287–313. <https://doi.org/10.1146/annurev-pathol-020117-043811>
- Scaletti, E., Huschmann, F.U., Mueller, U., Weiss, M.S., Sträter, N., 2021. Substrate binding modes of purine and pyrimidine nucleotides to human ecto-5'-nucleotidase (CD73) and inhibition by their bisphosphonic acid derivatives. *Purinergic Signal.* <https://doi.org/10.1007/s11302-021-09802-w>
- Schünke, M., Schulte, E., Schumacher, U., 2005. Prometheus. Hals und innere Organe: 78 Tabellen. Thieme, Stuttgart.
- Takemoto, M., Asker, N., Gerhardt, H., Lundkvist, A., Johansson, B.R., Saito, Y., Betsholtz, C., 2002. A new method for large scale isolation of kidney glomeruli from mice. *Am. J. Pathol.* 161, 799–805. [https://doi.org/10.1016/S0002-9440\(10\)64239-3](https://doi.org/10.1016/S0002-9440(10)64239-3)
- Tomas, N.M., Beck, L.H., Meyer-Schwesinger, C., Seitz-Polski, B., Ma, H., Zahner, G., Dolla, G., Hoxha, E., Helmchen, U., Dabert-Gay, A.-S., Debayle, D., Merchant, M., Klein, J., Salant, D.J., Stahl, R.A.K., Lambeau, G., 2014. Thrombospondin type-1 domain-containing 7A in idiopathic membranous nephropathy. *N. Engl. J. Med.* 371, 2277–2287. <https://doi.org/10.1056/NEJMoa1409354>
- Tomas, N.M., Meyer-Schwesinger, C., von Spiegel, H., Kotb, A.M., Zahner, G., Hoxha, E., Helmchen, U., Endlich, N., Koch-Nolte, F., Stahl, R.A.K., 2017. A Heterologous Model of Thrombospondin Type 1 Domain-Containing 7A-Associated Membranous Nephropathy. *J. Am. Soc. Nephrol. JASN* 28, 3262–3277. <https://doi.org/10.1681/ASN.2017010030>
- Ugorski, M., Dziegiel, P., Suchanski, J., 2016. Podoplanin - a small glycoprotein with many faces. *Am. J. Cancer Res.* 6, 370–386.
- Wanner, N., Hartleben, B., Herbach, N., Goedel, M., Stickel, N., Zeiser, R., Walz, G., Moeller, M.J., Grahammer, F., Huber, T.B., 2014. Unraveling the role of podocyte turnover in glomerular aging and injury. *J. Am. Soc. Nephrol. JASN* 25, 707–716. <https://doi.org/10.1681/ASN.2013050452>
- Welsch, U., Sobotta, J., 2009. Lehrbuch Histologie: Zytologie, Histologie, mikroskopische Anatomie; mit 21 Tabellen; [+ mit dem plus im Web, Zugangscode im Buch, www.studentconsult.de], 2., völlig überarb. Aufl., 4. Nachdr. ed. Elsevier, Urban & Fischer, München Jena.

7. Erklärung des Eigenanteils an der Publikation

Die Entwicklung der timMEP Zellisolationmethode erfolgte durch Catherine Meyer-Schwesinger, Uta Wedekind und mich.

Die Zellisolationen wurden durchgeführt von Uta Wedekind, Stephanie Zielinski, Wiebke und Marlies Sachs, Julia Reichelt und mir.

Alle konfokalen Mikroskopien wurden durchgeführt von Catherine Meyer-Schwesinger und mir.

Die qPCRs erfolgten durch Uta Wedekind, Julia Reichelt, Lukas Heintz und mich.

Die Western Blots erfolgten durch Wiebke Sachs.

Die Kultur sortierter Zellen erfolgte durch Marlies Sachs und Sinah Skuza.

Die Durchführung, Analyse und Visualisierungen der Proteomics erfolgte durch Markus Rinschen und Fatih Demir.

Die Literaturrecherche zur Identifizierung neuer Markermoleküle erfolgte durch mich.

Das Schreiben des Artikels erfolgte durch Catherine Meyer-Schwesinger, Markus Rinschen, Uta Wedekind und mich.

Die super-resolution structured illumination microscopy erfolgte durch Desirée Loreth.

Die Co-Immunopräzipitationen erfolgten durch Christopher Kosub.

Die UMAP-Visualisierungen erfolgten durch mich.

Die mT/mG Reportermäuse wurden von Tobias B. Huber zur Verfügung gestellt.

Die Generierung des anti-THSD7A Antikörpers für die Induktion der THSD7A-assoziierten membranösen Nephropathie in der Maus erfolgte von Nicola Tomas.

8. Danksagung

Diese Arbeit war lang und anstrengend, dennoch behalte ich sie als eine der schönsten Zeiten meines Lebens in Erinnerung, da sie mich mit zahllosen großartigen Menschen in Verbindung gebracht hat.

Catherine Meyer-Schwesinger, danke, dass du mir die Möglichkeit gegeben hast, eine Doktorarbeit in deinem Labor durchzuführen. Deine ansteckende Begeisterung für unsere Arbeit und deine stete Bereitschaft mit gutem Rat und Tatendrang zu Hilfe zu kommen, war der größte Katalysator für die letztlich erfolgreiche Entwicklung von timMEP und das Gelingen dieser Doktorarbeit. Ich werde nie vergessen, wie wir vor Sonnenaufgang gemeinsam im Labor mit dem Experimentieren begonnen haben.

Anna Reinicke-Vogt, Marlies Sachs, Wiebke Sachs und Julia Reichelt, danke, dass ihr mir mit steter Hilfsbereitschaft und unerschütterlicher Geduld die Arbeitsabläufe des Labors und die Durchflusszytometrie beigebracht habt.

Zusammen mit euch und natürlich Sinah Skuza, Johanna Herwig, Stefanie Zielinski, Karen Neitzel und Uta Wedekind sowie den Kollegen des IZIP und der III.

Medizinischen Klinik des UKE war die Zusammenarbeit stets abwechslungsreich und spannend. Vielen Dank für die großartige Zeit!

Gleichsam möchte ich mich bei meiner Familie bedanken, die mich auf diverse Weise immer unterstützt hat. Ohne euch alle wäre diese Arbeit nicht zustande gekommen.

9. Lebenslauf

Name: Favian Alexander Hatje
Geburtstag: 2. Oktober 1992
Geburtsort: Hongkong

Publikationen:

- Hatje FA, Wedekind U, Sachs W, Loreth D, Reichelt J, Demir F, Kosub C, Heintz L, Tomas NM, Huber TB, Skuza S, Sachs M, Zielinski S, Rinschen MM, Meyer-Schwesinger C. Tripartite Separation of Glomerular Cell Types and Proteomes from Reporter-Free Mice. J Am Soc Nephrol. 2021 Sep;32(9):2175-2193. doi: 10.1681/ASN.2020091346. Epub 2021 Jun 1. PMID: 34074698; PMCID: PMC8729851.

Schulbildung und Studium:

1999	Einschulung
2012	Doppelabschluss mit deutsch-französischem Abitur (Abitur / Baccalauréat Scientifique)
2012 – 2019	Studium der Medizin Universitätsklinikum Hamburg-Eppendorf
2017 – 2018	Einjährige Vollzeitarbeit in einem physiologisch-nephrologischen Labor zur Promotion
2020	Fortsetzung der Promotionsarbeit
23.3.2020	Approbation als Arzt

10. Eidesstaatliche Versicherung

Ich versichere ausdrücklich, dass ich die Arbeit selbständig und ohne fremde Hilfe verfasst, andere als die von mir angegebenen Quellen und Hilfsmittel nicht benutzt und die aus den benutzten Werken wörtlich oder inhaltlich entnommenen Stellen einzeln nach Ausgabe (Auflage und Jahr des Erscheinens), Band und Seite des benutzten Werkes kenntlich gemacht habe.

Ferner versichere ich, dass ich die Dissertation bisher nicht einem Fachvertreter an einer anderen Hochschule zur Überprüfung vorgelegt oder mich anderweitig um Zulassung zur Promotion beworben habe.

Ich erkläre mich einverstanden, dass meine Dissertation vom Dekanat der Medizinischen Fakultät mit einer gängigen Software zur Erkennung von Plagiaten überprüft werden kann.

Unterschrift: